DUPLICATE ALSO

HADLEY CENTRE
FOR CLIMATE PREDICTION AND RESEARCH

Workshop on simulations of the Climate of the Twentieth Century using GISST 28-30 November 1994, Hadley Centre, Bracknell, UK

Edited by

C K Folland and D P Rowell

CRTN 56 **April 1995**

CLIMATE
RESEARCH
TECHNICAL
NOTE

Hadley Centre
Meteorological Office
London Road
Bracknell
Berkshire RG12 2SY

ORGS UKMO C
National Meteorological Library
FitzRoy Road, Exeter, Devon. EX1 3PB

Workshop on simulations of the Climate of the Twentieth Century using GISST 28-30 November 1994, Hadley Centre, Bracknell, UK

Edited by

C K Folland and D P Rowell

CRTN 56

April 1995

CLIMATE RESEARCH TECHNICAL NOTE NO. 56

WORKSHOP ON SIMULATIONS OF THE CLIMATE OF THE TWENTIETH CENTURY USING GISST

28-30 NOVEMBER 1994, HADLEY CENTRE, BRACKNELL, UK

Edited by

C K Folland and D P Rowell

Hadley Centre for Climate Prediction and Research
Meteorological Office
London Road
Bracknell
Berkshire RG12 2SY

NOTE: This paper has not been published. Permission to quote from it should be obtained from the Director of the Hadley Centre.

Preface

The overall purpose of this ad hoc workshop was to bring together groups interested in multidecadal atmospheric general circulation model (AGCM) integrations forced with observed sea surface temperature (SST). The main emphasis was on models run against the Global sea Ice and Sea Surface Temperature (GISST) data sets being developed by the Hadley Centre. Major objectives of the meeting included:

1. Discussions on the development of an improved GISST and related data sets, and atmospheric data sets for model verification.

2. Presentations of results of integrations relating to model validation, seasonal predictability, decadal variability and limited aspects of climate change detection.

3. A special session devoted to diagnostics in support of the model validation chapter of the 1995 IPCC Scientific Assessment.

4. Possible future relationships between the "GISST initiative" and the Atmospheric Models Intercomparison Program (AMIP), the Decadal and Interdecadal Climate variability: dynamics and predictability Experiments (DICE), and the CLImate VARiability and predictability project (CLIVAR).

The workshop consisted of two days of presentations, followed by division into three subgroups which collated and assessed model diagnostics which had been agreed in advance of the workshop. A final session was devoted to diagnostics needed for the climate variability and trends subsection of the model validation chapter of the IPCC Scientific Assessment. These IPCC discussions are well covered by the "Key Time Series Diagnostics" report, which has been updated since the workshop to include diagnostics requested at the workshop.

Contents

Preface 1
Contents 3
Workshop Summary 5
Intercomparison Reports of Working Groups
List of intercomparison diagnostics 11
A methodology for using an ensemble of multi-decadal GCM simulations to assess the percentage variance explained by SST forcing 12
- D.P.Rowell
AGCM intercomparison diagnostics: Climatologies and ENSO teleconnections (1951-80) 14
- C.S.Frederiksen, A.Bevan, A.Navarra, M.Hoerling, K.Miyakoda and M.N.Ward
AGCM intercomparison diagnostics: SST-forced variability versus internal variability 35
- F.W.Zwiers, D.P.Rowell, A.Hense, J.R.Davies and M.Christoph
AGCM intercomparison diagnostics: Key time series 40
- R.Livezey, C.Folland, J.Davies, D.Karoly, J.Walsh, M.Sugi, P.Gleckler and D.Parker
Abstracts
The standard GISST data sets: Versions 1 and 2 50
- D.E.Parker and M.Jackson
Using EOF analysis to create a new GISST data set for forcing GCMs 52
- N.A.Rayner, M.N.Ward, D.E.Parker and C.K.Folland
A sea ice database 54
- J.E.Walsh
Global precipitation and surface temperature data sets 56
- M.Hulme
A provisional new global mean sea level pressure data set 58
- T.A.Basnett and D.E.Parker
A provisional new radiosonde temperature data set 60
- D.E.Parker and D.P.Cullum
NCEP/NCAR 40-year reanalysis 62
- E.Kalnay
Reconstruction of pre-1980 SST fields 63
- R.E.Livezey, R.W.Reynolds, T.Smith and D.C.Stokes
Forcing the Hadley Centre model with GISST: Introduction and seasonal predictability 64
- D.P.Rowell
Forcing the Hadley Centre model with GISST: Extratropical response to ENSO 66
- A.Bevan, D.P.Rowell and C.K.Folland
Forcing the Hadley Centre model with GISST: European variability 68
- J.R.Davies, D.P.Rowell and C.K.Folland
Forcing the Hadley Centre model with GISST: Interannual variability of African wave activity 70
- C.D.Thorncroft and D.P.Rowell
Forcing the ECHAM3 model with the GISST data: First results 72
- A.Hense, U.Röemer and T.Heinze
Forcing the ECHAM3 model with the GISST data: Variability of storm tracks 73
- M.Christoph and E.Roeckner
Forcing the GFDL model with GISST 75
- W.F.Stern, K.Miyakoda and J.Anderson
Forcing the BMRC model with GISST 76
- C.S.Frederiksen, P.Indusekeran, R.C.Balgovind and N.Nicholls

Forcing the CSIRO model with GISST and MOHSST 78
- I.N.Smith, B.G.Hunt and R.J.Allan
Simulation of atmospheric circulation with observed global SST and sea ice during 1949-1992 80
- J.Shukla and L.Marx
Forcing the JMA global model with MOHSST 83
- M.Sugi, R.Kawamura and N.Sato
Modelling and observational studies of a tropic-wide oscillation of boreal summer rainfall 85
- M.N.Ward, K.Maskell, C.K.Folland, D.P.Rowell and R.Washington
The Atmospheric Model Intercomparison Project (AMIP) 87
- W.L.Gates, P.J.Gleckler, B.D.Santer and K.R.Sperber
Intercomparison of observed and simulated potential predictability 88
- F.W.Zwiers
SST-forced simulation skill for versions of the NCEP/MRF model 92
- R.E.Livezey, M.Masutani, M.Ji, H.Rui, A.Kumar and A.Leetmaa
Response of the Asian summer monsoon to ENSO 93
- J.Slingo
Predictability of monsoons in ECMWF seasonal integrations 95
- C.Brankovic and T.N.Palmer
Climate predictability within two nearly identical atmospheric GCMs 99
- M.Hoerling, A.Kumar, M.Ji, A.Leetmaa and P.Sardeshmukh
Appendix 1: Program of Workshop 103
Appendix 2: Participants 107

Workshop Summary

Here we summarise some of the main points of discussion. There is no attempt to fully review the papers that were presented. This section is arranged according to subject matter.

1. GISST and related data

The main problem with the existing GISST data (GISST1.1) is that it is poor in data sparse areas (discussion after I.Smith's talk). N.Rayner described a new version of GISST using interpolation using empirical orthogonal functions that tries to reduce this problem. It was thought that the new LEPS (Linear Error in Probability Space) assessment technique was useful for testing the skill of these SST reconstructions.

R.Livezey discussed a broadly similar technique being developed for post-War SST data, analysed at high resolution, at the National Meteorological Centre, Washington DC (NMC). D.Rowell demonstrated a positive impact of a preliminary version of GISST that uses EOF interpolation (GISST 1.2) on the simulated atmospheric response to SST-forcing over the central Pacific during a data-sparse period (1904-13).

Should the SST EOFs be based solely on a modern, more reliable, period? Use of empirical orthogonal functions (EOFs) based on a modern period to interpolate SST fields for an earlier period assumes, strictly speaking, that the EOFs are temporally invariant. Several participants considered, however, that resulting interpolations would not be sensitive to changes in the EOFs. Only the total variance may need to be stationary (R.Livezey). Care would be needed, therefore, to account adequately for climate change (mostly warming) signals in SST (C.Folland).

It was noted that EOFs based on 1982-1993 SST anomalies (these include bias-adjusted satellite data) reconstructed the 1988 La Nina adequately, even with a 1950s data availability mask, and model simulations were not adversely affected when the reconstructed SSTs were used (R.Livezey). A severe test of the reliability of a new EOF-interpolated GISST for earlier years would be to create a version for say, 1982-1994, using a data coverage restricted to that for, say, 100 years earlier and use this version in (an ensemble of) simulations. The results would be compared with simulations based on the real GISST for 1982-1994. Test simulations could also be used to assess the optimum number of EOFs, though the number of simulations needed could be expensive.

It was noted (e.g. A.Navarra and D.Parker over coffee) that we could use Optimum Interpolation (OI) to improve EOF-interpolated GISST, using EOF GISST as input, with lower weights for interpolated data than for original data.

D. Parker noted that future GISST analyses would greatly benefit by the digitization of at least 17 million still unkeyed marine observations made between 1850 and 1950. These are mainly in currently data sparse regions or at nearly universally poorly sampled times.

J.Walsh brought out the subjectivity and heterogeneity of the earlier Arctic sea-ice extent and concentration data. He was confined to using climatology in the early 1940s owing to lack of data. He had found an artificial decrease in Antarctic ice concentrations (not

extents) in the post 1973 NOAA data. In future, autocorrelations of ice-concentration anomalies could be used in temporal interpolation. Russian data for 1920-1960 for the Asian sector will become available, but its reliability will need checking.

2. Model Verification data sets

2.1 Precipitation

Precipitation climatologies are currently developing quite rapidly, but for model validation purposes a really satisfactory climatology over land, and certainly over the oceans, has yet to emerge. M Hulme wondered whether models been tuned to agree with raw (land) raingauge data? If so, they may be yielding too little rainfall because many raingauge observations require positive adjustments for systematic undercatch. It was noted that the 'worst' rainfall climatology (Jaeger) is still better correlated with other climatologies, e.g. Legates and Willmott, than are model-simulated climatologies to observed climatologies (and very often model rainfall climatologies with each other). Owing to natural variability, 'timeless' rainfall climatologies like Legates and Wilmott are not sufficient: the reference period should be specified and adhered to. On the other hand, the "time specific climatology" of M.Hulme does not yet include bias corrections whereas Legates and Wilmott does.

For the oceans, it is uncertain which is the best of the Outgoing Longwave Radiation (OLR), Microwave Sounding Unit (MSU) and Defense Meteorological Satellite Program (DMSP) rainfall data bases. The new Global Precipitation Climatology Program (GPCP) analysis for 1986-1995 will weight oceanic rainfall data sources differently in different parts of the globe, according to their assessed performance there and include some model (ECMWF) analysed values.

2.2 Mean sea level pressure

This is an important variable for assessing climate variations. Analyses based on observations alone will be needed for periods prior to current reanalysis programs, i.e. certainly before 1946, and are very desirable after then. Biases were noted by I.Smith (of CSIRO) in the provisional CSIRO monthly gridded CSIRO historical mean sea level pressure (MSLP) data set (highs too weak, lows too shallow). This may result from the interpolation scheme and from the low (10° x 10°) resolution. It was noted that this problem affects the current Hadley Centre MSLP data set which incorporates CSIRO data. The Hadley Centre data set is now being reanalysed to include individual ship reports. EOFs could be used to fill gaps. However, care would be needed because if there are only a few observations in a month, MSLP data may be locally unrepresentative because of the frequently poor persistence of daily MSLP. A combination of MSLP, observed winds and surface air temperature (and precipitation over land in some regions) could be used to carry out an MSLP reanalysis superior to the use of MSLP alone back to say 1871. Whether reconstructions can be done with the help of a simple model to any further advantage is uncertain (J.Shukla, D.Parker and others).

2.3 Radiosonde data

Radiosonde data are being incorporated in the NMC reanalysis but it is still valuable to have an independent data set. A major problem is the inhomogeneity of many of these data, a problem that afflicts current reanalyses. It should be possible to use MSU channels 2R (troposphere) and 4 (lower stratosphere) to help homogenise radiosonde temperatures from 1979 onwards. EOFs based on reanalyses could be used to interpolate global temperature anomaly fields at specific levels of the atmosphere. (D.Parker).

2.4 Reanalyses

The NMC reanalysis is now under way and will extend back to 1957 and possibly 1946. It will may be repeated in a few years time. (R.Livezey, and E.Kalnay, personal communication). It was noted that the recent Naval Research Laboratory (NRL) reanalysis was not greatly affected by their poorer SST input (L.Gates).

3. Model simulations

3.1 Experimental design

If a model is forced with observed SST, do we really expect it to reproduce the correct SST-atmosphere relationships since the atmosphere is unable to simultaneously influence the SST? Thus in the extratropics, the real atmosphere may for a while favour a particular weather pattern. Underlying SST will then react to this change. Due to model internal atmospheric variability, a change may initially happen in the model atmosphere but the SST cannot not react (in any direct way). This problem could be acute if significant positive or negative feedbacks exist between an initial internal atmospheric perturbation and the underlying SST (D.Karoly). Could this affect the spectrum of modelled atmospheric variability?

We also need larger ensembles (J.Shukla). There should be a range of input SSTs applied to ensembles of simulations for given periods, to represent, and enable an assessment of the effects of, uncertainties in SST (K.Miyakoda, T.Palmer). In this context, the new NMC EOF interpolated data set now becoming available (R.Livezey, personal communication) from 1950 would complement GISST.

Simulations with SST anomalies limited to particular regions are needed in order to disentangle the complex influences of SST on atmospheric circulation. An example is SST in the Newfoundland area and its effects on European winter climate (T.Palmer).

Limited area nested high resolution models are useful for more detailed investigations of climate variability and its mechanisms. Such a model is being used over North Africa in summer by C.Thorncroft and D.Rowell to investigate how easterly waves modulate regional rainfall, and how they interact with the large scale circulation.

3.2 Shortcomings of models

The formulation of mountains, which is more difficult in spectral models, is crucial for the Indian Monsoon and affects the Southern Oscillation. The effects of mountains on

other aspects of global circulation and climate was questioned (K.Miyakoda).

The vertical profile of (latent) heating in the tropical Pacific may be inadequately calculated, degrading models' ability to simulate the amplitude and phase of the long waves, and blocking, in the extratropics (J.Shukla).

Better specification of land surface hydrology, especially soil moisture, and its interaction with the atmosphere, may enhance prediction skill. (J.Shukla, F.Zwiers).

3.3 Treatment of El Nino-Southern Oscillation (ENSO)

A. Bevan and Sugi both showed good simulated extratropical response to ENSO. However the response of the UK Met Office model (A.Bevan) to ENSO seems very linear - is this correct? (R.Livezey). However the real atmospheric response to ENSO might be more linear than current observations suggest, due to a bias in the frequency of warm events rather than cold events (M.Hoerling).

For assessing ENSO effects in northern winter, January to March is a better choice than December to February. February appears to show the highest predictability over North America so some of the ENSO interactions may be modulated on a calendar monthly time scale. Forcing from tropical features other than ENSO should not be ignored (R.Livezey).

Inter-decadal ENSO-related and/or interhemispheric variations of temperature, precipitation and atmospheric circulation were simulated with some success by a CSIRO model using MOHSST (as opposed to GISST) data (I.Smith). However the model did not succeed in reproducing recent changes in atmospheric circulation over the North Pacific and North Atlantic.

An apparent positive bias in models' Southern Oscillation Index (SOI) (Tahiti minus Darwin MSLP) in 1982-1987 does not necessarily indicate erroneous MSLP or input SST data. The atmosphere around Tahiti and/or Darwin may be responding to sub-regional or local forcings which in the models are overwhelmed by the ENSO SST forcing. The tropic-wide state of the atmosphere should be assessed in both observations and models using indices which are less affected by local features, eg a Southern Oscillation MSLP EOF, or perhaps a combined index of N.Ward et al's tropic-wide mode incorporating aspects of regional MSLP and rainfall. Sir Gilbert Walker's original Southern Oscillation Index was of this latter type. SSTs in the subtropical northwest Pacific, which are part of the El Nino / La Nina pattern, appear to modulate the latitude of the ITCZ over Indonesia in northern spring. This may be a key part of the link between El Nino / La Nina and the large-scale Asian summer monsoon (J.Slingo).

3.4 Assessment of predictability and skill

We need to investigate how SST anomalies affect the probability of low frequency weather types e.g. via changes in the frequency distribution of the coefficients of atmospheric EOFs representing such types (C.Folland). The probabilistic nature of climate predictions places upper bounds on skill. Random internal variability can at any time overwhelm the SST signal (M.Hoerling, D.Rowell, J.Davies).

Successful prediction of mid-latitude seasonal atmospheric anomalies will not be possible routinely; but if we have an accurate prediction of tropical SST anomalies and if these have large amplitude and the model is good, then reliable seasonal forecasts over North America are possible for some seasons in some years (J.Shukla). Simulation skill has been limited to the Pacific-North America (PNA) sector, January to May, and major ENSO events; but both observations and simulations show traces of a Tropics-Northern Hemisphere (TNH) pattern right through the summer, so predictability even then may not be zero (R.Livezey).

Indian monsoon rainfall is probably less predictable in principal than eg. N.E.Brazil because the latter is more clearly dominated by SST anomalies (A.Hense, M.Sugi, J.Shukla).

To obtain good skill we need both a correct response to local SST and realistic large scale atmospheric teleconnections (N.Ward, M.Hoerling). Importantly, predictability may be very sensitive to small changes in model code, particularly convection as was demonstrated by M.Hoerling for the MFR8 and MRF9 models in the PNA region. Predictability appeared better when resolution was degraded to T5, neatly fulfilling the expectation that the effects of chaos are larger at smaller space scales (F.Zwiers).

It is useful to show a relatively complete statistical model of the response for a given variable. F.Zwiers used the following breakdown of Canadian Climate Centre model response (run in ensemble mode) using an ANOVA model:

$$y_{i,j,t} = \mu + \alpha_i + \beta_j + \alpha\beta_{ij} + \epsilon_{i,j,t}$$

where i,j,t denote ith run, jth year, and time within a season; μ is the mean; α_i is the signal of initial atmospheric conditions, machine precision, etc in the ith run; β_j is the signal from interannual variability common to all i runs and ascribable to forcing such as SST; $\alpha\beta_{ij}$ represents the interaction between α_i and β_j i.e. mainly between the initial conditions and the forcing; $\epsilon_{i,j,t}$ is weather noise. α_i was shown to change through using a different computer for one run, and $\alpha\beta_{ij}$ was shown to have a small effect on 850HPa temperature over land, perhaps due to long time scales of soil wetness anomalies. However, both these terms are generally negligible, in which case the model reduces to that employed by D.Rowell and which was used for the diagnostic intercomparison.

3.5 Climate change detection (and attribution)

An approach to climate change detection discussed at the workshop that is being tried experimentally by the Hadley Centre is to force a model with GISST with and without increasing greenhouse gases and then add changing aerosol forcing etc. This is being done in ensemble mode. J.Shukla pointed out that if forcing a model with observed SST only yields land surface air temperature anomaly patterns which agree with those observed, then it will be difficult to detect the influence of increasing greenhouse gases, etc. The meeting considered though that the observed rise in land surface air temperature anomalies since 1950 was not fully simulated by the several models tested. So scope remains for adding increasing CO_2 etc to the simulations to improve the land surface air temperature response, thereby contributing towards climate change detection. Recent results from one of the Hadley Centre models appear to confirm this supposition.

However, a full geographical analysis of temperature at the surface and in the upper air is needed; detection requires the addition of the influences of time-varying man-made and probably volcanic aerosols.

3.6 Relationship with other projects

The GISST data set is being used within the DICE project by the Hadley Centre. A. Navarra and N.Ward may wish to use a version of GISST with the ECHAM model in long integrations.

L.Gates agreed that an opportunity for further discussion of the GISST data set and GISST-based simulations could be at the AMIP Conference to be held in Monterey, California in May 1995. A 2.25 hour session is being organised with some financial support from PCMDI.

Finally C.Folland advertised another opportunity for presenting C20C/GISST results at the IUGG Conference, Boulder, in early July 1995 where he is co-convening a session on The Industrial Period: Causes and Character in a Symposium called Climatic Variability and Forcing over the last Millennium. Since the workshop, there has been a good response from workshop attendees, and many other scientists.

4. Future Directions

Intercomparison of future diagnostics from the GISST-based Climate of the 20th Century Project will benefit if diagnostics are agreed and organized, output is systematically archived and documented, and results are carefully published (L.Gates in his reflections on AMIP). AMIP itself is expected to be extended to 1993 or later, the models being rerun with a revised SST and sea ice data set.

C.Folland said that he hoped to release a new EOF version of GISST (GISST2.2) from 1946 to 1994 in early spring 1995 that would also incorporate a new analysis of the underlying ship reports, improved Arctic sea ice extent data supplied by J.Walsh, and a new 1961-1990 climatology. Release is now not expected until June 1995, but GISST2.2 will be made available back much further, to 1903. A further release of GISST, for 1871-1995, is planned in 1996.

D.E.Parker, C.K.Folland and D.P.Rowell

Intercomparison Diagnostics

1) Climatologies and ENSO Teleconnections

Global maps for the seasonal means MAM, JJA, SON and DJF:

PMSL - Ensemble mean (1951-80)
PMSL - Standard deviation (using individual runs, and years 1951-80)
Rainfall - Ensemble mean (1951-80)
Rainfall - Standard deviation (using individual runs, and years 1951-80)
500hPa Height - Ensemble mean (1951-80)
500hPa Height - Standard deviation (using individual runs, and years 1951-80)

Global maps of correlation coefficients between Nino 3 (5°N-5°S, 90-150°W) SST anomaly and 700, 300hPa height anomaly for each of the four seasons. The length of each time-series of height data would be multiplied by the number of runs available, with the SST time-series repeated to attain the same length.

2) SST-Forced Variability versus Internal Variability

Global maps of the percentage of variance explained by SSTs, using seasonal means for MAM, JJA, SON, and DJF:

PMSL - Calculated using individual seasons
PMSL - Calculated using 5-year running means
PMSL - Calculated using 10-year running means
Rainfall - Calculated using individual seasons
Rainfall - Calculated using 5-year running means
Rainfall - Calculated using 10-year running means

3) Time-Series

Graphs of the following diagnostics, plotting a separate line/bar for each run. Also for each graph, the percentage of variance explained by SSTs.

SOI - Tahiti minus Darwin PMSL, normalised wrt 1951-80. 5-month running mean. Line graph, 1949-90.
Global annual mean land surface temperature, time series for 1949-93. Plus linear trend. Plus low pass filtered (> 10 years) time series of same data.
Rainfall. Anomaly bar graphs, wrt 1951-80 average. Area averages for:

- Sahel (approx. 12.5-17.5°N, 15°W-37.5°E), JAS means. Plus linear trend. Plus low pass filtered (> 10 years) time series of same data.
- India (using approx. national boundary), JJAS means.
- N.E.Brazil (the smaller area in Fig.1 of Ward and Folland, 1991, IJC, p712), FMAM means.
- Queensland (land points north of 30°S, east of 135°E), Annual means.
- North and South Queensland (as Queensland, but split at 25°S).
- High latitude precipitation linear trend and low pass filtered (> 10 years) time series. ONDJFM and DJF means, for all American and Eurasian (but not UK) land points north of 55°N.

NAO. Ponta Delgada (Azores) minus Stykkisholmur (Iceland) PMSL, normalised wrt 1951-80. Separate anomaly bar graphs for each season (MAM, JJA, SON, DJF), wrt 1951-80 average.
N Hemisphere Blocking. Frequency of blocked events at each longitude, for each of the decades 1951-60, 1961-70, 1971-80, 1981-90, and each season (MAM, JJA, SON and DJF) [using the index of Tibaldi and Molteni (1990, Tellus, 42A, 343-365)]. Separate graphs for each decade and each season.

A Methodology for Using an Ensemble of Multi-Decadal GCM Simulations to Assess the Percentage Variance Explained by SST Forcing

David P. Rowell

Hadley Centre for Climate Prediction and Research,
Meteorological Office, Bracknell, U.K.

Here we reproduce the statistics required to separate the estimated total variance of simulated rainfall amounts (or any other parameter) (σ^2_{TOT}), into an SST-forced component (σ^2_{SST}) and an internal variability component (σ^2_{INT}). This will prove useful as a general analysis tool for understanding natural climate variability and potential atmospheric predictability on any chosen time or space scale.

We consider a generalised case of N ensembles (years of SST-forcing), each with n members. The simulated rainfall amounts for each experiment are 'modelled' as the sum of two independent components:

$$x_{ij} = \mu_i + \varepsilon_{ij} \qquad (1)$$

where: x_{ij} = simulated rainfall

$i = 1, \ldots N$ is associated with a particular year

$j = 1, \ldots n$ is associated with a particular member of the ensemble

μ_i = component of rainfall due to SST-forcing

ε_{ij} = anomalous rainfall due to internal variability

The approach we use below to estimate the components of variance closely follows an 'Analysis of Variance' methodology, using a so-called 'random-effects' model (see for example, Scheffe, 1959, sect.7.2). The only assumptions required are that the internal variability is the same for each year, and that the effect of altering the initial atmospheric conditions has a purely random impact on the simulated seasonal rainfall anomalies.

First, the internal variability is easily estimated by computing the variance of each datum's deviation from its ensemble mean:

$$\hat{\sigma}^2_{INT} = \frac{1}{N(n-1)} \sum_{i=1}^{N} \sum_{j=1}^{n} (x_{ij} - \bar{x}_i)^2 \qquad (N(n-1) \text{ being the degrees of freedom}) \qquad (2)$$

where $\hat{y}$ denotes an estimate of y, and:

$$\bar{x}_i = \frac{1}{n} \sum_{j=1}^{n} x_{ij} \qquad (\text{the ensemble mean for the } i^{th} \text{ year}) \qquad (3)$$

In order to estimate the variability due to SST forcing, we must first estimate the variance of the ensemble means:

$$\hat{\sigma}^2_{EM} = \frac{1}{N-1} \sum_{i=1}^{N} (\bar{x}_i - \bar{\bar{x}})^2 \qquad (N-1 \text{ being the degrees of freedom}) \qquad (4)$$

where:

$$\bar{\bar{x}} = \frac{1}{nN} \sum_{i=1}^{N} \sum_{j=1}^{n} x_{ij} \qquad (\text{the mean of all data}) \qquad (5)$$

Now, using a standard result from 'Analysis of Variance', we can also express σ^2_{EM} in terms of σ^2_{INT} and σ^2_{SST} (eg. Scheffe, p226):

$$\sigma^2_{EM} = \sigma^2_{SST} + \frac{1}{n}\sigma^2_{INT} \tag{6}$$

This essentially states that the variance of the ensemble means is a *biased* estimate of the variance due to SST forcing. This is because with finite 'n' each ensemble mean ($\bar{x}_i$) still contains an element of internal variability (each ensemble mean is only an *estimate* of μ_i, not equal to μ_i), so that $\hat{\sigma}^2_{EM}$ overestimates σ^2_{SST}.

Thus from equations (6), (4) and (2), the variance due to SST-forcing may be estimated as:

$$\begin{aligned}\hat{\sigma}^2_{SST} &= \hat{\sigma}^2_{EM} - \frac{1}{n}\hat{\sigma}^2_{INT} \\ &= \frac{1}{N-1}\sum_{i=1}^{N}(\bar{x}_i - \bar{\bar{x}})^2 - \frac{1}{Nn(n-1)}\sum_{i=1}^{N}\sum_{j=1}^{n}(x_{ij} - \bar{x}_i)^2\end{aligned} \tag{7}$$

[see note(i)].

This then leads to an estimate of the total variance:

$$\hat{\sigma}^2_{TOT} = \hat{\sigma}^2_{INT} + \hat{\sigma}^2_{SST} \tag{8}$$

[see note(ii)],

and finally, the ratios of components of variance:

$$\frac{\hat{\sigma}^2_{SST}}{\hat{\sigma}^2_{TOT}} \quad \text{and} \quad \frac{\hat{\sigma}^2_{INT}}{\hat{\sigma}^2_{TOT}} \tag{9}$$

Notes:

(i) Because of the subtracted term in equation (7), the *distribution* of $\hat{\sigma}^2_{SST}$ includes a few negative values, which are sometimes produced by chance. However, this is only likely when n and N are small *and* when $\sigma^2_{SST} / \sigma^2_{TOT}$ is small. Such negative values are best reset to zero.

(ii) It is perhaps tempting to estimate σ^2_{TOT} as: $\frac{1}{Nn-1}\sum_{i=1}^{N}\sum_{j=1}^{n}(x_{ij} - \bar{\bar{x}})^2$. However, this is a *biased* estimate, because it fails to account for the impact that the make-up of the data has on the number of degrees of freedom, ie. that the data has *two* components of variability. The total variance is correctly estimated only by the *sum* of its two components (equation 8).

Reference:

Scheffe, H., 1959: The analysis of variance. John Wiley and Sons, New York, 477pp.

Formal publication:

This work is extracted from:

Rowell, D.P., Folland, C.K., Maskell, K. and Ward, M.N., 1995: Variability of summer rainfall over Tropical North Africa (1906-92): observations and modelling. Q. J. R. Meteorol. Soc., 121, 669-704.

Further applications of the methodology, and publications thereof, will follow.

AGCM Intercomparison Diagnostics : Climatologies and ENSO Teleconnections (1951-80)

Working Group : Dr C.S. Frederiksen (leader), Miss A. Bevan, Dr A. Navarra, Dr M. Hoerling, Prof K. Miyakoda, and Dr M.N. Ward

1. Introduction

The task of this working group was to evaluate the climatologies and ENSO teleconnections of a number of atmospheric general circulation models (AGCMs) used in multidecadal simulations for periods including 1951-80, and forced with various observed sea surface temperature (SST) datasets including the Hadley Centre's Global Ice and Sea Surface Temperature (GISST) dataset, the UK Met. Office SST (MOHSST) dataset, and the modified Reynolds SST dataset used in the AMIP experiments. Our group had access to results from seven AGCMs including the Hadley Centre (UKMO) UM-Climate 1 grid point model (2.5° lat, 3.75° lon, L19, GISST), the Canadian Climate Centre CCC-GCM2 spectral model (T31, L10, Reynolds), the Australian Bureau of Meteorology Research Centre BMRC v2.1 spectral model (R31, L9, GISST), the Centre for Ocean-Land-Atmosphere Studies COLA spectral model (T30, L18, GISST), the Japan Meteorological Agency JMA-GSM89 spectral model (T42, L21, MOHSST), the Geophysical Fluid Dynamical Laboratory GFDL spectral model (T30, L18, GISST), and the Max-Planck Institute's ECHAM3 spectral model (T21, L19, GISST) (see references below for description of models).

For each season March-May (MAM), June-August (JJA), September-November (SON) and December-February (DJF), we considered model ensemble means and standard deviations, with respect to the period 1951-80, of global MSLP, precipitation and 500hPa geopotential heights, and correlations between NINO3 (5°N - 5°S, 90-150°W) SST anomaly and 700hPa and 300hPa height anomalies. These were compared with a similar set of diagnostics derived from observations. Not all modelling groups provided a complete set of diagnostics, at the time of the meeting, and in some cases the simulations covered a shorter period such as, for example, the AMIP period. For some diagnostics, there were no directly comparable observational results. Below, we consider each of the diagnostics in turn, with particular emphasis on JJA and DJF, and show various results from a selection of the models.

2. MSLP

The models all capture reasonably well the observed global distribution of MSLP in each of the four seasons. Figure 1 shows (a) the observed DJF MSLP climatology, and the same field as simulated by (b) the BMRC, (c) the UKMO, and (d) the JMA models. Generally, all the models were able to capture salient features of the observed distribution, at least qualitatively. Thus, for example, in the Northern Hemisphere, the Aleutian low is fairly well simulated with centre in the northern North Pacific near the international dateline between 60°N and 45°N, but, in many cases, displaced further to the east than observed. While

the trough is generally lower in the simulations, all models show a single centre which is elongated in an east-west orientation. The position and magnitude of the Icelandic low is also remarkably well simulated. Similarly, the pattern of subtropical high pressure, in the Northern Hemisphere, is quite well captured by all models. In particular, the Siberian high is quite well simulated, although in some simulations the centre appears south of its observed location, and its strength is underestimated.

Throughout the equatorial region, all models show the observed belt of low pressure. In the Southern Hemisphere, the subtropical highs are correctly positioned to the west of the continents, although in many models the strengths of the highs are overestimated. The low pressure troughs over South Africa, Australia and South America are also reasonably captured by the models, but appear lower than observed in some models. All models generally locate the Antarctic circumpolar trough in approximately the correct position. The strength of the trough varies between the models with most showing lower than the observed pressure.

Figure 2 shows the standard deviation for DJF derived from the observations and the same three models above. Both the observations and the simulations show most variance in the winter hemisphere (i.e. the Northern Hemisphere) with centres of maximum variance east of the dateline and southeast of Greenland, and with comparable magnitudes. Most models locate the centre associated with the Aleutian low slightly east of its observed location. In the Southern Hemisphere, the midlatitude centres in the Indian Ocean and to the southeast of New Zealand are also captured by the models.

Simulations of the MSLP climatology during JJA also reproduce many of the main features seen in the observations (see Figure 3). In particular, the high pressure centres in the North Atlantic and North Pacific occur in approximately correct locations and with about the right strength. The models also reporduce the Northern Hemisphere summer monsoon structure, with a low pressure centre to the northeast of India, and high pressures over the oceans, in most models. In the arctic, some models produce a high pressure zone which is not seen in the observations, and in the Southern Hemisphere the subtropical high pressure systems to the west of the continents are again overestimated. Over southern Australia, the centre of high pressure is higher in most models than observed. The Antarctic circumpolar trough is again a feature of all simulations, although, in some cases, shifted slightly equatorward.

Again, from Figure 4, we see that the largest variance in MSLP during JJA occurs in the winter hemisphere (in this case the Southern Hemisphere). Most models correctly locate the centre of largest variance in the South Pacific, east of the dateline, but at higher latitude and displaced east of the observed maximum. The models generally overestimate the maximum variance. The secondary centre to the southeast of South Africa is less well simulated by the models.

3. Precipitation

This diagnostic shows much greater variability between the models, and between the models and observations. Figure 5 depicts the mean rainfall for 1951-80 for DJF from (a) the Hulme CRU dataset (land only) and (b) the BMRC, (c) the UKMO, and (d) the COLA models. The

group also had access to the Jaeger and Legates and Willmott global rainfall climatologies with which to evaluate the models peformance over the oceans.

Most models capture the rainfall maximum over Northern Australia associated with the Australian monsoon, and the rainfall distribution over this continent is reasonably well simulated with approximately correct strengths. Some models show an artificial maximum over Papua-New Guinea, which appears to be related to topography. Generally, the model rainfall is less reliable in areas of strong orographic features, such as, for example, on the west coast of South America.

While some models do not show all the features of the intertropical convergence zones (ITCZs), many do show qualitatively correct features. Thus, for example, the models simulate intense rainbelts in the equatorial regions, and most models show some evidence of a South Pacific convergence zone (SPCZ). The rainfall maximum over northeast Brazil is not as well simulated, being located generally too far east in the models. The observations show this feature more centrally located over the continent. The precipitation minima to the west of the continents, and the minima over central North America and North Africa, are also simulated in the models to a reasonable extent with approximately correct strengths and location. The rainbelts in the North Pacific, North Atlantic and over Europe, associated with the Northern Hemisphere stormtracks, are also captured, at least qualitatively, in the model simulations.

An indication of the variability of DJF precipitation in the observations and simulations is shown by the plots of the standard deviation in Figure 6. The models correctly simulate large variance in the region of the Australian monsoon, the SPCZ, the Indonesian archipelago and in the western Indian Ocean near Madagascar. Some models, however, show quite large variance over the southern half of Africa which is not evident in the observations.

During JJA (Figures 7 and 8), some models simulate the rainfall distribution over the Indian monsoon region quite well, although some have a tendency for too little rain over western India. In addition, the rainfall maximum over eastern Indian is generally located a little too south in the Bay of Bengal, and the strength of the Indian rainfall varies considerably between models, and between models and observations. The models simulate intense equatorial belts in approximately the right locations over the African continent and central America. The models are also able to simulate the minima over north and south Africa, the Middle East, South America and Australia, and to the west of the North American and South America continents. Some models show a distinct SPCZ while this feature is missing in others. The models all capture the rainfall maximum over the tip of South America.

Consistent with the observations, the models have maxima in rainfall variance over the Indian Monsoon region, throughout the South China Sea, and the the region of the Pacific Ocean ITCZ. Some models, however, show large variance in the west Indian Ocean, northeast of Madagascar, which is not evident in the observations.

4. 500hPa Geopotential Height

Figure 9 shows (a) the observed 500hPa geopotential height DJF climatology based on the

period 1984-1993, (b) a 1979-1988 climatology from the CCC model, and 1951-80 climatologies from (c) the BMRC and (d) JMA models. While it is difficult from these diagrams to quantify similarities and differences between the observations and the model results, there is clearly broad qualitative agreement. In particular, the models capture the Northern Hemisphere wave pattern with ridges and troughs in approximately the correct locations, although the strengths vary between models. The regions of strongest meridional gradient, in the midlatitudes of the west Pacific and west Atlantic, associated with the Northern Hemisphere storm tracks and wind maxima, are also features of the simulations. Again the strengths of these gradients vary between models with some showing much weaker gradients, and hence smaller wind maxima, than observed. The more zonal flow of the Southern Hemisphere circulation during DJF is also evident in the simulations.

The corresponding 500hPa height standard deviations are shown in Figure 10. The models capture quite well the region of maximum variance off the west coast of North America, with location and strength approximately correct. However, the second maximum centred over the UK,is not as well simulated, with some models showing this feature further upstream in the central North Atlantic. The models all show high variance at high latitudes in the Northern Hemisphere, but with varying strengths. In the Southern Hemisphere, the models generally show lower variance than seen in the observations, and most noticeably fail to simulate the region of high variance in the South Pacific centred at (60°S, 130°W). So while the models largely capture the observed pattern, there is room for improvement.

As can be seen from Figure 9 and Figure 11 (for JJA), the models are able to pick up the seasonal cycle in the global circulation, showing in JJA a more zonal flow in the Northern Hemisphere and larger waves in the Southern Hemisphere. In the Northern Hemisphere, the models correctly simulate much weaker meridional gradients in the regions of wind maxima, and position the jetstream in approximately the right location. Similarly, in the Southern Hemisphere, the models show large meridional gradients in the Indian Ocean, associated with the storm track and wind maxima in this region. In the South Pacific, the models are also able to simulate reasonably well the subtropical and polar jetstreams.

The variance of the JJA 500hPa heights (Figure 12) show much more consistency between the models than was evident for DJF. There is also generally good agreement with the observations in both location and relative strengths. As in the observations, the models show largest variance in the winter hemisphere (i.e Southern Hemisphere) with a maximum to the southwest of southern South America. The strength of this feature is approximately correct in most models, but is centred a little upstream in some simulations.

5. ENSO-Related Teleconnections

This diagnostic was the most difficult for the working group to evaluate given the lack of observations with which to compare, and given that the models showed different sensitivities leading to large differences between them. Figure 13 shows for DJF the correlation between NINO3 SSTs and (a) observed MSLP, and 700hPa heights from (b) the BMRC, (c) the UKMO, and (d) the JMA models. Figure 13(a) shows a negative correlation pattern over

the major part of the eastern Pacific with largest magnitude in the Southern Hemisphere. Positive correlations are a feature of the remaining parts of the tropics with highest correlations over the Indonesian archipelago and the south Atlantic Ocean. Correlations at higher latitudes are generally weaker. While this diagnostic was not requested for the Climate of the Twentieth Century workshop, Bengtsson et al. (1994), do provide this diagnostic in an analysis of 5 climate simulations (1979-1992) with the ECHAM3 model, and their simulated results (their Figure 15(a)) concur well with Figure 13(a).

Figures 13(b)-(d) illustrate the large differences, both in the correlation patterns and strength, between the model results for the 700hPa correlations with NINO3 SSTs. However, there are some similarities between the patterns seen in Figures 13(b) and (d), and some of the other model results not shown here. Bengtsson et al. (1994), show the same diagnostic for the 500hPa height and their pattern (their Figure 15(b)) shows a global pattern very like Figure 13(d). Some of the features, seen in Figures 13(b) and (d), also project consistently onto the pattern for the observed MSLP correlations. These figures show generally a pattern of positive correlations throughout the tropical regions. Quite large negative correlations are centred over the southeast of the United States, in the eastern North Pacific, in the central South Pacific, southeast of South America, and South of Australia. There are also large positive correlations over Canada and to the southwest of southern South America. The pattern at 300hPa (not shown) is very similar. As pointed out by Bengtsson et al., such a pattern during an El Niño, would be expected to strengthen the subtropical jetstreams, especially over the western hemisphere, and shift it equatorward. The opposite would happen during a La Niña.

During JJA (Figure 14), there appears to be more consistency between the models in the 700hPa and 300hPa (not shown) correlations patterns. The patterns are broadly similar to those for DJF, but the correlations are much weaker, with maxima being about half those in DJF.

6. Conclusions

While it was dificult for the working group to quantify the success of the seven models in simulating the given set of climatological and ENSO related diagnostics, it was clear that the models showed considerable qualitative success. Generally, the simulated global circulation, its seasonality and variance, agree reasonably well with observations, although the strength and location of some features may vary slightly from the observed, and also between the models. Precipitation, for which there was much more variability between the models and between the models and observations, also showed broad qualitative similarities in its distribution and variance. The ENSO related teleconnections were the most difficult to evaluate due to the lack of comparable observations, and the different model sensitivities, especially during DJF. However, the 700hPa and 300hPa correlation patterns with NINO3 SSTs, simulated in a number of models, were consistent with the observed surface patterns and with expected changes in strength and location of the subtropical jetstreams during El Niño and La Niña phases.

The members of this working group found this intercomparison to be a very useful exercise.

It was felt that, for future similar intercomparisons of multidecadal simulations, it would be useful to standardize the presentation of diagnostics and attempt to quantify differences between model simulations and observations, in a way similar to AMIP. Some recommendations suggested by group members include

(i) the provision of datasets of observed diagnostics from which the modelling groups could generate difference fields, anomaly correlations and RMS errors

(ii) for some diagnostics, such as precipitation, it would be useful to have a map of the global topography used by the various models

(iii) observations should coincide with the model periods

(iv) Hovmöller diagrams would be useful to show the climatological annual cycle of some fields over key centres

(v) some fields, such as the 500hPa height, might more usefully be shown without the zonal component, and eddy maps be presented for intercomparison

(vi) composites of warm and cold events for specified years would be useful to study the simulation of ENSO relationships

(vii) for ENSO related teleconnections, it was suggested that precipitation and 300hPa height should be included in a common analysis

(viii) rather than concentrating, in all diagnostics, on all seasons, DJF and JJA should be the main periods considered. For other individual diagnostics other periods may be more appropriate

(ix) participants should agree on a standard map format and contouring for presentation of results.

References

Bengtsson, L., K. Arpe, E. Roeckner and U. Schulzweida, 1994 : Climate predictability experiments with a general circulation model. *Max-Planck Institut fuer Meteorologie.,* Report **145**, 45pp.

Cullen, M.I.P., 1993 : The Unified Forecast/Climate Model. *Meteor. Mag.*, **122**, 81-94.

Fennessy, M.J., et al., 1994 : The simulated Indian monsoon : A sensitivity study. *J. Climate,* **7**, 33-43.

McAvaney, B.J., J.R. Fraser, T.L. Hart, L.J. Rikus, W.P. Bourke, M.J. Naughton and P. Mullenmeister, 1991 : Cirulation statistics from a non-diurnal seasonal simulation with the BMRC atmospheric GCM:R21L9. *BMRC Research Report*, **29**, available from Aust. Bur. Met., 231pp.

McFarlane, N.A., G.J. Boer, J.-P. Blanchet and Lazare, 1992 : The Canadian Climate Centre Second Generation General Circulation Model and its Equilibrium Climate. *J. Climate,* **5**, 1013-1044.

Roeckner, E., K. Arpe, L. Bengtsson, S. Brinkop, L. Duemenil, M. Esch, E. Kirk, F. Lunkeit, M. Ponater, B. Rockel, R. Sausen, U. Schlese, S. Schubert, and M. Windelband, 1992 : Simulation of the present-day climate with the ECHAM model : Impact of model physics and resolution. *Max-Planck Institut fuer Meteorologie.,* Report **93**, 171pp.

Stern, W.F., K. Miyakoda and J. Anderson, 1995 : Forcing the GFDL model with GISST. (This volume.)

Sugi, M., K. Kuma, K. Tada, K. Tamiya, N. Hasegawa, T. Iwasaki, S. Yamada and T. Kitade, 1990 : Description and performance of the JMA operational global spectral model (JMA-GSM88). *Geophys. Mag.,* **43**, 105-130.

(a)

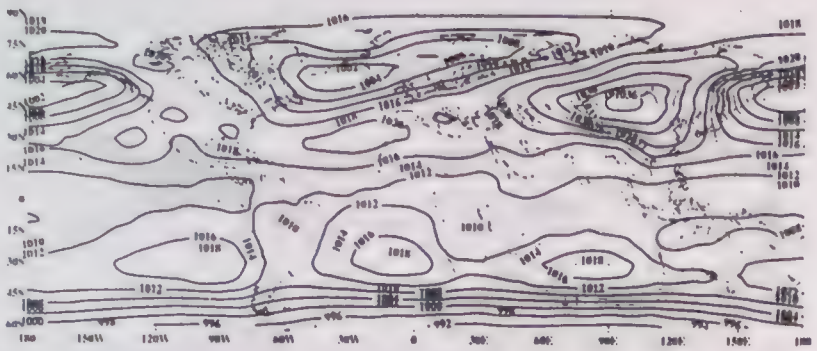

(b)

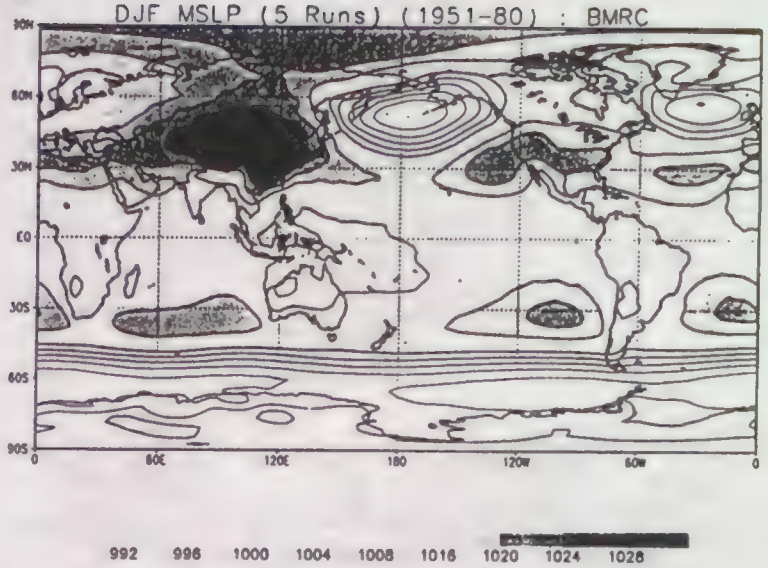

(c)

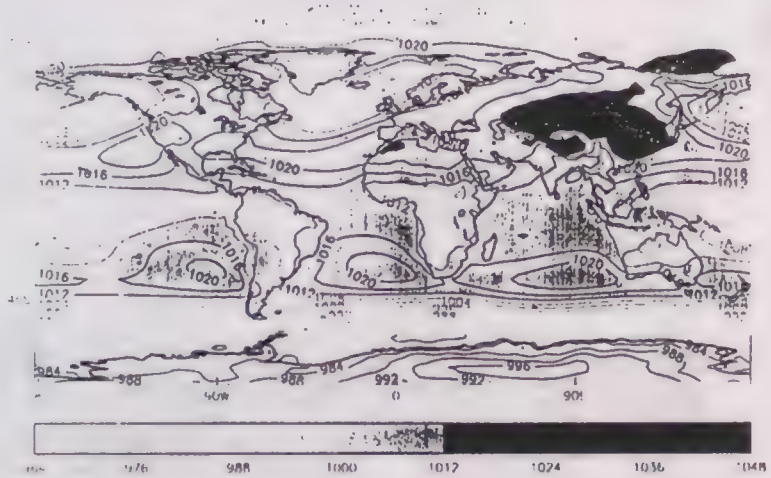

(d)

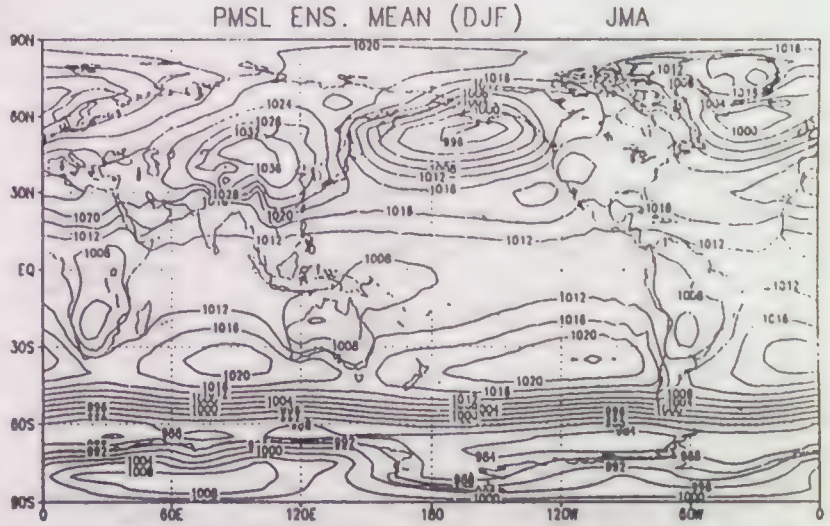

Figure 1

(a)

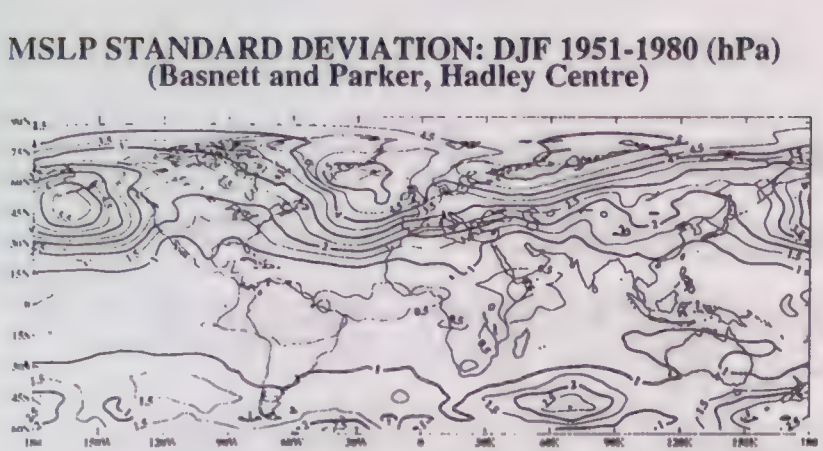

(b)

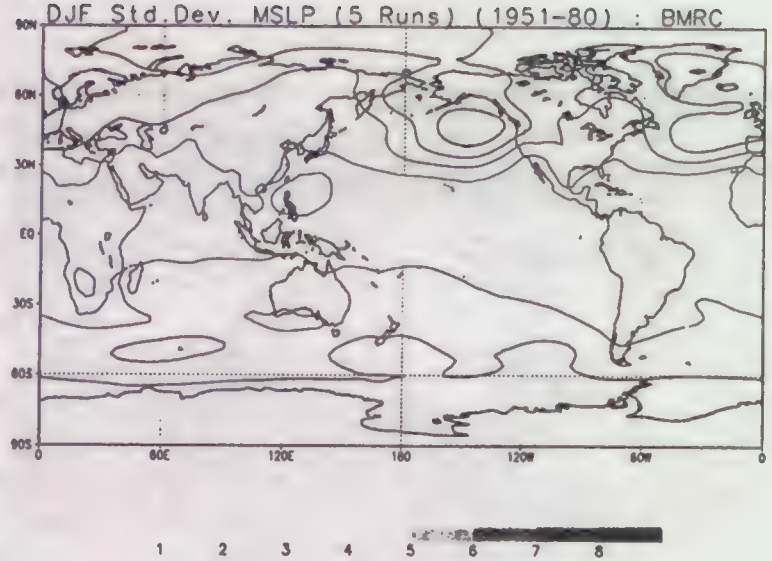

(c)

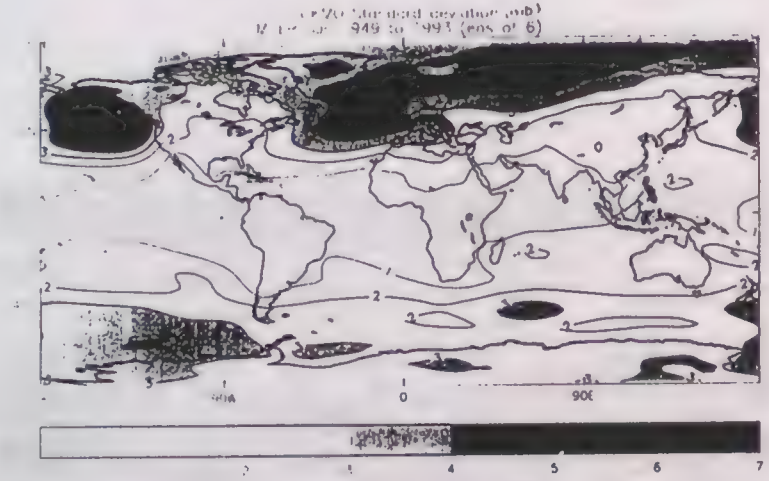

(d)

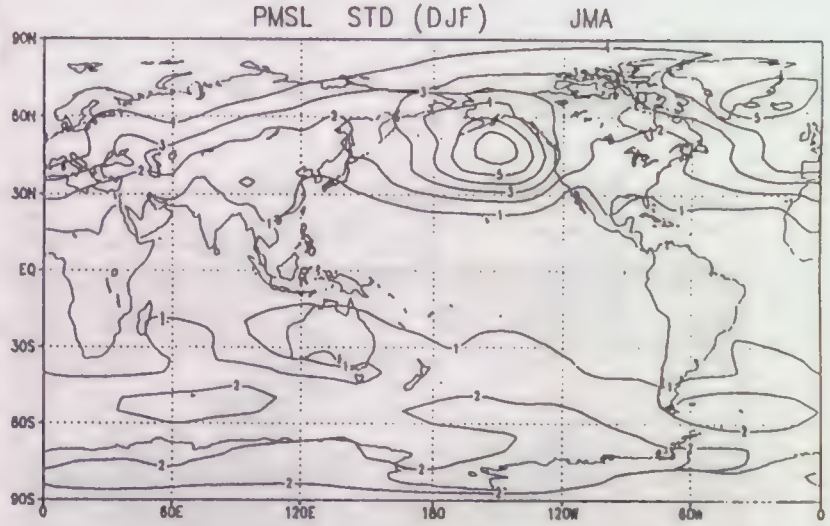

Figure 2

(a)

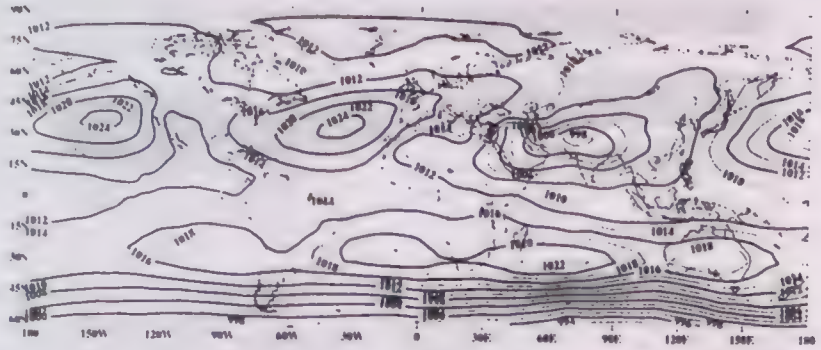

(b)

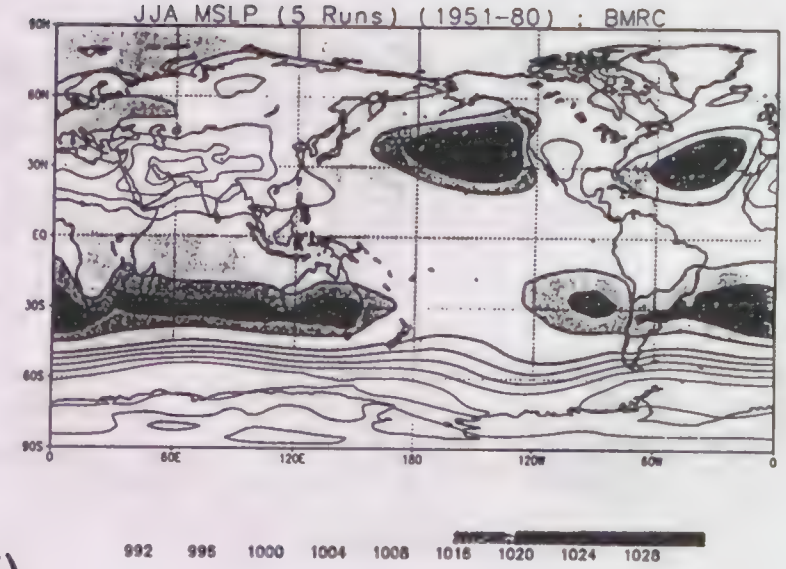

(c)

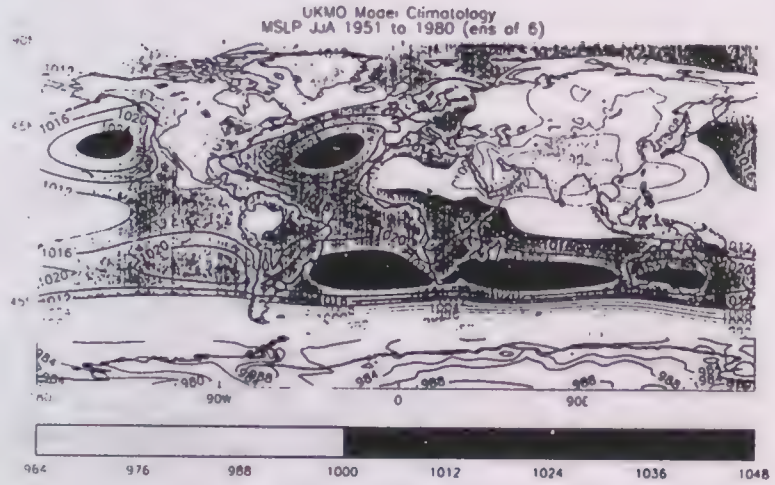

(d)

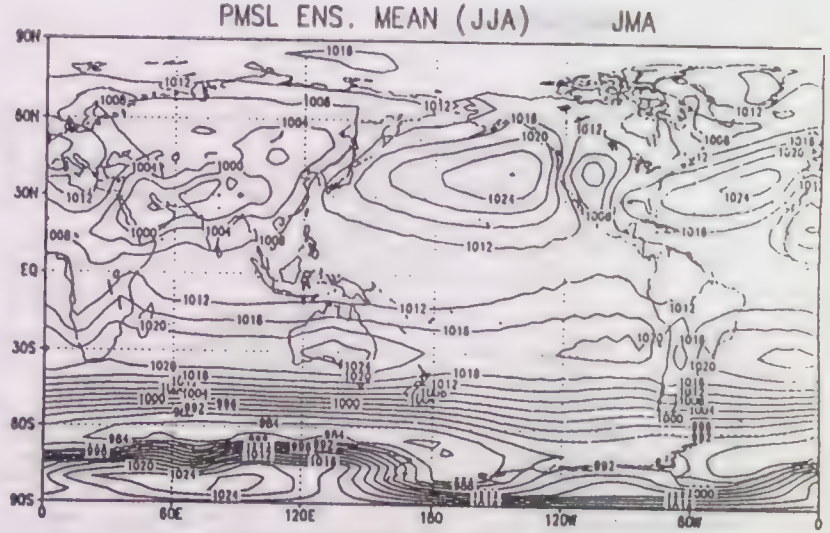

Figure 3

(a)

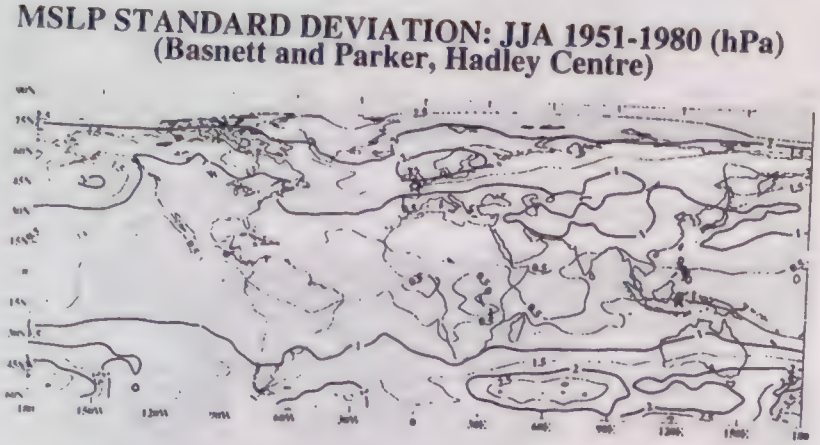

(b)

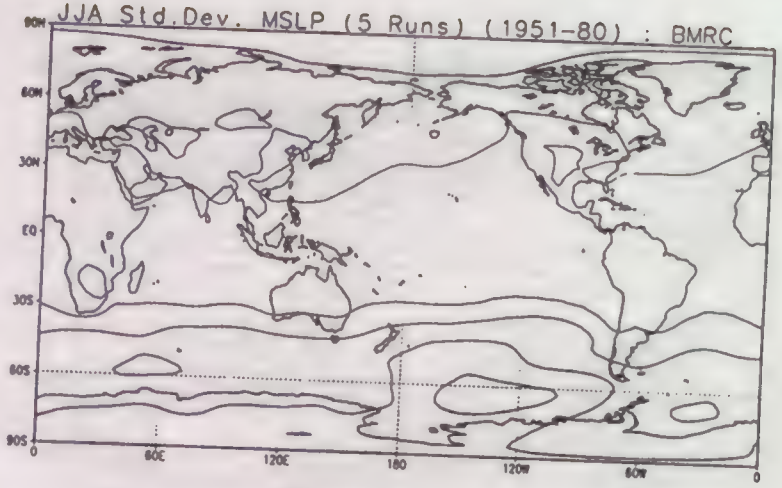

(c)

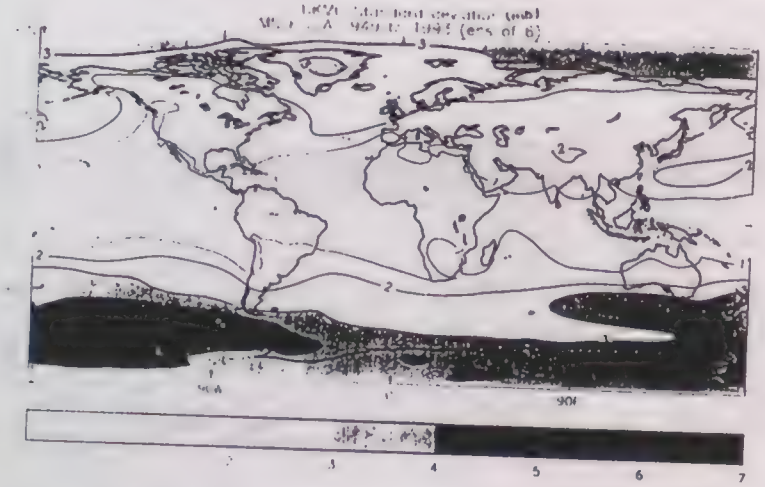

(d)

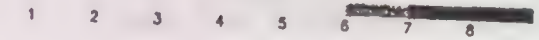

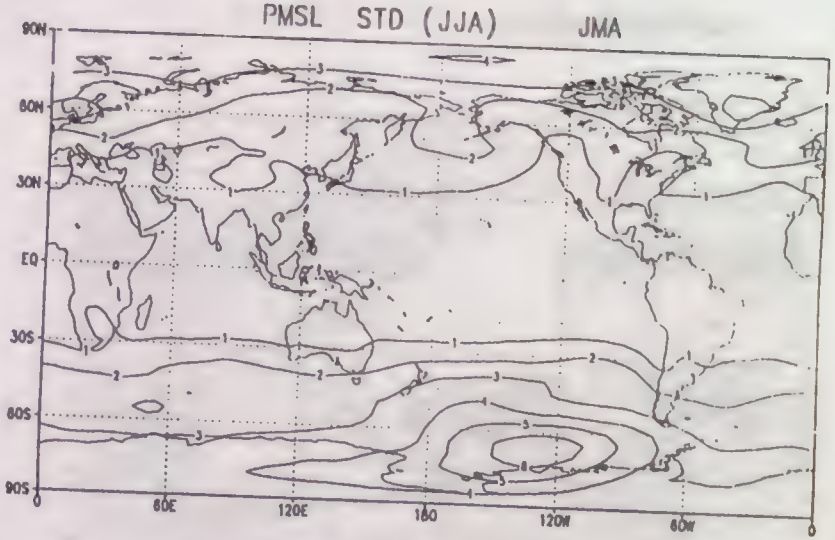

Figure 4

(a)

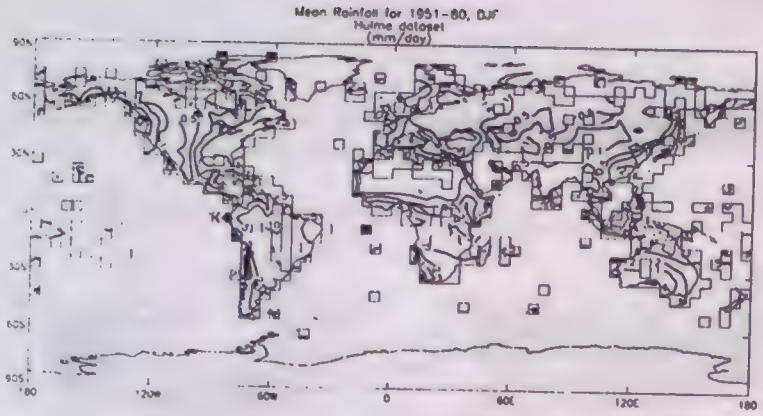

(b)

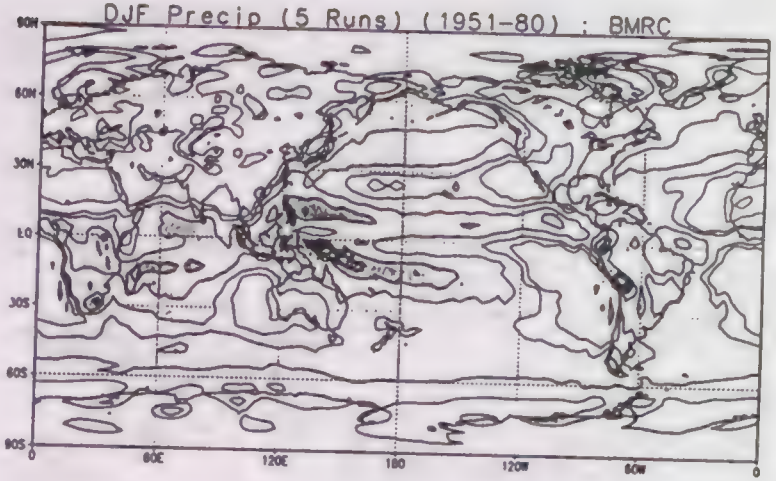

(c)

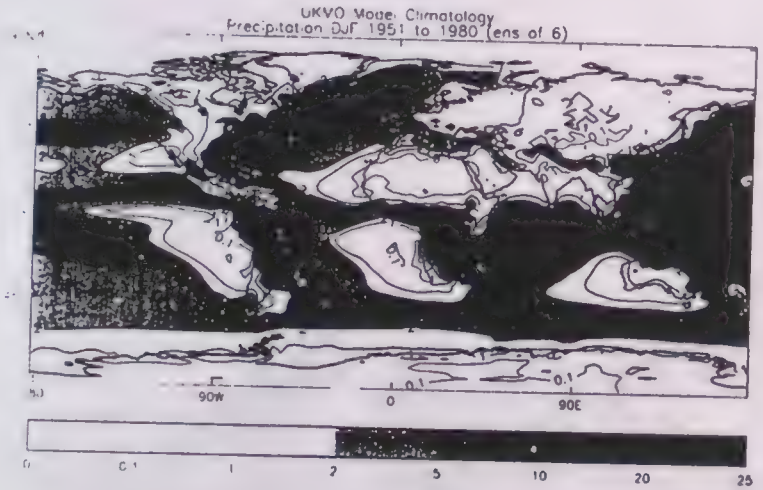

(d)

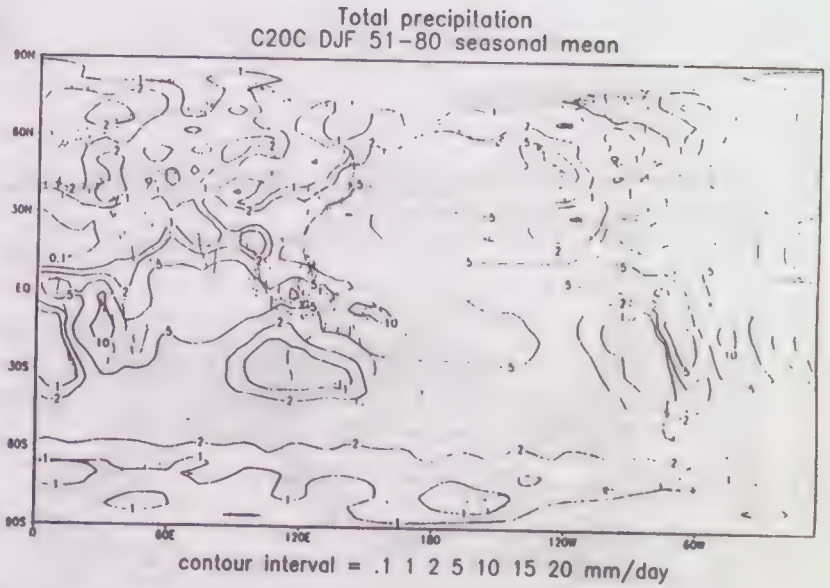

Figure 5

(a)

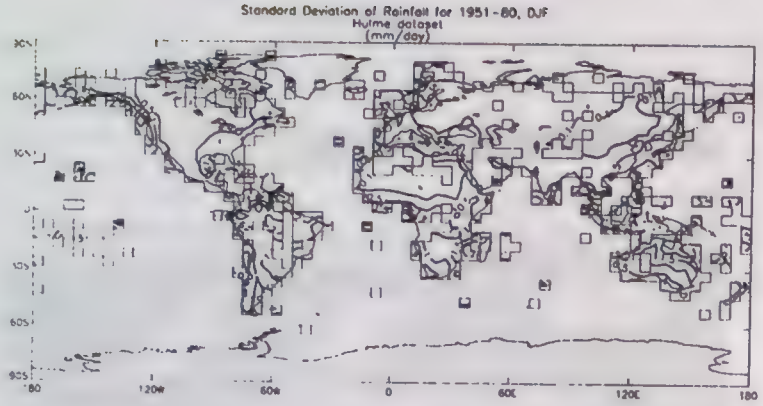

(b)

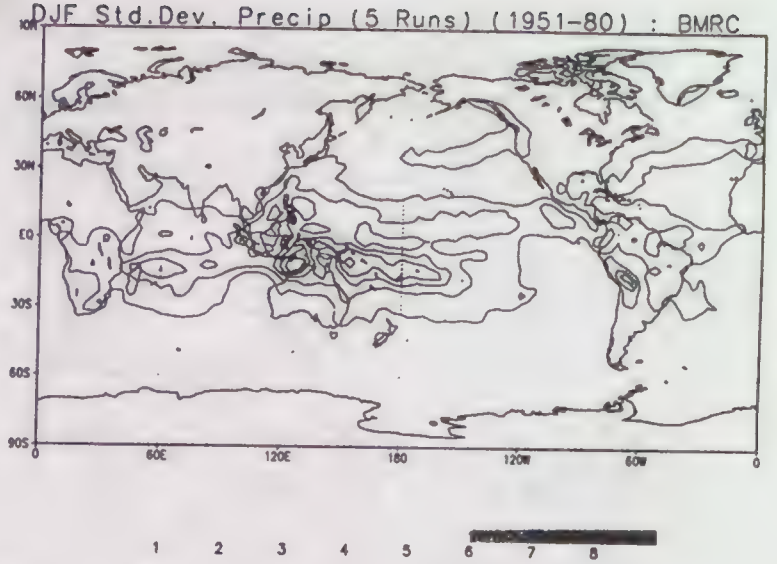

(c)

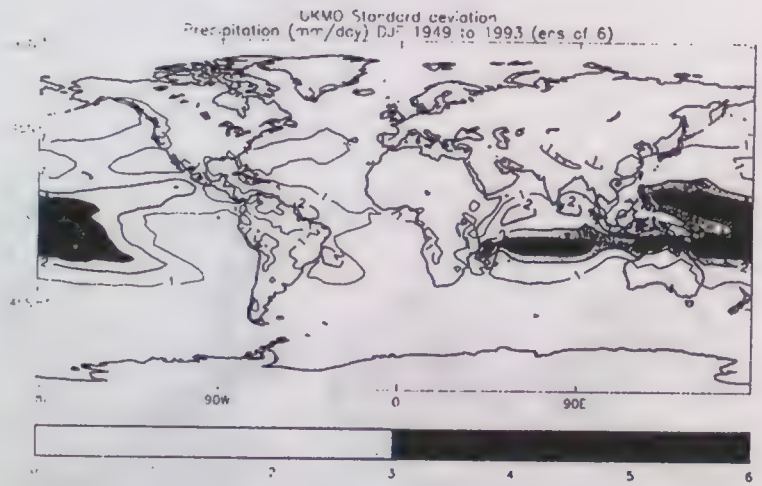

(d),

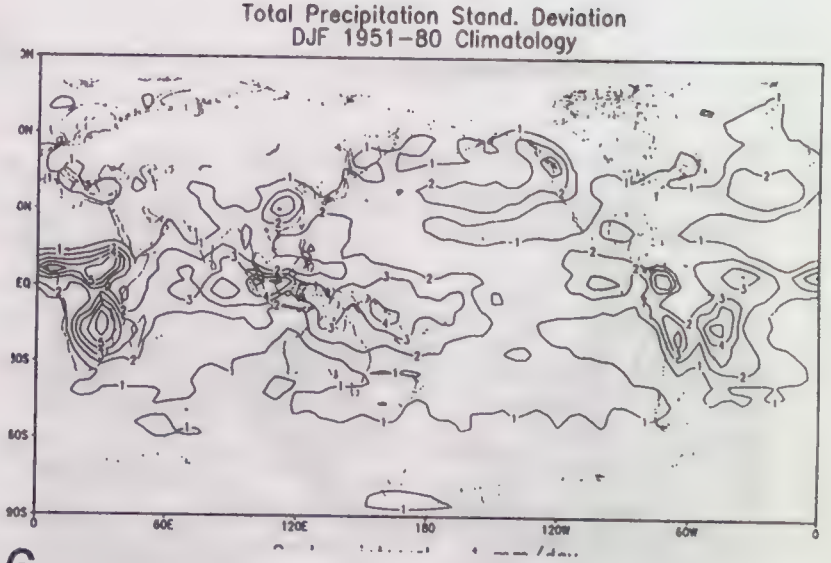

Figure 6

(a)

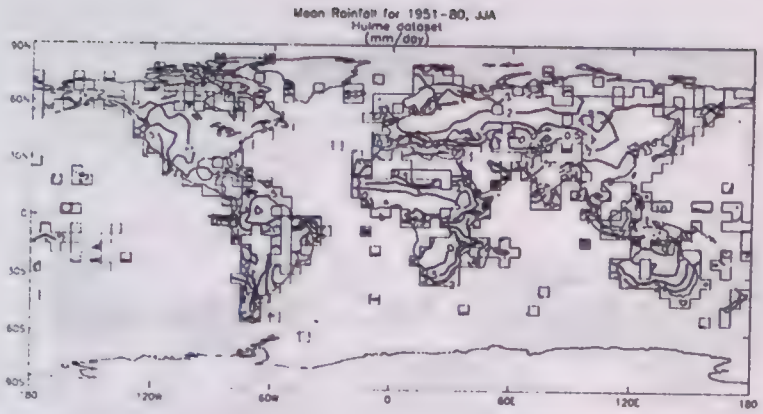

(b)

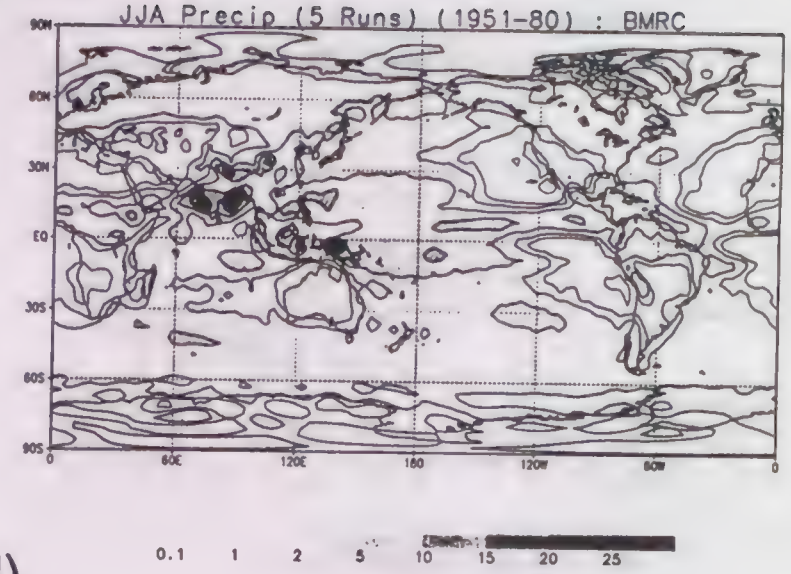

(c)

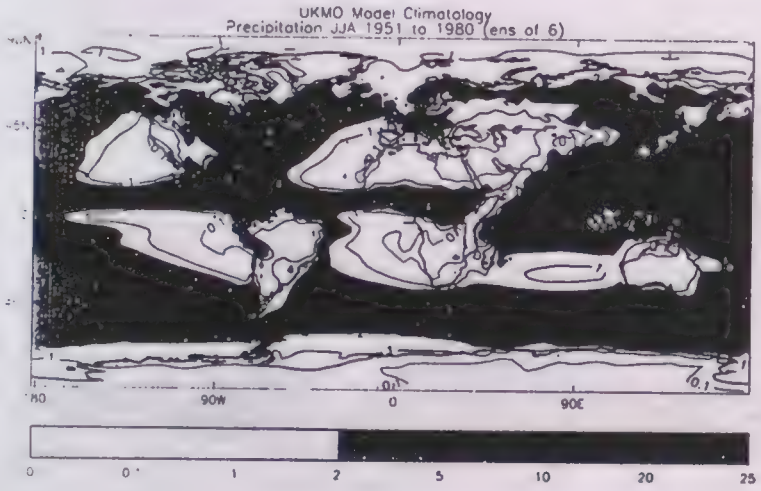

(d)

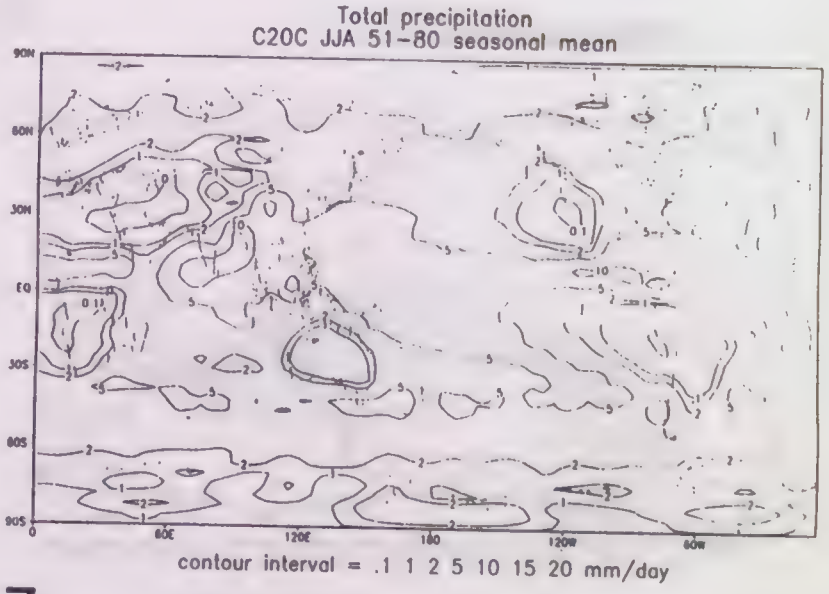

Figure 7

(a)

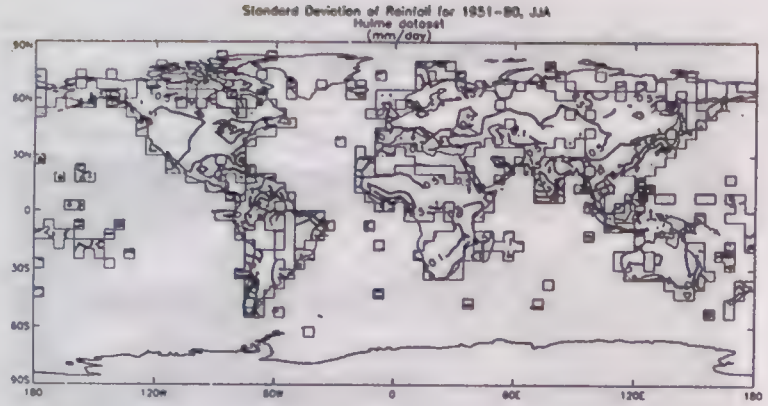

(b)

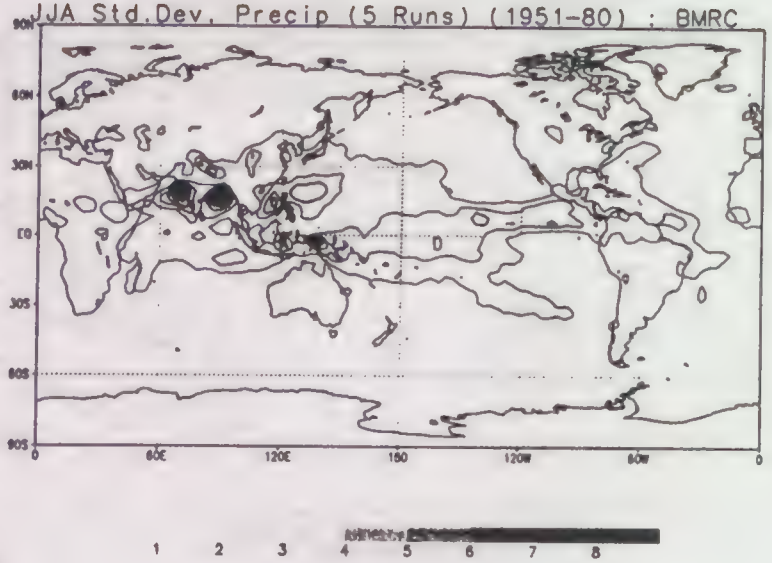

(c)

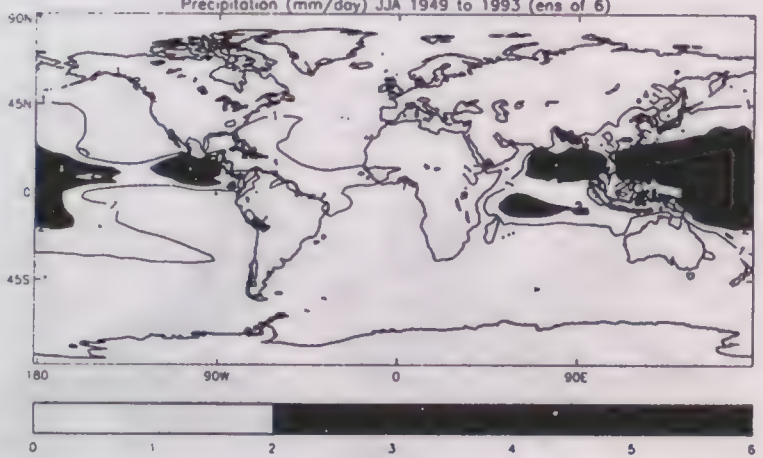

(d)

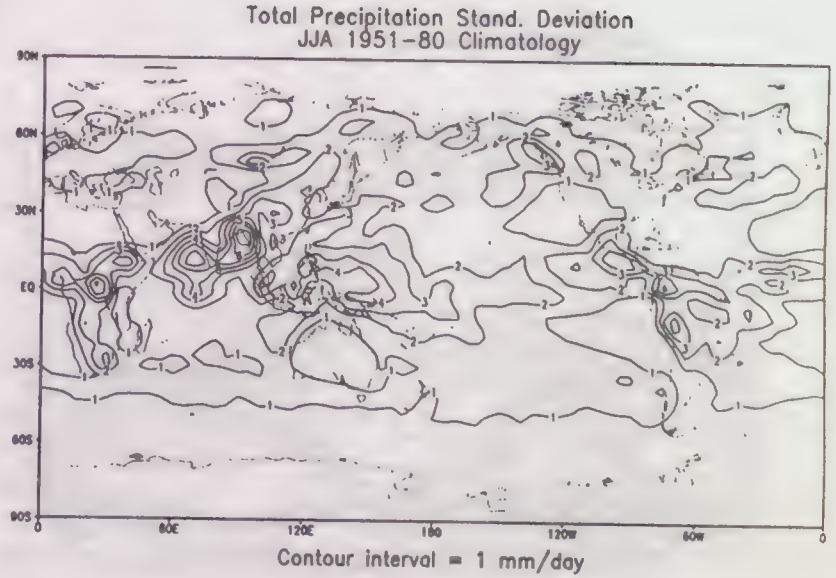

Figure 8

(a)

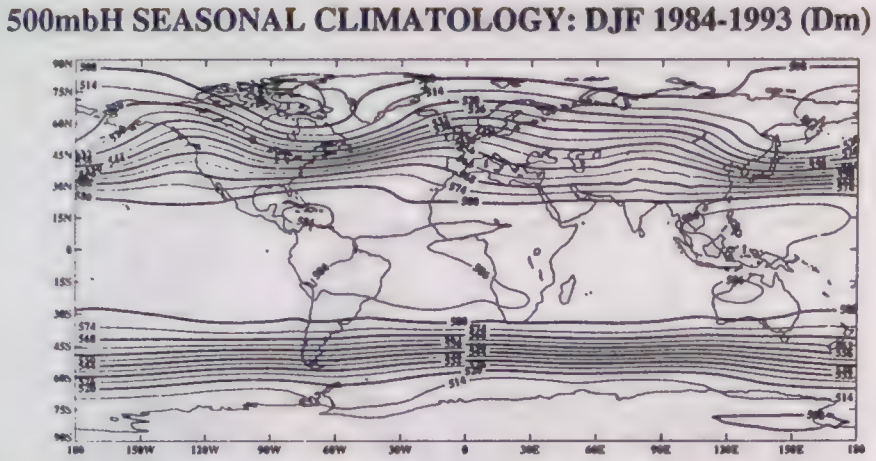

(b)

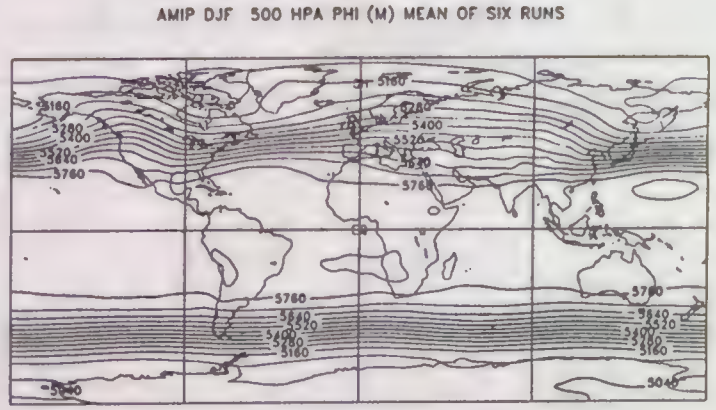

(c)

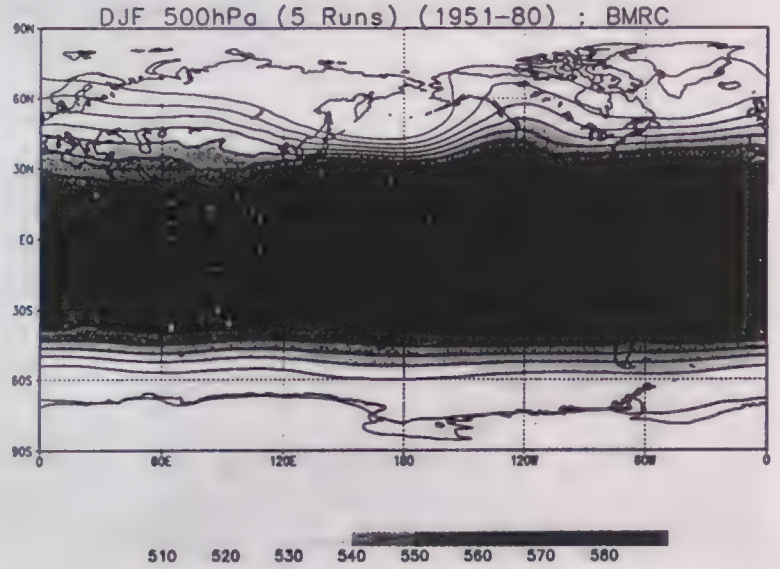

(d)

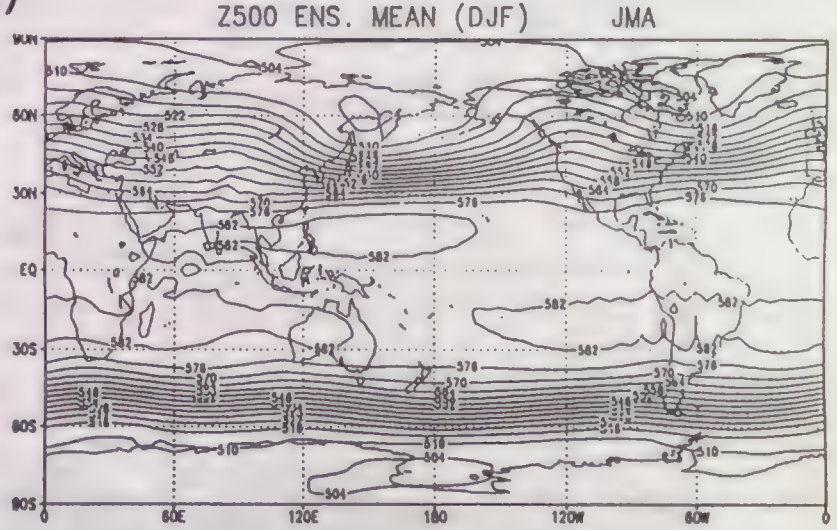

Figure 9

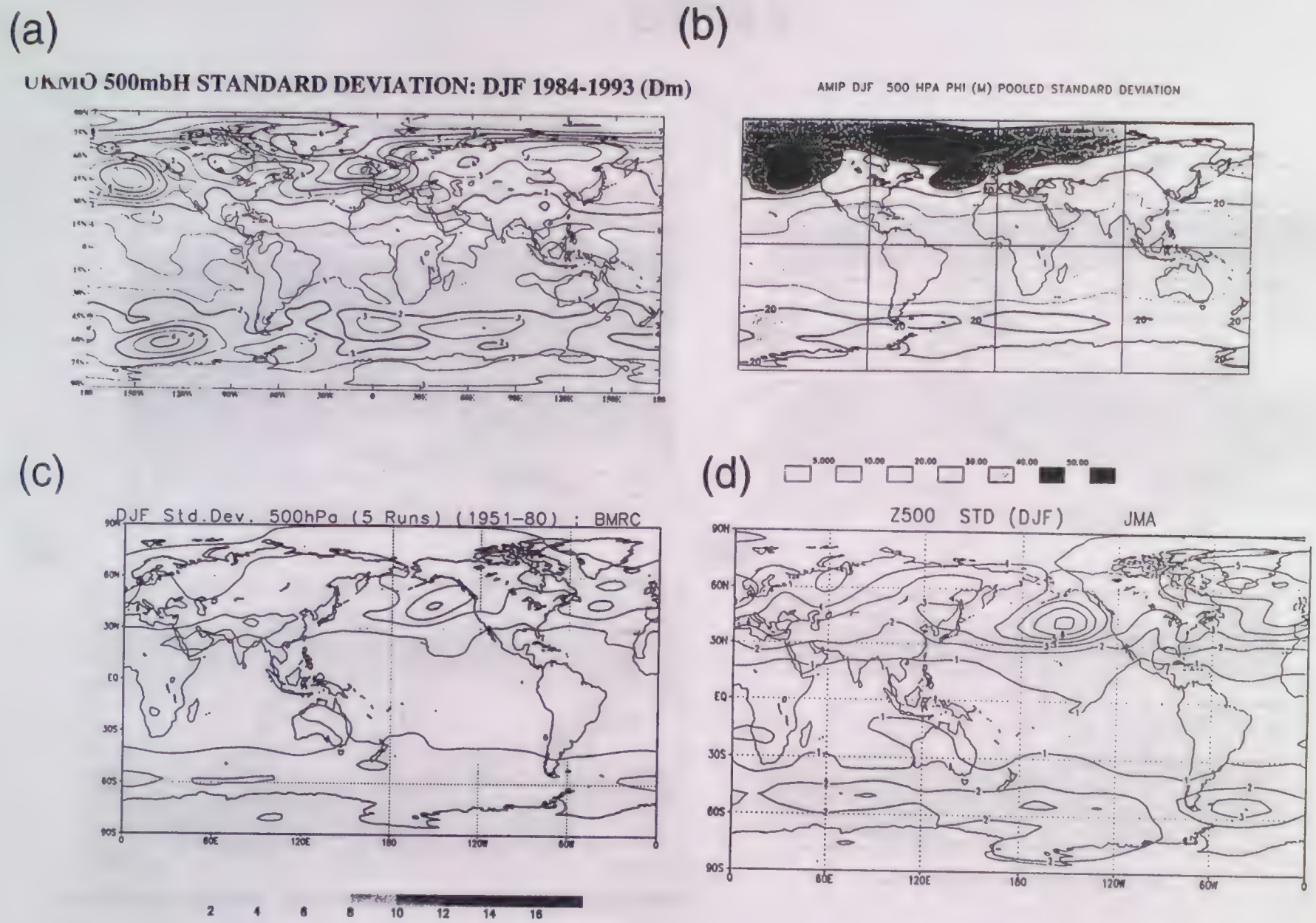
(a)
UKMO 500mbH STANDARD DEVIATION: DJF 1984-1993 (Dm)
(b)
AMIP DJF 500 HPA PHI (M) POOLED STANDARD DEVIATION
(c)
DJF Std.Dev. 500hPa (5 Runs) (1951-80) : BMRC
2 4 6 8 10 12 14 16
(d)
Z500 STD (DJF) JMA

Figure 10

(a)

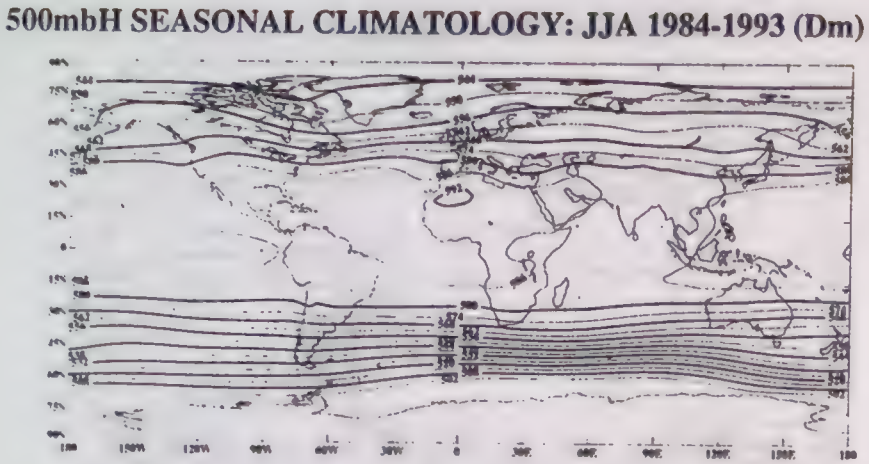

(b)

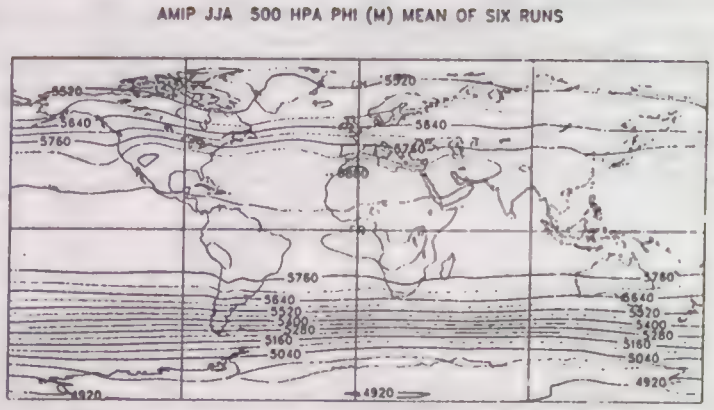

(c)

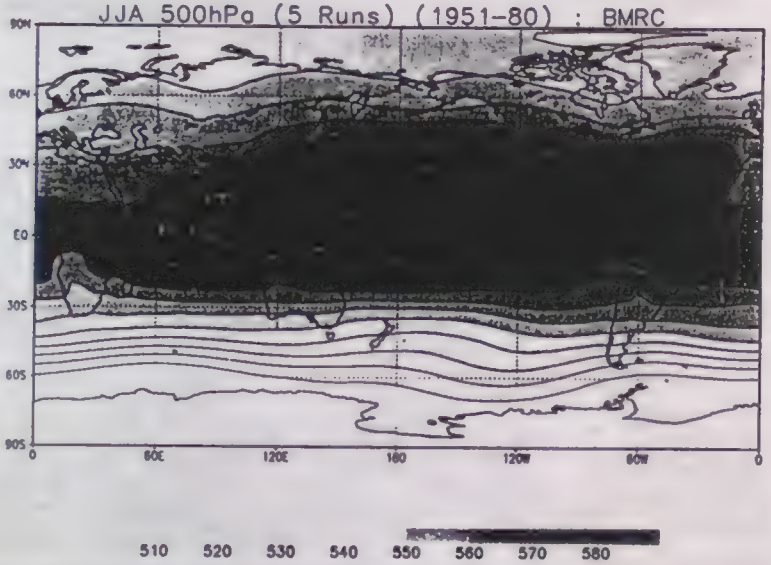

(d)

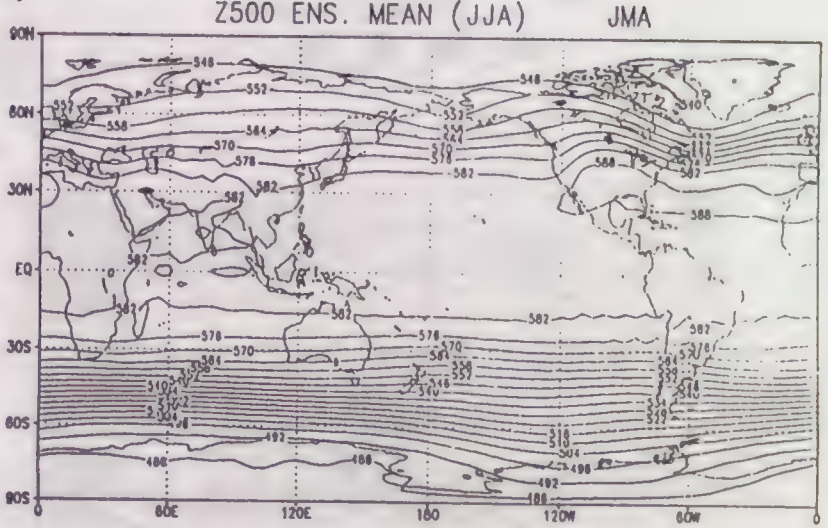

Figure 11

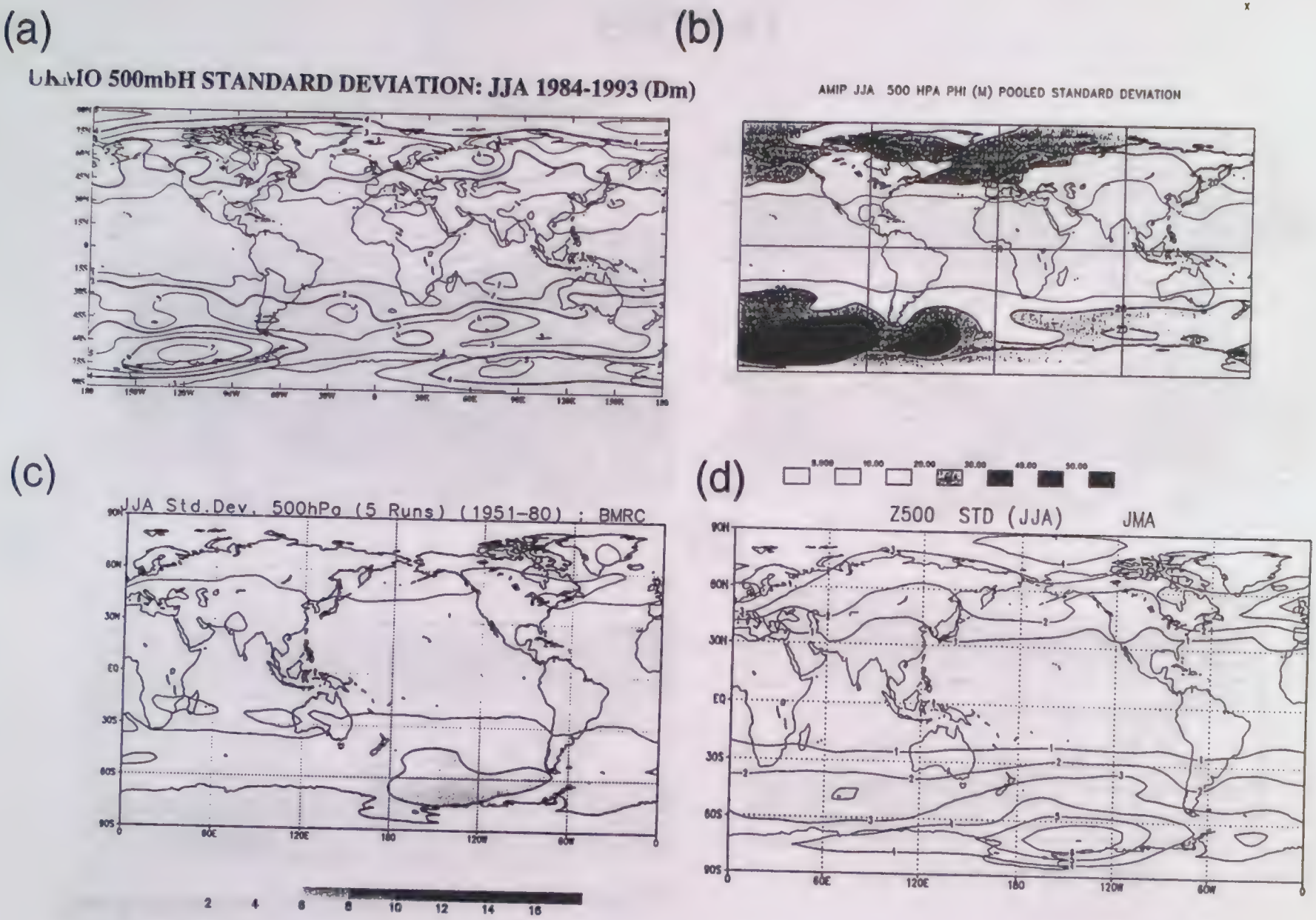
(a)
UKMO 500mbH STANDARD DEVIATION: JJA 1984-1993 (Dm)
(b)
AMIP JJA 500 HPA PHI (M) POOLED STANDARD DEVIATION
(c)
JJA Std.Dev. 500hPa (5 Runs) (1951-80) : BMRC
2 4 6 8 10 12 14 16
(d)
Z500 STD (JJA) JMA

Figure 12

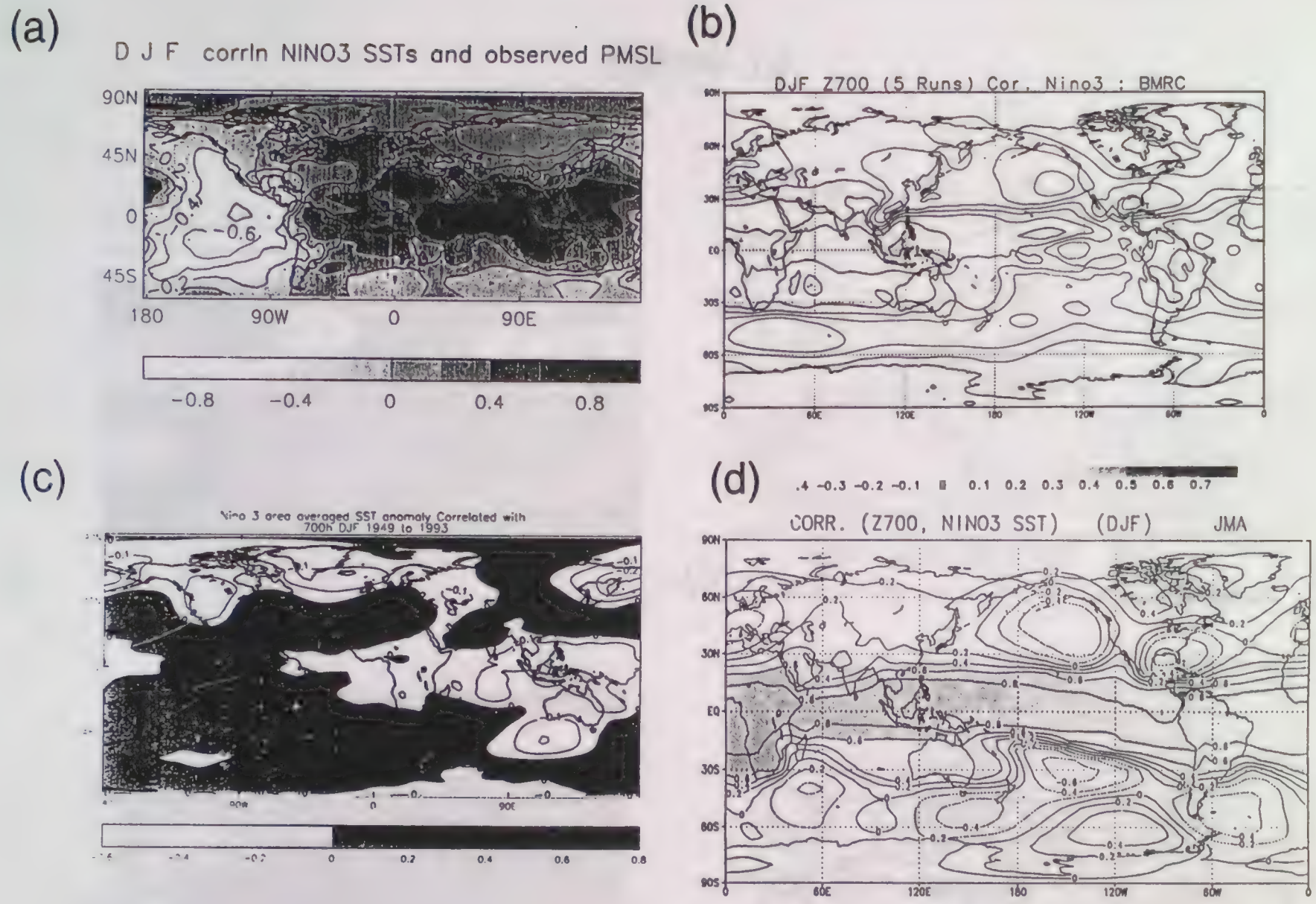
(a)
D J F corrln NINO3 SSTs and observed PMSL
90N
45N
0
45S
180
90W
0
90E
-0.8
-0.4
0
0.4
0.8
(b)
DJF Z700 (5 Runs) Cor. Nino3 : BMRC
(c)
Nino 3 area averaged SST anomaly Correlated with
700h DJF 1949 to 1993
(d)
CORR. (Z700, NINO3 SST) (DJF) JMA
60N
30N
EQ
30S
60S
90S
60E
120E
180
120W
60W

Figure 13

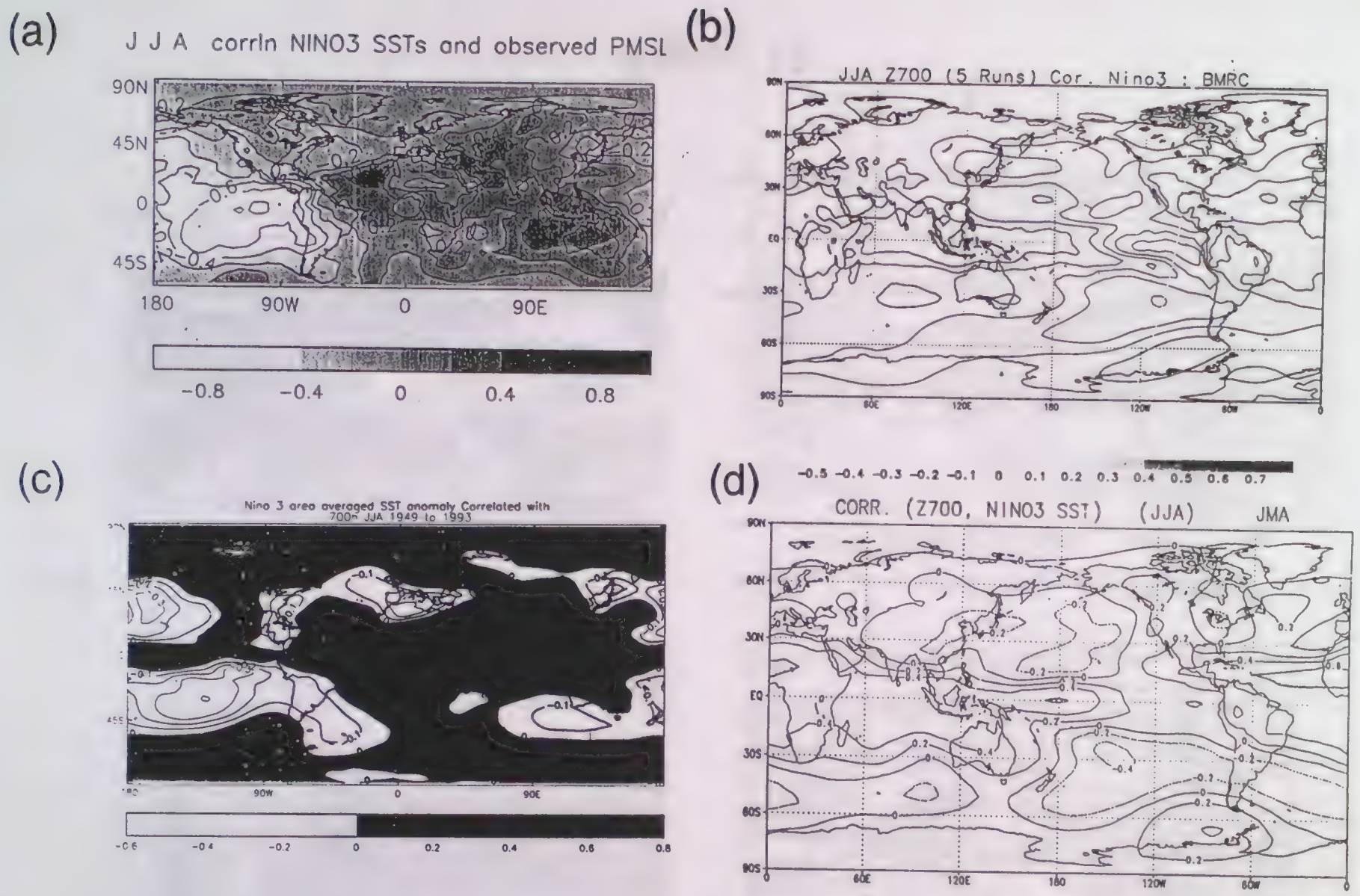
(a)
J J A corrln NINO3 SSTs and observed PMSL
90N
45N
0
45S
180
90W
0
90E
-0.8
-0.4
0
0.4
0.8
(b)
JJA Z700 (5 Runs) Cor. Nino3 : BMRC
(c)
Nino 3 area averaged SST anomaly Correlated with
700mb JJA 1949 to 1993
(d)
-0.5 -0.4 -0.3 -0.2 -0.1 0 0.1 0.2 0.3 0.4 0.5 0.6 0.7
CORR. (Z700, NINO3 SST) (JJA) JMA

Figure 14

AGCM Intercomparison Diagnostics: SST-Forced Variability Versus Internal Variability

F. W. Zwiers (Rapporteur), D.P. Rowell, A. Hense, J.R. Davies, M. Christoph

1 Introduction

The simulations which were inter-compared by this small working group were the 6 run UKMO ensemble for 1949-93, the 5 run BMRC ensemble for 1950-91, the 2 run MPI ensemble for 1950-89 and the 3 run JMA ensemble for 1955-88. The UKMO model, known as UM-Climate 1, is a grid point model with 2.5° latitude and 2.75° longitude horizontal resolution and 19 levels in the vertical (see Cullen, 1993, for details). The BMRC model is a spectral model with R31 horizontal resolution (approximately $2.8° \times 3.8°$) and 9 levels in the vertical. A recent description of the model and its lineage may be found in McAvaney and Coleman (1993). The MPI model used which for this experiment is known as ECHAM3. It is a spectral model with T21 horizonal resolution (i.e., approximately $5.625° \times 5.625°$) and 19 levels in the vertical. ECHAM3 is described in Roeckner, et al., 1992. The version of the JMA model used for this experiment is JMA-GSM89. It is a spectral model which has T42 horizontal resolution and 21 levels in the vertical. The model is described in Sugi, et al., 1990. The UKMO, BMRC and MPI simulations were forced using GISST version 1.1 (Parker and Jackson, 1995) sea surface temperatures (SSTs) and sea-ice boundaries. The JMA simulations were forced using MOHSST (Bottomley et al., 1990) SSTs and sea-ice boundaries.

The task of this group was to intercompare the proportion of variance attributable to SST and sea-ice boundary forcing in these ensembles of simulations. These variance ratios were computed following Rowell (1995, this volume). Critical values for these variance ratios are easily derived under standard Gaussian assumptions from those of the F-distribution (Rowell, 1995; in preparation).

SST induced variance for both PMSL and precipitation was examined on three different time scales by studying the estimated variance ratios computed from unfiltered seasonal means and from 5- and 10-year running means of seasonal means. Variance ratios diagnosed at the two longer time scales were very similar. Therefore discussion in this report will be limited to that of the unfiltered seasonal means and of the 10-year running means of seasonal means.

Significantly large variance ratios were diagnosed for both variables in all 4 models over a very large fraction of the globe. That is, the *signal* induced by the prescribed SSTs and sea-ice boundaries were detectable over much of the globe, often even in the interiors of continents. However, ratios which are "usefully" large (e.g., ratios greater than about 40%) were confined primarily to the tropics.

2 Unfiltered PMSL

A common extra-tropical feature which appears in all models was a local maximum of explained variance in the north eastern Pacific in DJF together with a corresponding local minimum over North America. The results for the UKMO, which are typical, are displayed in Figure 1. Some models (UKMO, ECHAM3) display evidence of enhanced predictability over western North America during MAM while another (BMRC) does not. All models show some evidence of enhanced predictability over the southern half of North America during JJA.

There did not appear to be a consensus amongst models concerning enhanced predictability over Europe. ECHAM3 displays relatively large variance ratios (local maximum > 50%) over Europe in MAM while the UKMO model displays a modest local maximum in MAM (> 20%) over the Caspian sea. Both variance ratios are significantly greater than zero. On the other hand, BMRC shows no evidence of enhanced inter-annual variability over Europe at any time of the year. The JMA results appear to agree with those of BMRC, although the reader should be aware that the extra-tropical results from the JMA simulations were difficult for us to interpret because of the large contour intervals used in the displays of their variance ratios.

All models except JMA displayed a local minimum in SST/sea-ice induced variance in the tropical Atlantic in DJF. This phenomenon was observed in the JMA model in SON. We noted that the local SST inter-annual variance is similar in both the tropical Atlantic and Pacific. Thus a difference in local forcing at the inter-annual time scale is not an explanation for this phenomenon. We also noted that there was a local minimum in explained variance over the Indian Ocean in JJA (in the JMA and UKMO models) and in MAM (in the BMRC and MPI models). It was noted that this local minimum corresponds to the weakest points in the SOI. For example, the proportion of SOI variance explained by SST in the MPI simulations is approximately 30% in MAM while it is approximately 60% during other seasons.

3 10-year Running Mean PMSL

We are able to intercompare only the BMRC, JMA and UKMO simulations on the 10-year time scale because analysis of variance results for filtered data were not available for the ECHAM3 simulations.

At this time scale much of the inter-annual variability in the forced component of PMSL appears to have been filtered out. The connection between the prescribed SST/sea-ice field and PMSL is generally weaker than in the unfiltered data except during SON when variance proportions are actually larger than with the unfiltered data. We also noted that the spatial scale of the regions with strong connections between the local PMSL values and the global SST/sea-ice field is smaller.

Interpretation of "significance" becomes difficult at this time scale because the tests which are used (simple F-ratios derived from classical one-way analysis of variance) do not account for the serial correlation which is induced by filtering.

A band of strong connections between the global SST/sea-ice field and PMSL is seen at about 20N between 160E and 60W. This is most pronounced in the BMRC results (see Figure 2) but was also apparent in the JMA and UKMO simulations. All 3 models agreed that a substantial portion of the simulated PMSL variability on the decadal time scale over western and southern North America is attributable to the imposed SST/sea-ice variation in JJA and SON.

Strong connections were also observed between the prescribed SST/sea-ice fields and PMSL over the Indian ocean in all seasons. The pattern of explained variance in this region which is illustrated in Figure 2 represents this in a more or less schematic manner because this pattern is somewhat stronger than that displayed in the results of the JMA and UKMO simulations. This strong signal maybe due to inter-decadal variability or warming in the Indian Ocean. We noted that the pattern does not extend into the southern ocean, perhaps because of data problems or perhaps because the signal to noise ratio is weak at higher latitudes. The gradients in the strength the SST/sea-ice signal illustrated in Figure 2 represent those of the other models schematically. Both the JMA and UKMO models display strong gradients, although not as strong as those of the BMRC model.

4 Unfiltered Precipitation

All models showed a tropical band in which SST/sea-ice variation is strongly related to inter-annual variation in precipitation. This band is narrowly focussed on the ITCZ and is skewed towards the summer hemisphere. In some models the proportion of precipitation variance which is explained by SST/sea-ice is greater than that for PMSL. The results for the UKMO model which are displayed in Figure 3 are representative of those of other models.

In all simulations, less precipitation variance was explained on the equator in the Atlantic during SON than during other seasons. This conflicts somewhat with our finding that in 3 of the 4 models, the minimum explained PMSL variance was occured during DJF.

In all models the band of large explained variance does not spread into land areas except over in regions bordering the tropical Atlantic (N.E. Brazil and the Guinea coast). We also noted that connections between the prescribed SST/sea-ice strengthen over the SPCZ in DJF. Both preferred locations of the SPCZ could be discerned in all of the simulations (but note that the depiction in Figure 3 is clearer than most). There was some evidence of precipitation predictability from the prescribed SST/sea-ice over south western North America during MAM in the BMRC, ECHAM3 and UKMO simulations. There was also some evidence of a predictive relationship between the SST/sea-ice field and precipitation at the ice edges. Finally, the simulations suggested that approximately 30-40% of variability in the Asian summer monsoon precipitation is attributable to SST/sea-ice variations.

5 10-Year Running Mean Precipitation

The patterns of explained variance obtained from the 10-year running means of precipitation are noisy and have structures with smaller scales than those of the unfiltered precipitation. There is some evidence that there is a stronger connection between the prescribed SST/sea-ice evolution and precipitation over tropical land areas (particularly tropical Africa and N.E. Brazil) at the decadal time scale than at the inter-annual time scale. Also, the effects of variations in boundary currents is evident on the decadal time scale in all 3 models considered and the effects of variations in ice-edges are evident.

6 Additional Analyses

The discussion within the group covered a number of possible extensions to this sort of investigation.

- More might be learned by conducting the analysis of variance on basis function coefficients such as principal components (obtained by projecting simulated fields onto EOFs), spherical harmonic coefficients, or the coefficients of the eigenmodes of simple linearised models of tropical modes.
- Linear contrasts (see for example, Scheffe (1959)) could be computed to compare groups of years such as "warm" and "cold" ENSO events.
- Additional simulation experiments could be conducted in which SSTs are fixed in all ocean basins except one. Such experiments would de-confound contributions to inter-annual and decadal variability originating from different geographical sources.
- Regression type models could be used to diagnose the proportion of variation which is due to the location of the ice edge (in locations where there are ice edge effects). Extreme care would be required to take into account adjustments which are made to SSTs near ice edges (as noted by Parker, personal communication).

References

[1] Bottomley, M., Folland, C.K., Hsiung, J., Newell, R.E. and Parker, D.E., 1990: *Global Surface Temperature Atlas.* HMSO, London, 20pp + 313 plates.

[2] Cullen, M.J.P., 1993: The Unified Forecast/Climate Model. *Meteor. Mag.*,, 122, 81-94.

[3] McAvaney, B.J. and Colman, R.A., 1993: The AMIP Experiment: The BMRC AGCM Configuration. BMRC Research Report 39, BMRC, GPO Box 1289K, Melbourne, Victoria, Australia 3001.

[4] Parker, D.E. and Jackson, M., 1995: The standard GISST data sets: Versions 1 and 2. This volume.

[5] Roeckner, E., Arpe, K., Bengtsson, L., Brinkop, S., Dumenil, L., Esch, M., Kirk, E., Lunkeit, F., Ponater, M., Rockel, B., Sausen, R., Schlese, U., Schubert, S., and Windelband, M., 1992: Simulation of the present-day climate with the ECHAM model: Impact of model physics and resolution. Max Planck Institute for Meteorology, Report No. 93, 171 pp.

[6] Rowell, D.P., 1995: A methodology for using an ensemble of multi-decadal GCM simulations to assess the percentage variance explained by SST forcing. This volume.

[7] Scheffe, H., 1959: *The Analysis of Variance.* John Wiley and Sons, New York, 477pp.

[8] Sugi, M., Kuma, K., Tada, K., Tamiya, K., Hasegawa, N., Iwasaki, T., Yamada, S., and Kitade, T., 1990: Description and performance of the JMA operational global spectral model (JMA-GSM88).Geophys.Mag., 43,105-130.

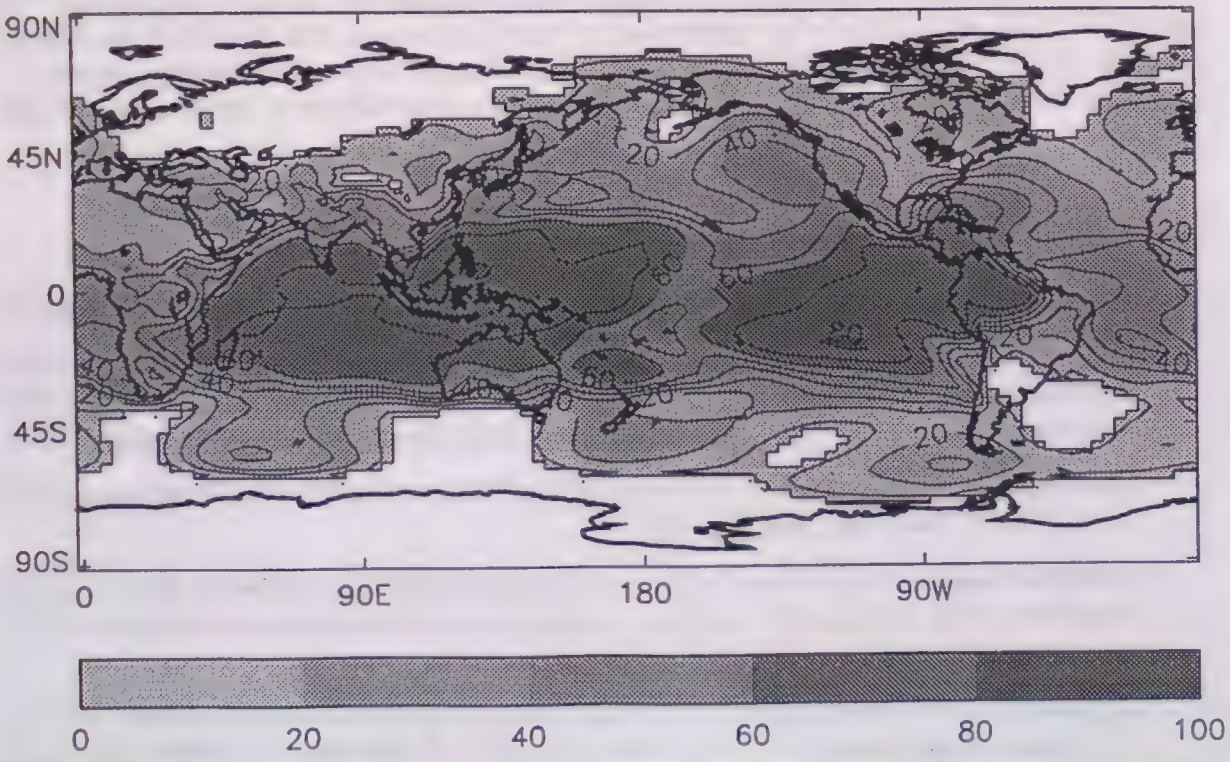

Figure 1: *The ratio of SST induced inter-annual variance to total inter-annual variance of DJF PMSL for the UKMO ensemble of simulations. Only the ratios significantly greater than zero at the 5% significance level are displayed.*

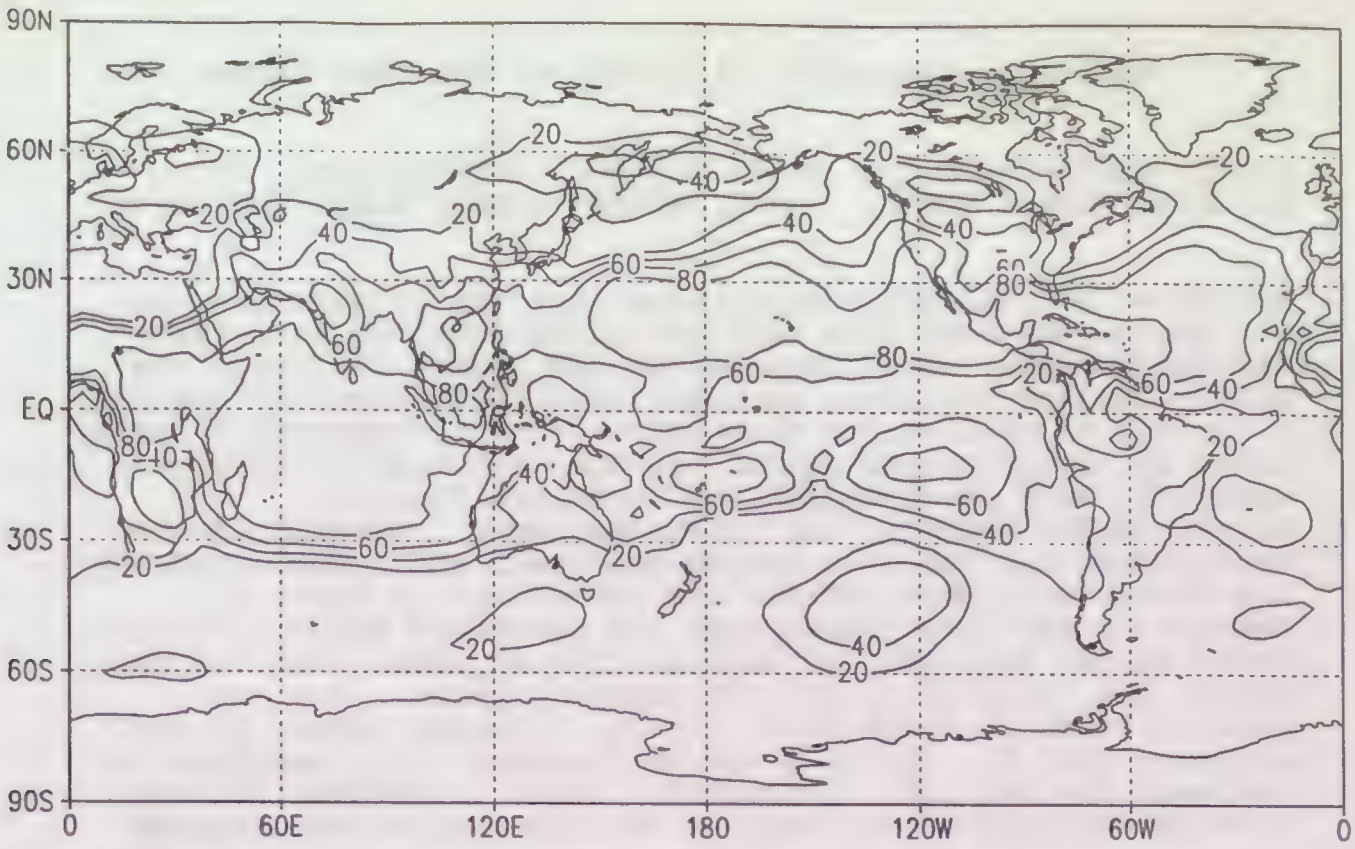

Figure 2: *The ratio of SST induced inter-annual variance to total inter-annual variance of JJA PMSL on the decadal time scale for the BMRC of simulations.*

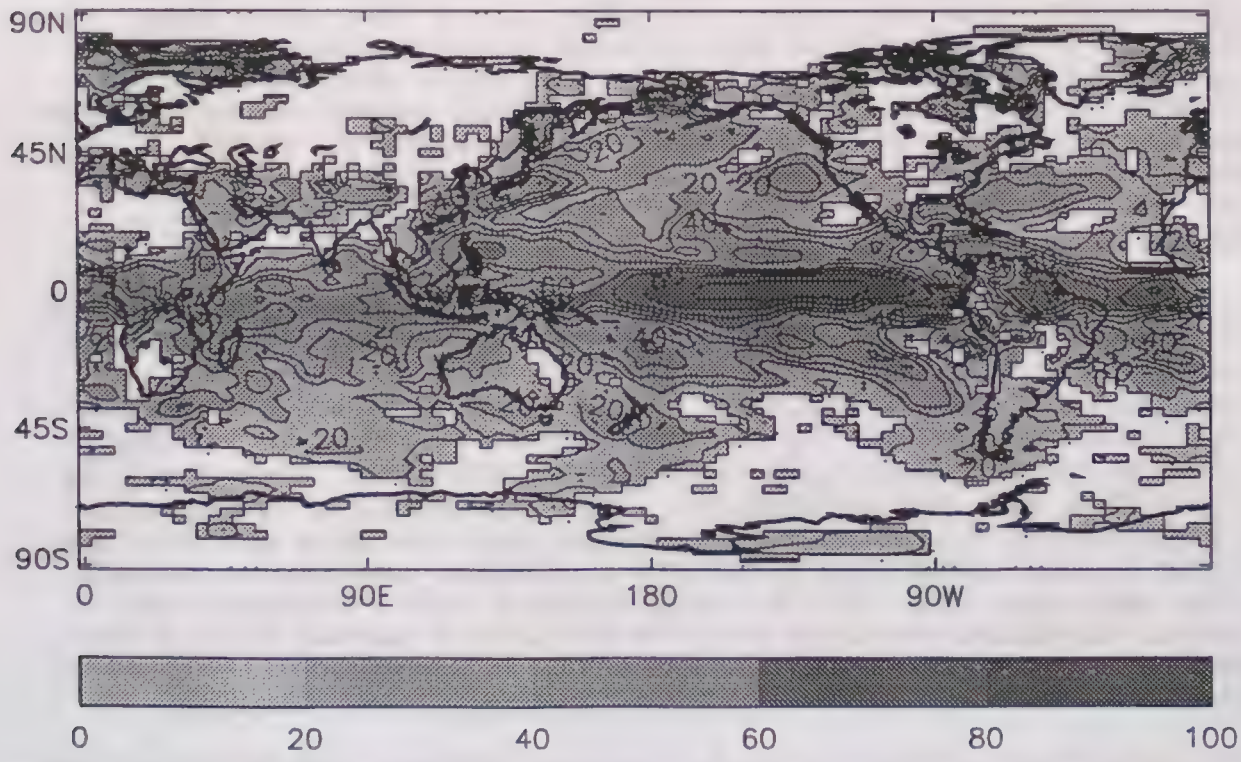

Figure 3: *The ratio of SST induced inter-annual variance to total inter-annual variance of DJF precipitation for the UKMO ensemble of simulations. Only the ratios significantly greater than zero at the 5% significance level are displayed.*

AGCM intercomparison diagnostics: Key Time Series

Robert Livezey (Chair), Chris Folland, John Davies, Peter Gleckler, David Karoly, David Parker, Masato Sugi, John Walsh.

Ensembles of long GCM integrations, varying in size from one to fourteen members with most extending from the late 1940s and early 1950s, were conducted by ten groups utilizing the GISST analyses for lower boundary conditions over the oceans. A variety of time series from these runs, accompanied in some cases by linear trends and/or low-pass filtered (> 10 years) versions, were produced for the Twentieth Century Climate/GISST Workshop for intercomparison. Details of the experiments and the time series produced, and correlations of the latter with observations are summarized in Table 1. Results of the intercomparisons are presented below. Only those series available in digital form at press time for this report are included in the referenced figures. For any particular model where there is more than one member in the ensemble (all but the COLA and EDF models) it is possible to estimate the per cent of variance linked to SST variability from an analysis of variance of the ensemble of simulations.

Two cautionary notes about the results are appropriate. First, because of internal atmospheric variability, those experiments with very small ensemble sizes (say less than three or four) should be interpreted with caution, although the use of three month or longer time means ameliorates the problem to some extent. Second, even for recent decades there are opportunities for meaningful improvements to GISST analyses. Such improvements are underway and should sharpen the role of SSTs in atmospheric variability in similar experiments.

Southern Oscillation Index (SOI). The five-month running mean difference in normalized Tahiti and Darwin PMSL, the SOI, was overall the best simulated series of all those examined (cf. the correlations in Table 1). Over half of the eight series available extend back to the early 1950s. From Fig. 1 the success (particularly after the early 1960s) of almost all of the models and, by implication, the huge portion of variance in the series attributable to the prescribed SSTs are obvious. Prior to the early 1960s the six ensembles available overall only reproduce the 1955-57 cold episode well. Because the larger ensemble averages are not obviously better during this period suggests that there may still be problems with the SST analyses that are not as serious in more recent decades.

The other most interesting difference between the modeled time series and the observations are the frequency of positive biases in the modeled SOIs during the period from about 1981 to 1987. These biases are particularly evident for the 1985

cold episode. Curiously, the models tracked the swings in SSTs well during this period in the sense that tropical Pacific waters (as monitored by the NINO3 index) did cool to well below normal temperatures in 1985. The model results may be a consequence of the inadequacy of a single index, like the SOI, for monitoring ENSO.

Global Annual Mean Land Surface Temperature. This series was available for intercomparison for at least most of the study period from five of the models. Estimates from the UKMO and JMA models of SST-attributable variance were between 65 and 70%. Low-pass filtered and unfiltered versions of the available series along with linear trend lines are shown in Fig. 2. From the figures and the correlations in Table 1 it is apparent that none of the simulations really capture the long-term linear trend and that the main reason for the larger correlations for four of the filtered series is the reproduction of the interdecadal swing between the 1970s and 1980s. None of the low-pass filtered series do exceptionally well at matching the observations prior to this, but the UKMO series comes closest. Note also that many interannual changes are captured by the models and that the levels of both interannual and interdecadal variability are generally well simulated.

North Atlantic Oscillation (NAO) Index. The normalized (with respect to 1951-80) differences between PMSL at Ponta Delgada (Azores) minus Stykkisholmur (Iceland) were formed for MAM, JJA, SON, and DJF and examined for four of the models. No model evidence (for example note the insignificance of the correlations in Table 1) is found that the variability **in these series** is coupled to SSTs. This does not preclude the possibility that relationships do exist for other time averages or other windows in the annual cycle.

Tropical Rainfall Indices. Areal-averaged rainfall anomaly (w.r.t. 1970-88) series for three different tropical locations in Figs. 3-5 exhibit several important differences between them. These differences involve the amount of variance in each set of series that can be attributed to SST variability, whether this SST-linked variance is mainly on interannual or interdecadal time scales and the extent to which it is potentially predictable.

SAHEL (approximately 12.5-17.5N,15W-37.5E, JJAS means): For ensembles in which it has been calculated and is available 35-40% of model variance was linked to SST variability. From the figures and the correlations in Table 1 this variance is dominantly on interdecadal time scales. The low-pass filtered observations were generally well simulated except for a tendency in all of the six models available in the early part of the study period to not be wet enough then. This has the effect (like in Fig. 2) of a considerable underestimation of the long-term trend. Only modest success was apparent in the

reproduction of interannual variability; for example even though the dry 1984 season was reasonably well handled and the wet 1952 season excellently, the dry 1972 and wet 1988 seasons were for the most part missed by the models.

INDIA (approx. national average, JJAS means): The per cent of variance attributable to SST fluctuations for models for which it is available is overall about the same (30-50%) for Indian monsoon rainfall as it is for the Sahel series, but otherwise the series in Fig. 4 are quite different than those exemplified by Fig. 3. There is no pronounced interdecadal variability in the observed or modeled Indian data, and even though the total interannual variance is well-estimated by the models, the timing of very few important events is captured (as reflected in the correlations in Table 1). Because the SST-related variability must primarily reside on interannual time scales these facts together imply that either the models' links between SSTs and monsoonal rainfall are incomplete or incorrect or the SST analyses are inadequate in crucial regions.

NORTHEAST BRAZIL (smaller area in Ward and Folland, 1991, FMAM means): In sharp contrast to the previous two areas, the sets of modeled series for Northeast Brazil rainfall for which the statistic is available all had close to 80% of their variance explainable by SST variability. Further, all six ensemble series available (Fig. 5) show little interdecadal variability and all but one exhibited considerable accuracy in the reproduction of year to year changes (Table 1). In fact the accuracy of at least the UKMO model can be characterized as extraordinary. This matches the experience of statistical modelers who have attributed comparable amounts of variance in this rainfall series to tropical Atlantic and ENSO-related SST fluctuations in that order of importance.

High Latitude Precipitation. Areal averages over all North American and Eurasian (excluding the UK) land points north of 55N for ONDJFM (DJF for JMA) are compared to the observational series (Fig. 6) whose principal feature of interest is a positive long-term trend. None of the three model ensemble series available reproduced such a trend. Thus, it is difficult at this point to attribute the trend to global SST trends. Note also in Figs. 2, 3, and 6 that **without exception every model ensemble-mean series either substantially underestimates or altogether misses the corresponding observed series long-term trend.** Whether these three occurrences are related is uncertain, but individually they must be the result of either deficiencies in the SST analyses in the early part of the record or some universal deficiency in the models. The former is militated against at least for high latitude precipitation by the simulation error for the most recent few years.

Recommendations. While the above series proved to be of

substantial interest it is clear that many of them are too crude to adequately describe many of the aspects of SST-related atmospheric forcing. In particular it is clear that a new SOI or ENSO index is needed that takes into account the spatial structure of the PMSL field and the seasonal variability of this structure. Additionally, richer detail in the intercomparison of ocean/atmosphere teleconnective links will require a variety of modal indices, based perhaps on Barnston and Livezey (1987) patterns and Ward's (1994) tropical-wide mode, and additional regional series following at least the work of C. Ropelewski and M. Halpert of the CPC but also including additional very large-scale series.

With the exception of some results from analysis of variance and from correlations, the comparisons made above between model and model and model and observations were largely subjective. Future intercomparisons should have a strong quantitative base and utilize a number of objective tools. Individual series should be characterized by their spectrum and autocorrelation function, while series should be compared through cross-spectral analysis, error analyses (including Murphy-Epstein, 1989, statistics; LEPSCONT; LEPSCAT with contingency tables; etc.), and multivariate techniques (like CCA or combined PCA).

Finally, intercomparisons should be conducted on stratifications of the complete data series that are based on at least ENSO episode type. Often it is more straightforward to evaluate model performance under certain scenarios because the picture is not clouded by a large number of irrelevant cases.

Table 1. GCM/GISST simulations and available ensemble time series (see text for desriptions) along with correlations of latter with observations (for filtered series in parenthesis).

Modeling Group	Period of Runs		Ensemble Size	Series						
	Start	End		SOI	Global Land Sfc. Temp.	NAO Indices*	Rainfall			
							Sahel	Indian Monsoon	NE Brazil	High Latitude
BMRC	3/50	9/91	5	0.84	0.52(0.70)	0.05	0.52(0.87)	-0.15	0.76	
CCC	1/79	12/88	6	0.88						
COLA	1/49	9/92	1	0.70	0.57(0.67)	0.16	0.44(0.81)	0.13	0.72	-0.12
CSIRO	1/50	12/88	3	0.65	0.59(0.47)		0.53(0.79)		0.23	
ECHAM	7/50	7/89	2				0.57(0.96)		0.74	
EDF	7/70	7/88	14				0.25(0.82)	0.20		
GFDL	3/46	10/88	4	0.74			0.08(0.56)			
JMA	1/55	12/88	3	0.86	0.63(0.92)	0.11	0.33(0.83)	-0.23	0.85	0.18
MRI	10/69	9/93	1	0.77			0.05(-0.21)			
UKMO	10/48	11/93	6	0.85	0.70(0.80)	0.05	0.58(0.93)	0.13	0.91	0.06

* Average for four seasons.

Figure 1: SOI Index standiardised w.r.t. 1979 to 1988 and 5pt smoothed
Correlation with obs given in brackets

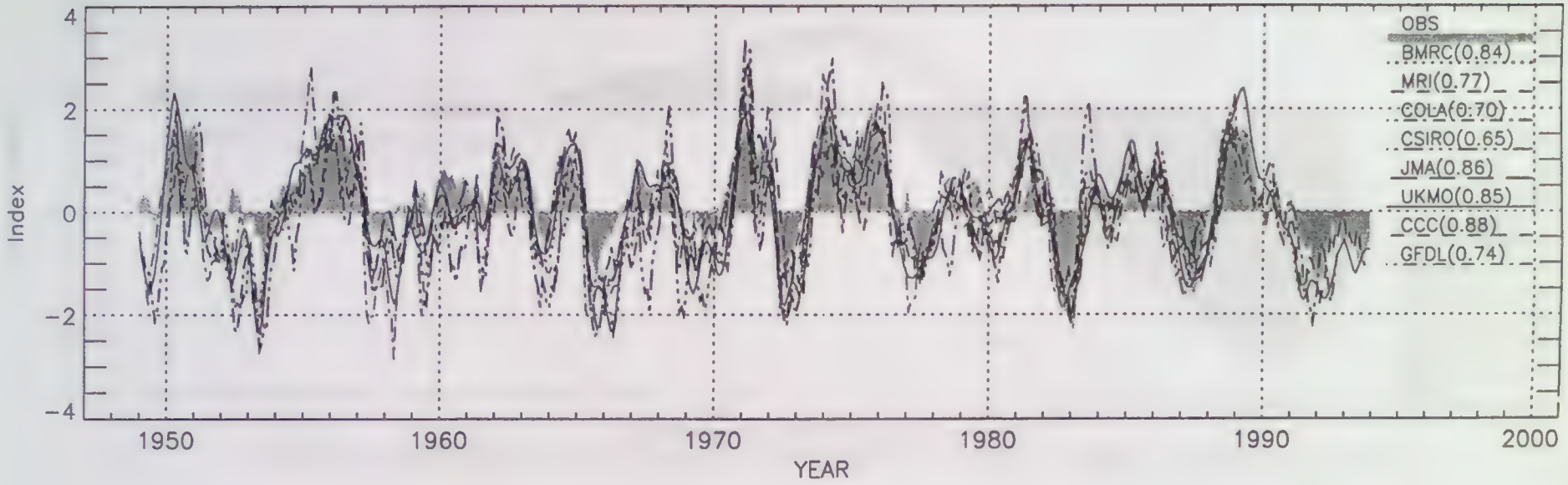

Figure 2a: Land surface air temperature anomalies w.r.t. 1970 to 1988
Lines show the linear trends. The thick line is the observed trend
Correlations with obs in brackets

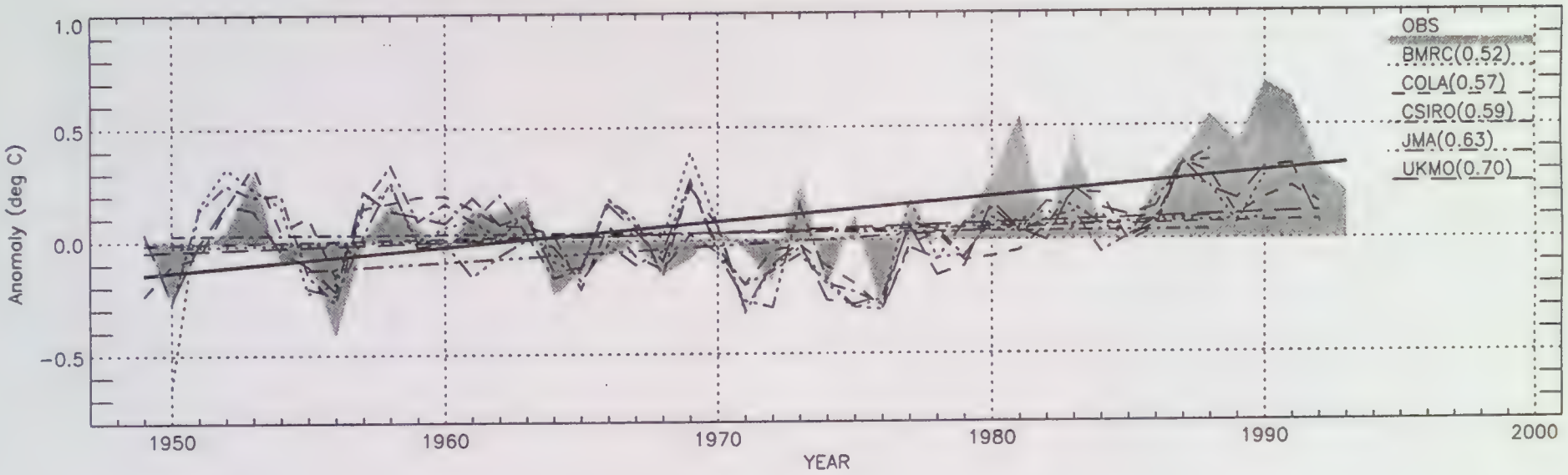

Figure 2b: Land surface air temperature anomalies w.r.t. 1970 to 1988 and low pass filtered
Correlations with obs in brackets

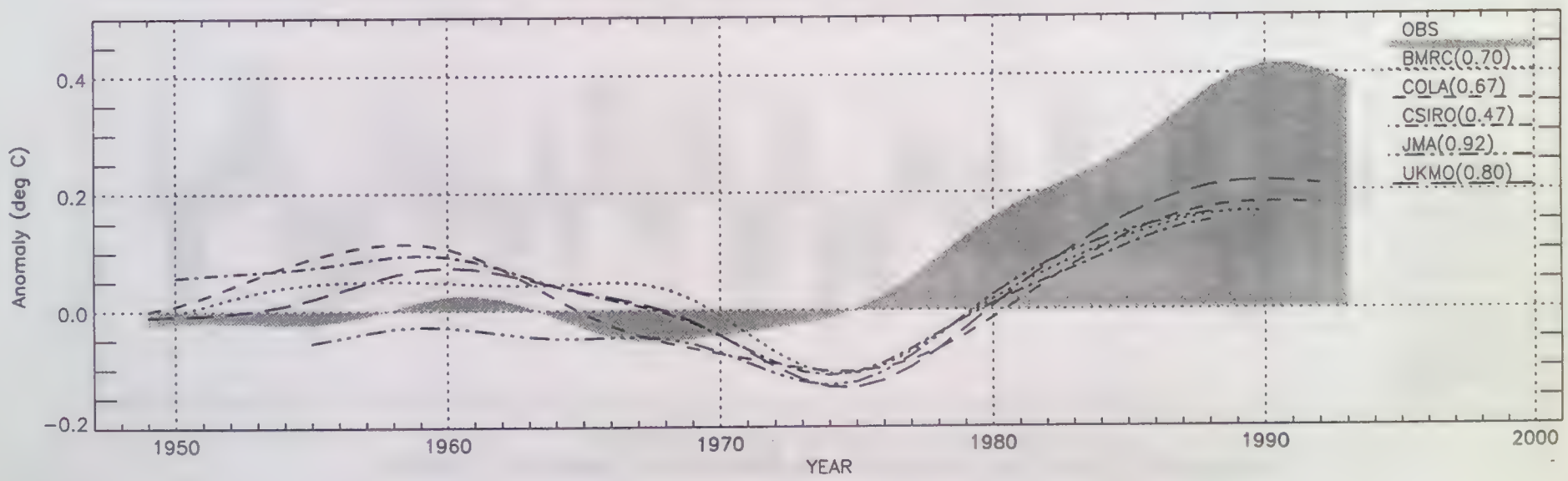

Figure 3a: Sahel rainfall (JAS) anomalies w.r.t. 1970 to 1988
Correlations with obs in brackets

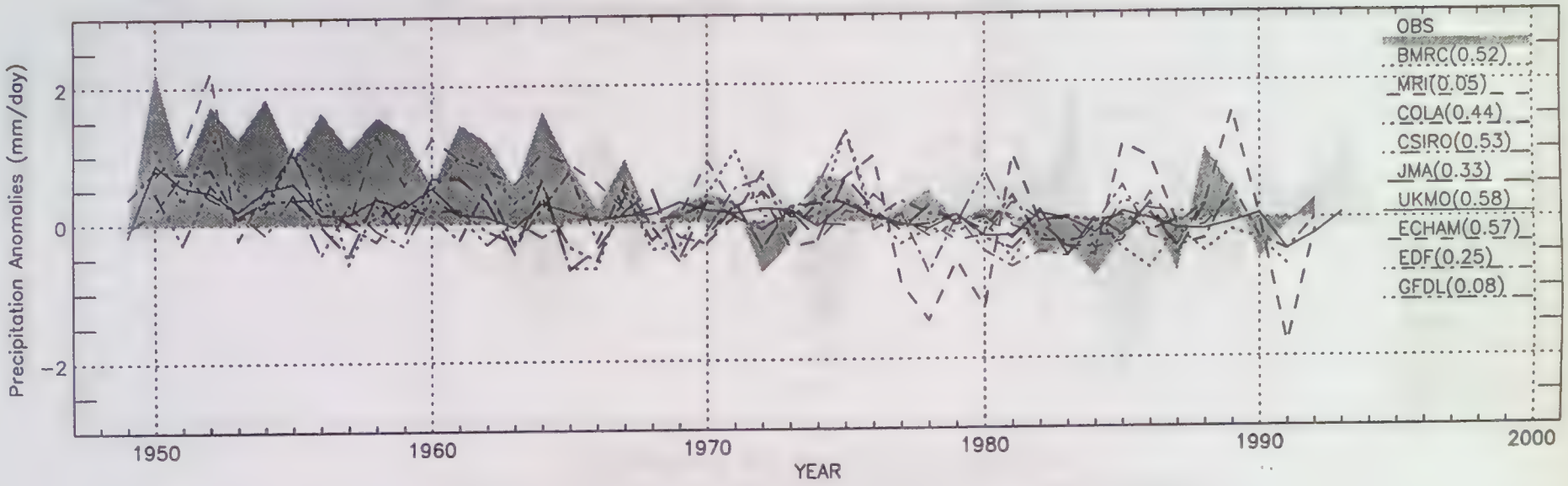

Figure 3b: Sahel rainfall (JAS) anomalies w.r.t. 1970 to 1988 and low pass filtered
Correlations with obs in brackets

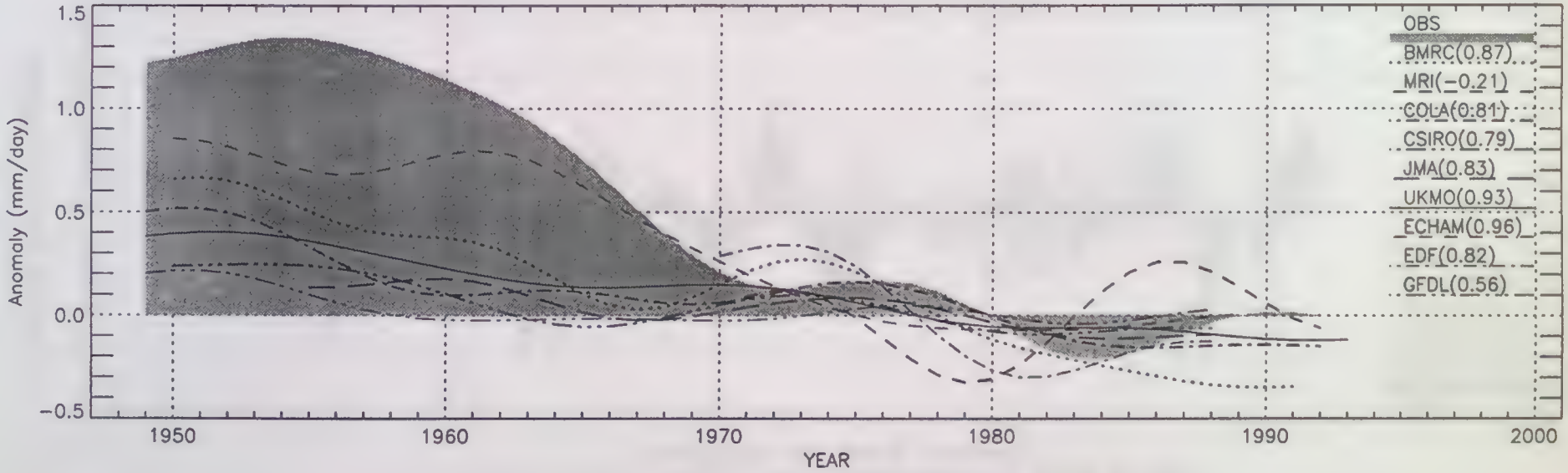

Figure 4: Indian rainfall (JJAS) anomalies w.r.t. 1970 to 1988
Correlations with obs in brackets

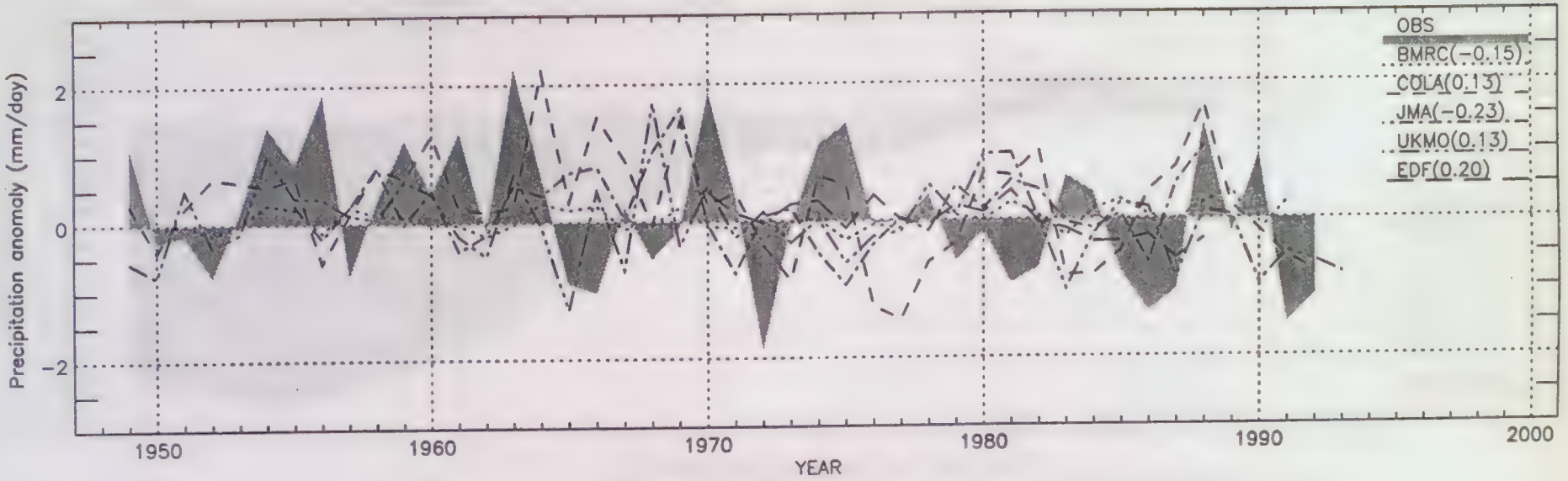

Figure 5: Brazil rainfall (FMAM) anomalies w.r.t. 1955 to 1988
Correlations with obs given in brackets

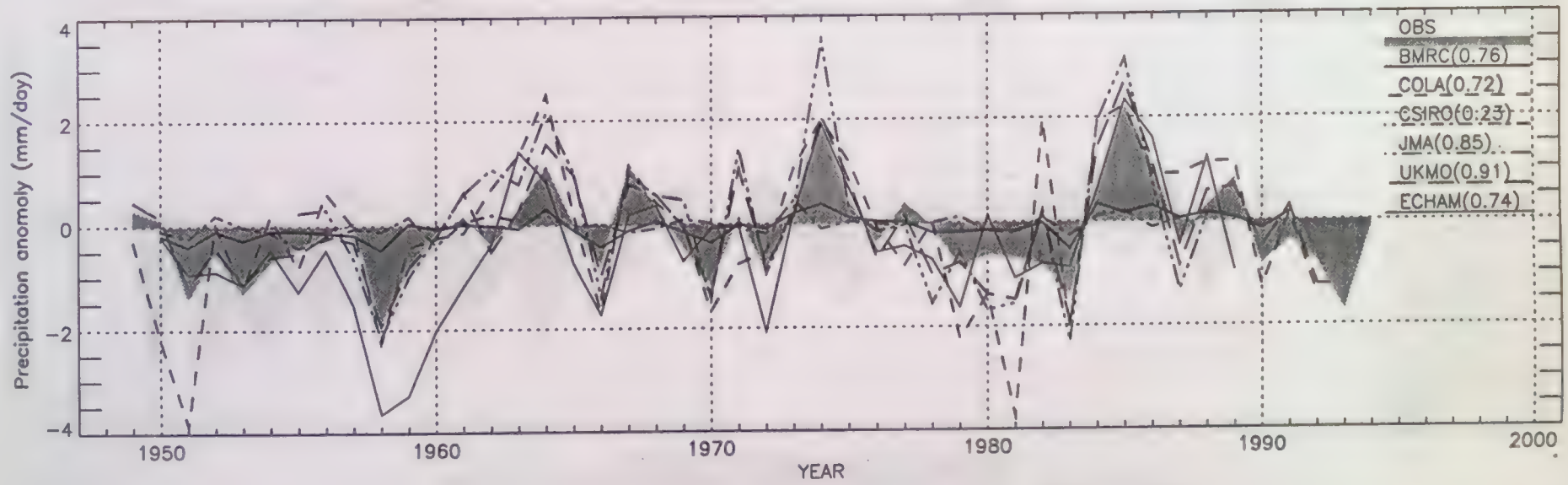

Figure 6: High latitude precip (ONDJFM) anomalies w.r.t. 1970 to 1988
Correlations with obs given in brackets

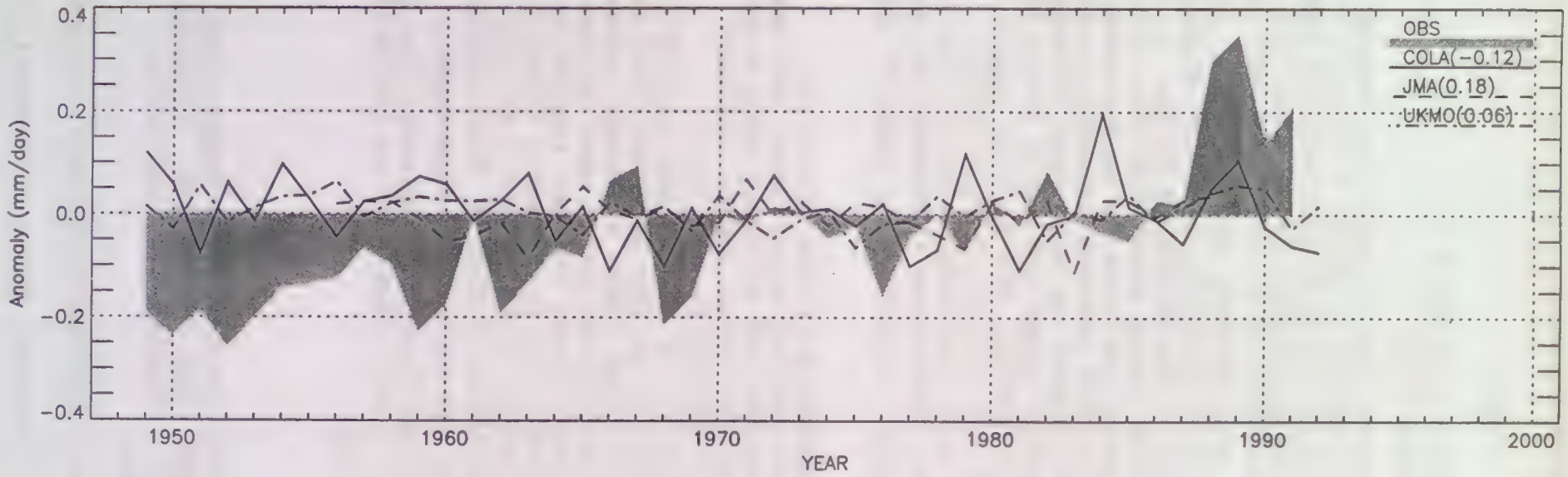

The standard GISST data sets: Versions 1 and 2

D E Parker and M Jackson

Hadley Centre for Climate Prediction and Research.
Meteorological Office, Bracknell, U.K.

The first version of GISST (Fig 1) is described in detail by Parker et al. (1994a). The monthly sea surface temperature (SST) data base ("MOHSST") of Bottomley et al. (1990) was augmented with monthly COADS data (Woodruff et al., 1987), while applying better corrections for the use of uninsulated and semi-insulated buckets up to 1941 (Folland and Parker, 1995). Missing and extreme 5° area monthly SST anomalies were then replaced by averages of spatially or temporally adjacent anomalies if sufficient of these were available (also described by Parker et al. , 1994b). The coverage was further enhanced using satellite data from 1982, but otherwise by using weighted anomalies from up to 5 months before or after a missing value. This latter process tended to generate too weak anomalies in data-sparse areas (Rayner et al., this workshop). Sea-ice extent was taken from NOAA datasets since the early 1970s and from a variety of sources, mainly climatologies, for earlier years. SSTs were assigned along ice-edges with the aid of climatological statistics, and the SSTs were extended into remaining missing areas with the aid of the Laplacian of the 1951-80 climatology (Bottomley et al., 1990). A final smoothing retained anomaly variations on about 5° spatial resolution.

The second version of GISST is being created with the following improvements. New accessing and quality-control algorithms, and the use of extra recent logbook data, yield smoother and slightly more complete initial MOHSST fields. The temporal interpolation scheme has been refined by allowing for geographical variations of the lag-autocorrelation of SST anomalies. Erroneous Antarctic sea-ice data for 1985-7 are being replaced, and in the Arctic we are incorporating sea-ice concentrations and using the data of Walsh (this workshop) between 1901 and the early 1970s. Refined statistics are being used in the assignment of ice-edge SST. The background field for the Laplacian interpolation is a better climatology developed by blending GISST 1 averages for 1982-93 with the improved MOHSST data for 1961-90 and satellite data for 1982-90. This climatology is thus a 'best estimate' for 1961-90 and is at 1° x 1° resolution and on a daily time-scale. GISST 2 anomalies will retain 1° resolution from 1982 onwards (Fig 2). All data used to form GISST 2 are first being referenced to the daily climatology for the appropriate 1° x 1° area.

References

Bottomley,M. et al., 1990. Global Ocean Surface Temperature Atlas. Met Office/MIT. Printed by HMSO. Available in the Hadley Centre.

Folland,C.K. and Parker,D.E. 1995 Quart.J.Roy.Meteorol.Soc., in press.

Parker,D.E. et al., 1994a. U.S. National Research Council, in press.

Parker,D.E. et al., 1994b. J.Geophys.Res., 99, 14373 - 14399.

Woodruff,S.D. et al., 1987. Bull.Amer.Meteorol.Soc., 68, 1239 - 1250.

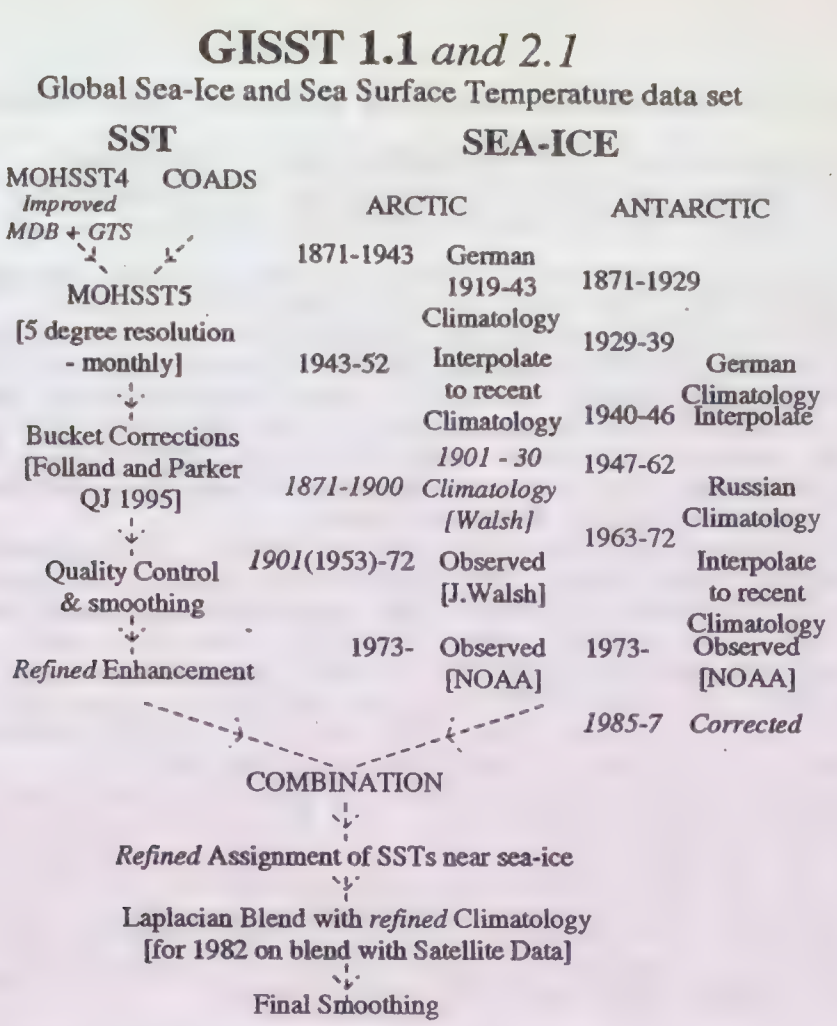

Figure 1 Creation of GISST 1.1 and 2.1. Features of GISST 1.1 are italicised.

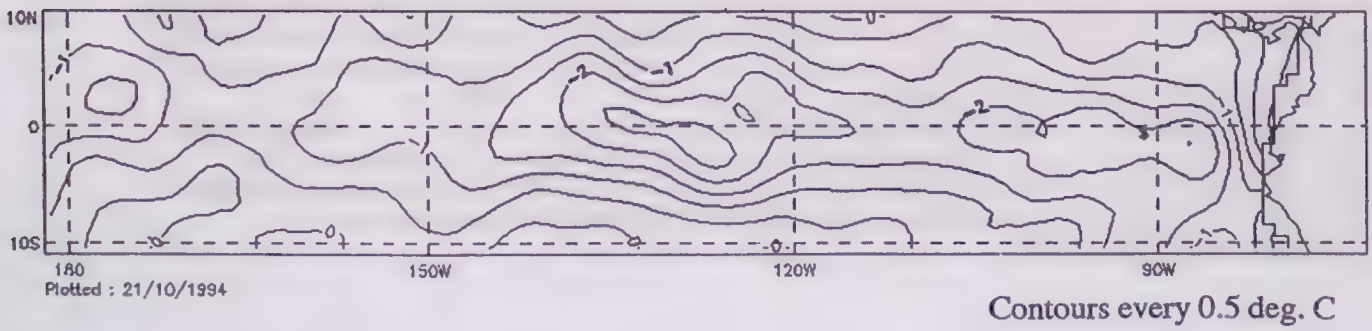

Figure 2 Preliminary GISST 2.1 anomalies (with respect to 1961-90) in the eastern tropical Pacific in La Nina conditions, July 1988. Note the narrow equatorial tongue of cold anomalues.

Using EOF Analysis to create a new GISST Data Set for Forcing GCMs.

N.A.Rayner,M.N.Ward,D.E.Parker and C.K.Folland
Hadley Centre for Climate Prediction and Research,
Meteorological Office, Bracknell, UK.

In order to produce a complete Global sea-Ice and Sea Surface Temperature (GISST) data set for forcing GCMs, sea surface temperature (SST) data must first be interpolated into data-sparse regions of the in situ Meteorological Office Historical SST data set (MOHSST). Empirical Orthogonal Function (EOF) analysis has been used to capture the essential characteristics of the spatial and temporal variation of the record, in order that these characteristics may be used to reconstruct the field in data-sparse areas in a manner most in keeping with the available observed data.

Individual covariance matrices for the Atlantic, Indian and Pacific ocean basins are formed and EOFs calculated on an equal area grid. The existing version of GISST[1] for 1901-1990 was used as a complete set of data is needed. Only the first few EOFs are necessary to explain the majority of the spatial variance of the data. The remainder represent noise (e.g. erroneous observations) and may possibly be discarded. Once the significant EOFs have been identified, they are used to interpolate missing data by reconstruction of the whole field. This is done by using the data which **are** available in the MOHSST data set to identify how strong the contribution from each EOF pattern is in each individual month.

The strength of the kth EOF pattern for any month is given by a scalar quantity known as the time coefficient, z_k. We are able to make a first estimate of this by calculating the coefficient from the observed data, z_k^*, which can then be used to calculate z_k, an estimate of the 'true' value for the whole field:

$$z_k=(1-c_{kk})^{-1}z_k^*$$

c_{kk} here is a diagonalised matrix comprising the sum of squares of each EOF weight over all missing data positions[2].

The method is verified using data-sparse periods simulated by removing data from the decade 1981-1990. Reconstructed portions of data are compared with observed data and measures of skill are attached to the reconstruction using various statistics, including the new Linear Error in Probability Space (LEPS)[3]; which is sensitive to both the phase and absolute magnitude of reconstruction errors. Skill has been calculated for several reconstructions using increasing numbers of EOFs in order to ascertain the optimum number. An example of one such analysis can be seen in Figures 1 and 2.

Initial results have been encouraging (Figs.1 and 2). Comparisons between the skill of this method and the existing interpolation methods used to create GISST 1.0 and 1.1 will be discussed together with future work, including the use of global eigenvectors to reconstruct the data.

---

[1] D.E.Parker, C.K.Folland, A.Bevan, M.N.Ward, M.Jackson and K.Maskell 'Marine Surface Data for Analysis of Climatic Fluctuations on Interannual to Century Timescales.'(1994) in press in 'Natural Climate Variability on Decade-to-Century Time Scales.' National Academy Press, Washington.

[2] N.A.Rayner and M.N.Ward. Hadley Centre Internal Note (1994).

[3] J.M.Potts, C.K.Folland, I.T.Jolliffe and D.Sexton,'Revised 'LEPS' Scores for Assessing Climate Model Simulations and Long-Range Forecasts'(1994) submitted to Journal of Climate.

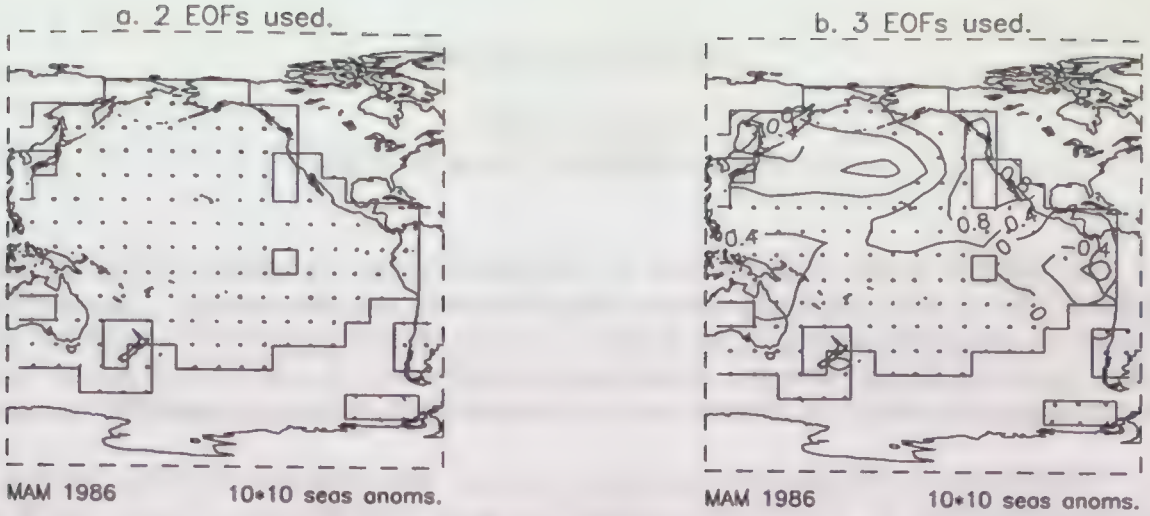

Figure 1. Reconstruction of Pacific SST Anomalies for March to May 1986 using Coverage Limited to that Available in 1876 and a. 2, b. 3, c. 8 EOFs
d. is observed. Interpolated data only shown. (Values greater than 0 are shaded.)

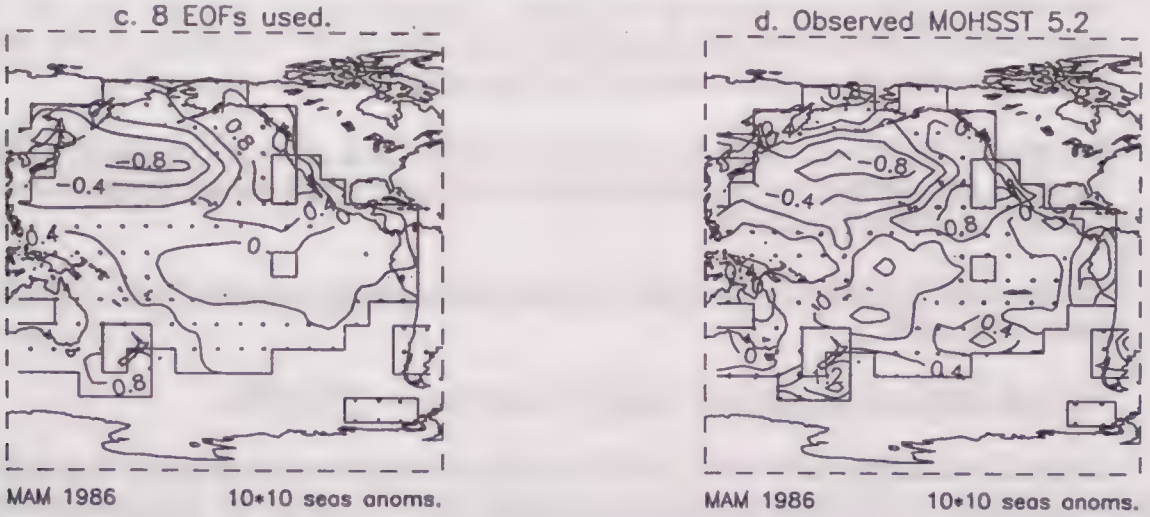

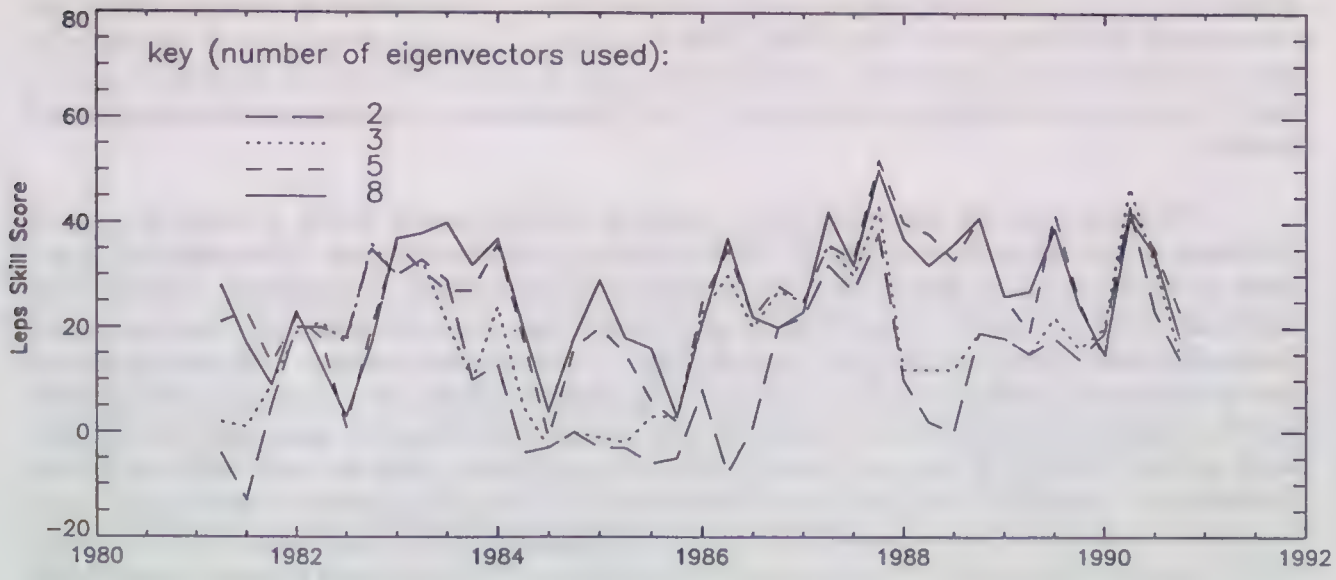

Figure 2. Summary of LEPS Skill for Pacific in Reconstruction of 1981–90 using 1871–80 Coverage.

A SEA ICE DATABASE

John E. Walsh
University of Illinois, Urbana, IL USA

The primary objective of a recent sea ice project at the University of Illinois was the compilation of a database depicting sea ice variations during the 20th century. The compilation procedure was designed to maximize the dataset's utility in modeling applications requiring surface boundary conditions in high latitudes. A secondary objective was an evaluation of recent trends of sea ice coverage and a diagnosis of these trends in terms of the associated atmospheric variables.

Existing sea ice information from various sources was gridded at monthly intervals and 110 km resolution (Fig. 1). The gridded variable was sea ice concentration, when available; in the absence of data on ice concentration, the location of the ice edge was digitized. The data compilation drew primarily upon four sources:

1. The annual reports and charts of the Danish Meteorological Institute for 1951-1956 (digitization of charts for April-August was performed by the University of East Anglia; digitizations for other months were based on the Danish narrative summaries).

2. Regional maps from the U.K. Meteorological Office, U.S. Naval Oceanographic Office, Canadian Atmospheric Environment Service and Icelandic Glaciological Society for various years of the 1953-1971 period.

3. The ice charts compiled for the Alaskan region by Sea Ice Consultants (W. S. Dehn) for the years 1953-1990.

4. The U.S. NOAA/Navy Joint Ice Center's digital data for 1972-1990.

Figure 2 is a sample time series for 1953-1990 showing the areal coverage of sea ice on a monthly basis for the North Atlantic subregion bounded by 0°W and 40°W. Noteworthy features of this time series are the minimum around 1960, the decline to a minimum in the early 1980s, and a secondary maximum in the late 1980s. The envelope of the winter maxima is considerably smoother than the envelope of the summer minima, and the winter maxima in this region seem to have a stronger low-frequency component than do the maxima and minima in other longitudinal sectors.

Variations over the longer period beginning in 1901 are shown in Fig. 3, which is a plot of the extent of sea ice in same sector (0°-40°W) during April of each year. (Note that Fig. 3 is a times series of ice extent, defined here as the ocean area poleward of the ice edge). While the ice maximum of the late 1960s is also apparent in this time series, there are indications that sea ice was somewhat more extensive during the early decades of the twentieth century. The most extensive sea ice coverage is indicated in 1911. It should be noted, however, that the data quality/quantity and the charting conventions of the earlier decades introduce considerable uncertainty into the left-hand portion of Fig. 3, thereby making direct comparisons with the later data somewhat questionable. In addition, the gridded data for some of the other longitudinal sectors (especially in the Pacific hemisphere) are characterized by a predominance of estimates based on climatology. An alternative version of this dataset includes non-climatological estimates in these regions based on spatial and temporal interpolation, with appropriate damping of the monthly anomalies derived from the available data.

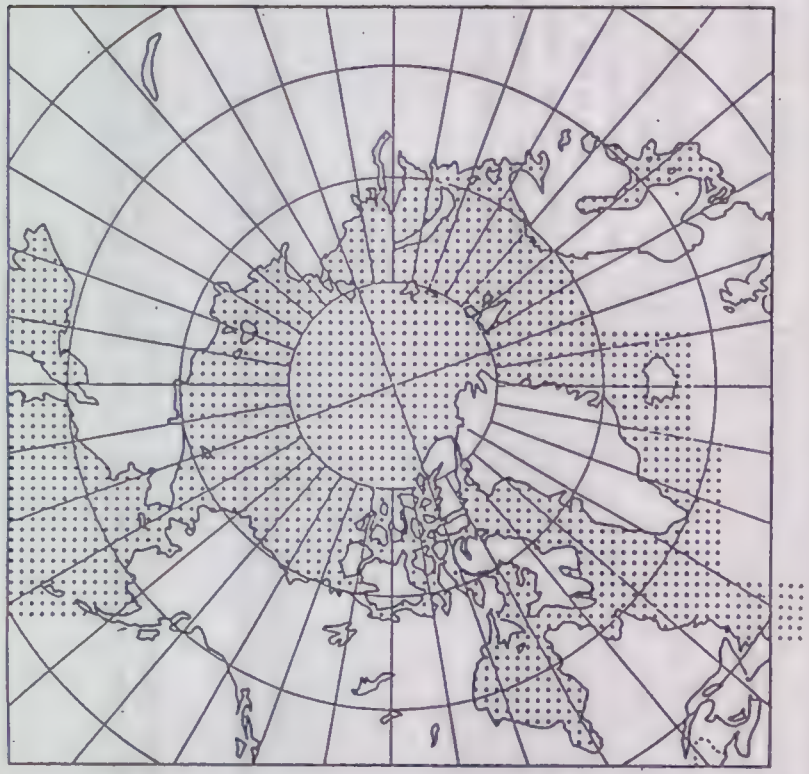

Fig. 1. The sea ice concentration grid.

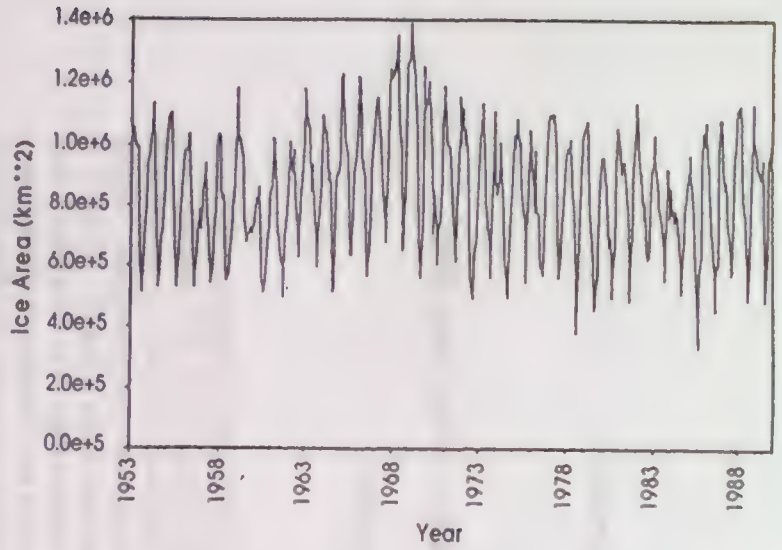

Fig. 2. Area covered by sea ice at the end of each month of 1953-1990 in longitudinal sector (0°-40°W) of Greenland and Iceland.

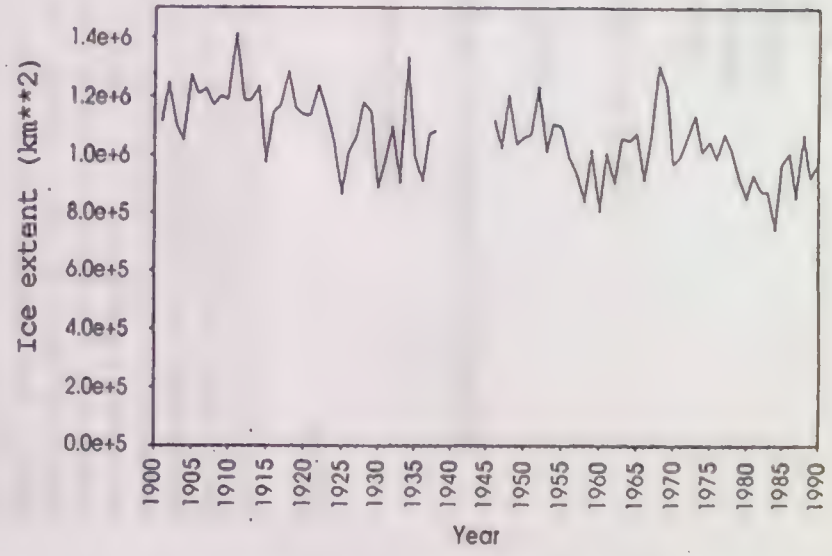

Fig. 3. Ice extent at the end of April, 1901-1990, in longitudinal sector (0 -40 W) of Greenland and Iceland.

Global Precipitation and Surface Temperature Datasets

Mike Hulme
Climatic Research Unit
University of East Anglia
Norwich NR4 7TJ

(tel: 01603 593162; fax: 01603 507784)

Paper prepared for the:

Workshop on Simulations of the Climate of the Twentieth Century using GISST

Hadley Centre, 28-30 November 1994

Abstract

For surface climatologies to be of greatest use in climate modelling studies their characteristics should ideally include the following: gridded on a model-compatible grid; possess mean and variance (time series) statistics; and describe known time periods. For precipitation and mean temperature, a number of climatologies exist (see Table), although not all of these possess the above three characteristics. Jaeger for example, is gridded at 4° by 5° resolution, but contains no information about variance. CLIMAT is gridded at 10' resolution for global land areas, but is only loosely related to the 1941-60 period; it also contains no information about variance. The Climatic Research Unit have constructed precipitation (Hulme, 1994) and mean temperature (Jones, 1994) climatologies which *do* possess the characteristics described above. The precipitation climatology (CRU0093) is gridded at 2.5° by 3.75° resolution (the Hadley Centre GCM grid) and possesses monthly time series for the period 1900 to 1993 thus enabling different time periods to be extracted and variance statistics to be calculated (e.g. see Figure). This climatology does not, however, include ocean areas, nor are adjustments for gauge undercatch included. For ocean areas the climatology of Spencer (1993) for the tropical oceans covers the period 1979 to date and a tropical precipitation climatology using OLR data for the period 1974 to date has been constructed by CRU. Other related activities include the Global Precipitation Climatology Project (GPCP) which has embarked on a mission to construct a global (land and ocean) climatology for the period 1986-95, combing both conventional surface observations and satellite-derived estimates (Huffman *et al.*, 1994).

Higher resolution limited-area models will require higher resolution climatologies against which to compare their simulations. Legates & Willmott and CLIMAT exist at 0.5° and 10' resolutions, respectively, for mean temperature and precipitation (CLIMAT also includes cloud cover). New work in CRU has established a 1961-90 climatology for European land areas, also at 0.5° resolution, but this encompasses a larger ensemble of nine surface climate variables (Hulme *et al.*, 1994). Time series for mean temperature and precipitation are also supplied with this climatology. Work is now proceeding to extend this project to all global land areas, thereby establishing the most comprehensive land surface climatology yet produced.

References:

Hulme,M. (1994) Validation of large-scale precipitation fields in General Circulation Models in, **Global precipitation and climate change** (ed. Desbois,M.and Desalmand,F.), D.Reidel, Dordrecht (in press)

Hulme,M., Conway,D., Jones,P.D., Jiang,T., Barrow,E.M. and Turney,C. (1994) A 1961-90 climatology for Europe for climate change impacts and modelling applications **Int. J. Climatol.** (submitted)

Huffman,G.J., Adler,R.F., Rudolf,B., Schneider,U. and Keehn,P.R. (1994) Global precipitation estimates based on a technique for combining satellite-based estimates, raingauge analyses and NWP model precipitation information **J. Climate** (submitted)

Jones,P.D. (1994) Hemispheric surface air temperature variability - a reanalysis and an update to 1993 **J. Climate**, 7, 1794-1802

Spencer,R.W. (1993) Global oceanic precipitation from the MSU during 1979-91 and comparisons to other climatologies **J. Climate**, 6, 1301-1326

	Domain	Time period	Resolution	Gauge adjustments	Statistics
CRU0093	Land only	1900 to 1993	2.5° by 3.75°	No	Time series
Jaeger	Global	1931-60	4° by 5°	No	Mean
CLIMAT	Land only	1941-60[1]	10'	No	Mean
Legates & Willmott	Global	unspecified	0.5°	Yes/No	Mean
Shea	Global	1950-79	2.5°	No	Mean and s.d.
Spencer	Oceans	1979-92	2.5°	n/a	Time series
GPCP	Global	1986-1995[2]	2.5° (also 1° for land)	Yes/No	Time series

Table: Some characteristics of precipitation climatologies [[1]: not precise; [2]: only 1987 and 1988 has been released to date]

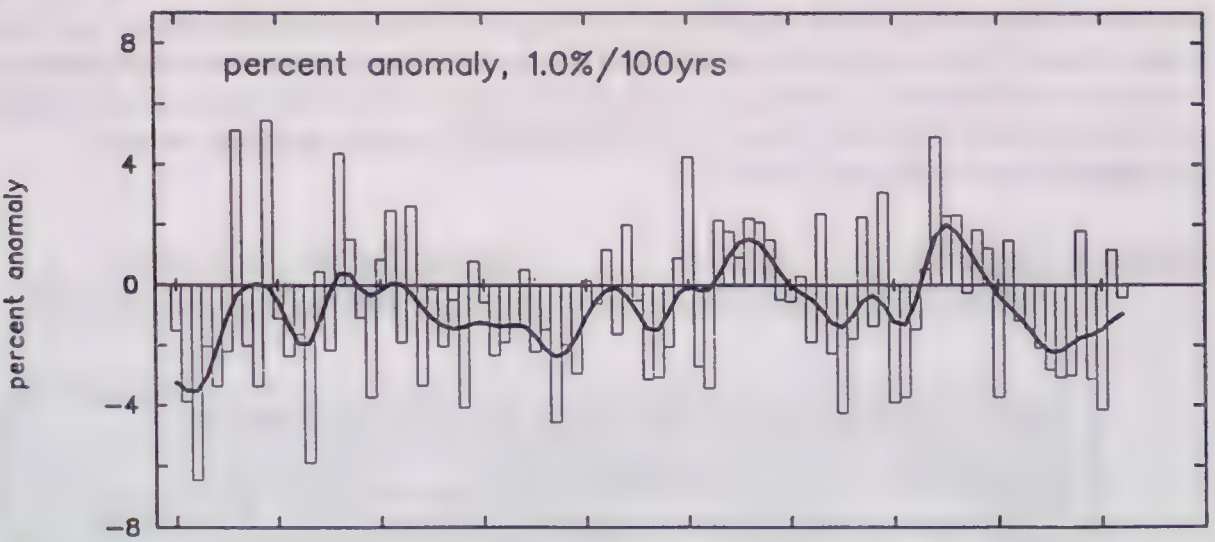

Figure: Terrestrial-mean annual precipitation (1900-1992) derived from the CRU0092 dataset. Trend shown is obtained from standard linear regression (sig. at 90% level).

A provisional new global mean sea level pressure data set

T A Basnett and D E Parker

Hadley Centre for Climate Prediction and Research.
Meteorological Office, Bracknell, U.K.

A global, observed, historical mean sea level (MSL) pressure data set is being developed in order to facilitate the validation of model results from simulations of the climate of the twentieth century and the interpretation of observed global and regional climate variations (Parker et al., 1994). The data set will be composed of monthly gridded values on a 5° resolution, dating back to 1871. It is being constructed from a blend of existing gridded data sets, provided by the Hadley Centre (UKMO), NCAR, Scripps Institution of Oceanography (SIO), PD.Jones and TML.Wigley (Univ. E. Anglia (UEA)) and RJ.Allan (CSIRO) (Table 1), plus data from observing stations.

The basic method of blending is to use the median of all available gridded values at each grid-point in each month. Observing stations' data are used to arbitrate in cases of serious disagreement or scatter between the gridded inputs.

This method was first tested on UKMO, NCAR and SIO northern hemisphere data dating back to 1951 and resulted in noticeable improvements relative to the original Hadley Centre data set, especially over Greenland and north-east Asia during the period 1981-1991. However, when the same technique was applied on a global scale using all the data sources available, discontinuities were generated across the geographical boundaries of the constituent data sources. These were mainly the result of attempting to combine data on differing resolutions. In particular the CSIRO 10° resolution data set gave underestimates in high pressure regions and overestimates in low pressure regions. For the Azores anticyclone, Figure 1 shows seasonal differences between values interpolated from each of three gridded data sources: NCAR (5° grid), UKMO (5x10° grid) and CSIRO (10° grid), and observed MSL pressure at Ponta Delgada, between 1900 and 1950. Further shortcomings include discrepancies over the Central Asian Massif and the lack of gridded MSL pressure data over the southern hemisphere oceans.

In an attempt to counter these problems a new observed grid-point data set based on a 5° grid is being created from ship and buoy data in the UKMO Marine Data Bank and in the Comprehensive Ocean-Atmosphere Data Set (Woodruff et al., 1987) and from monthly land station data. This should improve coverage and reliability globally and especially over the southern hemisphere. However, the existing blended MSL pressure data set is likely to be marginally acceptable in the meantime for model verification over much of the extratropical northern hemisphere, where the inputs have 5° latitude resolution; and over the tropics, where monthly average MSL pressure generally varies on geographical scales much larger than 10°.

References: Parker, D.E. et al., 1994. J.Geophys.Res., 99, 14373-14399.
Woodruff, S.D. et al., 1987 Bull.Amer.Meteorol.Soc., 68, 1239-1250.

Table 1: Data sources contributing to the new global dataset.

Data source	Area covered	Period	Resolution
UKMO	15N-90N	1873-1994	regular 5°lat.x10°long.
UKMO	Globe	1984-1994	regular 2.25°lat.x3.75°long.
NCAR	15N-90N	1899-1993	regular 5°lat.x long.
SIO	42.5S-72.5N	1951-1993	regular 5°lat.x 10°long.
CSIRO	60S-60N	1871-1989	regular 10°lat.x long.
Jones	15S-60S	1951-1985	staggered 5°lat.x 10°long.
Jones and Wigley	60S-75S	1957-1985	staggered 5°lat.x 10°long.

Figure 1: Differences between MSL pressures interpolated from gridded datasets and observed values for Ponta Delgada (37°44'N, 25°42'W), 1900 – 1950.

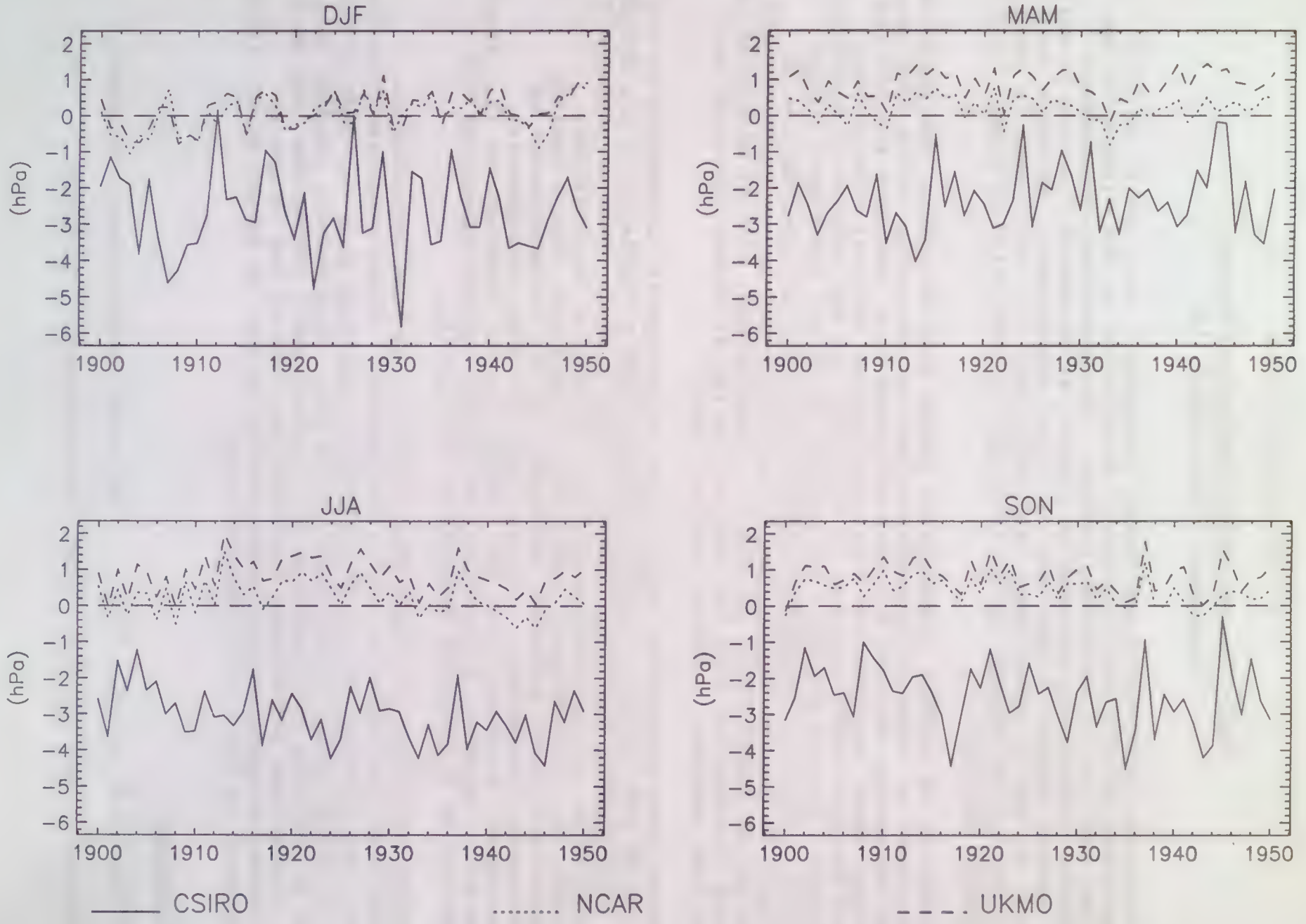

A provisional new radiosonde temperature data set

D E Parker and D P Cullum

Hadley Centre for Climate Prediction and Research.
Meteorological Office, Bracknell, U.K.

A complete, homogeneous radiosonde temperature data set is of major importance for the verification of simulations of the climate of the latter half of the twentieth century. The greenhouse-gas-induced climatic changes are expected to include stratospheric cooling as well as maximum warming in the tropical upper troposphere. Evidence for these changes in homogeneous radiosonde data will serve both to verify the atmospheric models and to reinforce the detection of human-induced climatic changes.

An archive of monthly temperatures (along with dewpoints, geopotentials and winds) at standard tropospheric and stratospheric levels from about 800 radiosonde stations has been developed from routinely transmitted monthly data, supplemented with published or national archive data. Many stations' data commence in the 1950s and the archive is continually updated. Quality controls are applied to detect and remove random errors. However, systematic biases affect the archive because of changes of instrumentation and of radiation- and lag-corrections, and changes of ascent times (eg Fig 1). Accordingly, station histories are being incorporated into the archive (eg Fig 2),though these are still far from complete. (Parker and Cox, 1995)

Future plans include the application of systematic adjustments on the basis of more complete station histories and a knowledge of the effects of instrumental and other changes. These effects would be assessed from comparisons of neighbouring stations straddling international boundaries, international radiosonde comparisons, checks against operational model analyses, and models of the thermodynamics of radiosonde instruments. Liaisons with the NOAA Comprehensive Aerological Reference Data Set (CARDS) project (Eskridge et al., 1995) and with a European Climate Support Network (ECSN) subproject are expected to bring major benefits to the archive.

Temperatures from the **unadjusted** archive have been converted to anomalies from stations' 1971-1990 averages. These anomalies have then been interpolated on to a 5° latitude x longitude grid for each of the 11 standard levels from 850 hPa to 30 hPa. This monthly gridded data set is perforce heterogeneous and geographically incomplete, but we plan to incorporate adjustments when they are derived and to use an eigenvector-based interpolation related to that of Rayner et al. (this workshop) to fill in the missing areas.

References

Eskridge,R.E. et al., 1995 Bull.Amer.Meteorol.Soc., in press.

Parker,D.E. and Cox,D.I., 1995 Int.J.Climatol., in press.

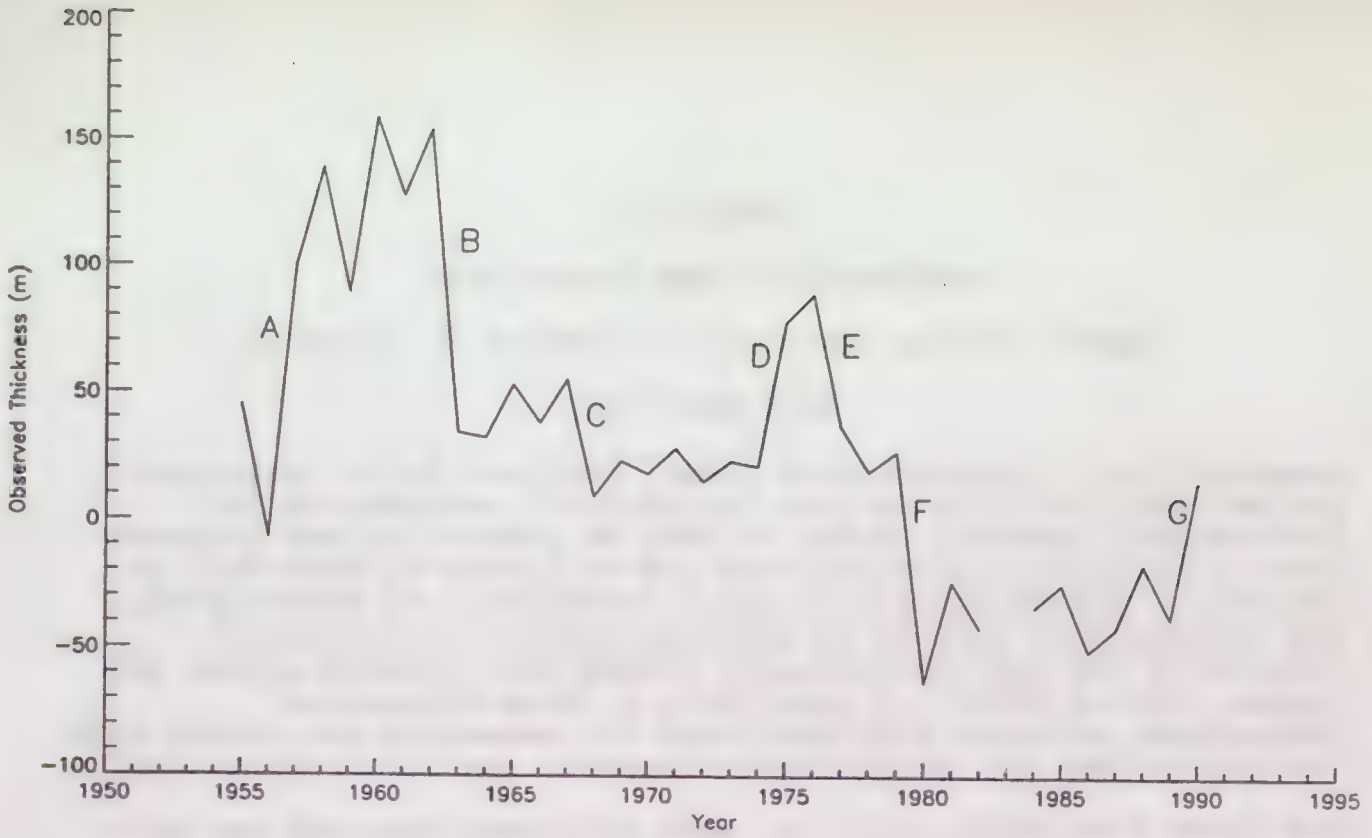

Fig 1 Observed thickness (m) of the 850-300 hPa layer at Bombay, relative to that at Madras, July. Most of the discontinuities A, B ... G can be related to changes of equipment (Parker and Cox, 1995).

Fig 2. Radiosonde instrumentation in use in Europe, 1960. The different symbols correspond to different sonde types as listed in Parker and Cox (1995).

Abstract

NCEP/NCAR 40-Year Reanalysis

Eugenia Kalnay (presented by Robert E. Livezey)

NCEP/NMC/NOAA

Reanalysis of a comprehensive global data set for a forty-year period from 1957 through 1996 is currently underway at the Evironmental Modeling Center of NCEP to provide global analyses free of analysis inhomogeneities and utilizing as much data as feasible. The reanalysis is being conducted with state-of-the-art systems that include an advanced physics, T62/28-level version of the NCEP global model driven with refined global SST fields (likely GISST for pre-1982), a three-dimensional variational analysis that precludes the necessity for normal mode initialization, and sophisticated complex quality control (CQC).

The first five years (1985-89) have been completed and the 40-year reanalysis is expected by the end of 1996 with interim mileposts which include 1985-1994 by April 1995 (which will be continued into the future through CDAS), 1979-1985 by September 1995, and 1957-1961 in 1996. This progress (more than one year per month) is possible because of preliminary QC conducted on one year of data at a time in the data preparation step. Data from a large number of international sources are processed and all outcomes (events) of the QC and analysis process are archived with the observations in Binary Universal Format (BUFR) in push-down stacks with accompanying meta-data so that the result of all processing steps are available to the interested user.

Three principal types of archives are being prepared for users: A comprehensive archive, an archive that includes time series of most variables and some diagnostics, and a one per year CD-ROM set containing a large variety of popular fields. The latter will be issued starting in early 1995. There will also be posted output in the NCEP public server. Copies of all archives will be distributed by NCAR, NCDC, and CDC.

Early diagnostics demonstrate that the reanalysis system is performing well. Although the system has excessive precipitation over the southeastern United States, the interannual variability of precipitation pattern is generally well represented over the globe.

Abstract

Reconstruction of Pre-1980 SST Fields

Robert E. Livezey, Richard W. Reynolds, T. Smith, and D. C. Stokes

NCEP/NWS/NOAA

A number of crucial tasks for the development of GCM-based seasonal prediction depend on simulation and prediction experiments that extend as far back as at least the 1950s. A major obstacle to success in these model runs is the quality of GISST- or COADS-based SST analyses that are the result of local "data-filling" procedures which fail to account for the rich covariance structure of the data. Such analyses are generally somewhat noisy and have been known to seriously misrepresent the character of some ENSO warm and cold events. Either of these problems can potentially compromise the value of simulation or forecast studies that utilize the analyses. UKMO and NCEP have been independently motivated to solve this problem and have come up with related but different solutions.

At NCEP the approach is very simple: The least-squares fit of a truncated set of EOFs to in-situ observation anomalies ocean basin by ocean basin constitutes the "reconstructed" analysis. The anomalies are taken with respect to a 10-year "climatology" from the GISST "filled" analyses centered on the map period being reconstructed. The EOFs are all-month modes derived from post-1981 NCEP OI monthly-mean SST analyses. The OI analyses are considered the "truth" for tests of the reconstructions. Theory predicts that the EOFs only have to crudely span the variance in earlier decades to be appropriate for application to reconstructions then. The number of EOFs used for reconstruction in each ocean basin is chosen *a priori* from examination of the eigenvalue curves.

Two criteria for success have been adopted, namely that the reconstructions do not degrade the in-situ analyses and that they not suffer from the problems that motivated their use. The most severe test of the procedure consisted of cross-validation of the 1980s -- with removal of 17 months of data at a time -- but with restriction of fitted data to densities and distributions slightly inferior to that available at corresponding times in the 1950s. It was evident from these and other tests that the reconstruction procedure achieves all of its objectives. In one spectacular example a recently-established cold tongue along the equator in May 1988 that was completely missed by the in-situ analysis was analyzed with a sizable fraction of its amplitude by the reconstruction procedure. Two ideas that have been tested and did not lead to obvious improvement were use of extended EOFs or global EOFs. To extend the procedure to pre-1950s we will test a fitting procedure that employs screening regression of rotated EOFs.

Forcing the Hadley Centre model with GISST: Introduction and Seasonal Predictability

David P. Rowell

Hadley Centre for Climate Prediction and Research,
Meteorological Office, Bracknell, U.K.

The "Climate of the Twentieth Century" project at the Hadley Centre has three main aims: to understand the nature and mechanisms of climate variability, to validate models used for climate prediction, and to assess the potential for seasonal prediction. The project is also being extended to include climate change detection research. The cornerstone is ensembles of multi-decadal AGCM integrations, forced by the observed SST and sea-ice data described by Parker and Jackson (this volume). Using the so-called "first climate version" of the Hadley Centre global model (the same version as that submitted to AMIP in 1993), an ensemble of 6 runs from Oct. 1948 to Nov. 1993 has been performed.

In order to assess the relative importance of SST forcing on atmospheric climate variability, "Analysis of Variance" is applied to the ensemble of integrations. The basic approach is described by eg. Rowell et al. (1995, QJRMS, p669-704), and essentially separates the total variance of some time-averaged quantity (σ^2_{TOT}) into two components, one due to oceanic (SST and sea-ice) forcing (σ^2_{SST}), and the other due to the random chaotic variations which are purely internal to the atmosphere (σ^2_{INT}). The ratio $\rho = \sigma^2_{SST}/\sigma^2_{TOT}$ then describes the fraction of interannual climate variability that can be ascribed to oceanic forcing. ρ can also be viewed as a measure of the potential predictability of the system.

An example of the application of "Analysis of Variance", with values of ρ computed at each grid point, is shown in Fig.1. The largest influence of SSTs is not surprisingly over the tropical oceans, especially the Atlantic and East and Central Pacific. Land areas displaying high potential seasonal predictability in MAM are the entire northern coast of South America, the Indonesian Archipelago, and parts of Coastal Africa. Extra-tropical land areas with moderate levels of predictability include the southern and western United States, Southwest Asia, and southern Japan.

These maps of ρ provide only an 'overall' assessment of predictability; in reality, there may also be variations of predictive skill from year to year. Such interannual variability of predictability might arise in two ways: unusually large oceanic forcing in occasional years (this is best assessed on a case-by-case basis), and/or, unusually large or small chaotic variability in some years. The second of these factors is assessed here. The possibility that this may be important is best understood if the atmosphere is viewed as a system in which SST forcing alters the residence-probability of attractors which are fixed in phase space (rather than altering the locations of these attractors) (cf. Palmer, 1993, Bull. Am. Met. Soc., p49-65), and this then induces year-to-year variations of intraseasonal variability, and thus interannual variations of the 'robustness' across the ensemble of the seasonal mean response to SSTs.

We have therefore computed at each grid point the variance of seasonal rainfall across the ensemble for each simulated year. Consider the null hypothesis that at each location the population variances for all years are identical (ie. equal to σ^2_{INT}), and hence any year-to-year variability of the sample variances is due to chance. Under this null hypothesis, the sample variances (computed from the ensemble data) should then follow an F distribution, assuming that the internal variations (deviations from each year's ensemble mean) are sampled from a Gaussian distribution. Fig.2 shows the result of testing against this null hypothesis at each grid point, for MAM seasonal precipitation. Over most of the globe the null hypothesis is accepted. The only regions where it might be rejected are where the Gaussian assumption is invalid; mainly extreme arid regions. In these regions, the interpretation of Fig.2 should be treated with caution, although in fact an assessment of predictability in most of these areas is of little practical value. Thus, to summarise our findings on this topic, it seems that these runs show *no evidence for a statistically significant influence of oceanic forcing on the interannual variability of ensemble spread*. A caveat however, is that only very large interannual variations of ensemble spread could be detected with a 6-member ensemble; detection of more subtle variations, which are suspected to exist, must await the resources to create much larger ensembles.

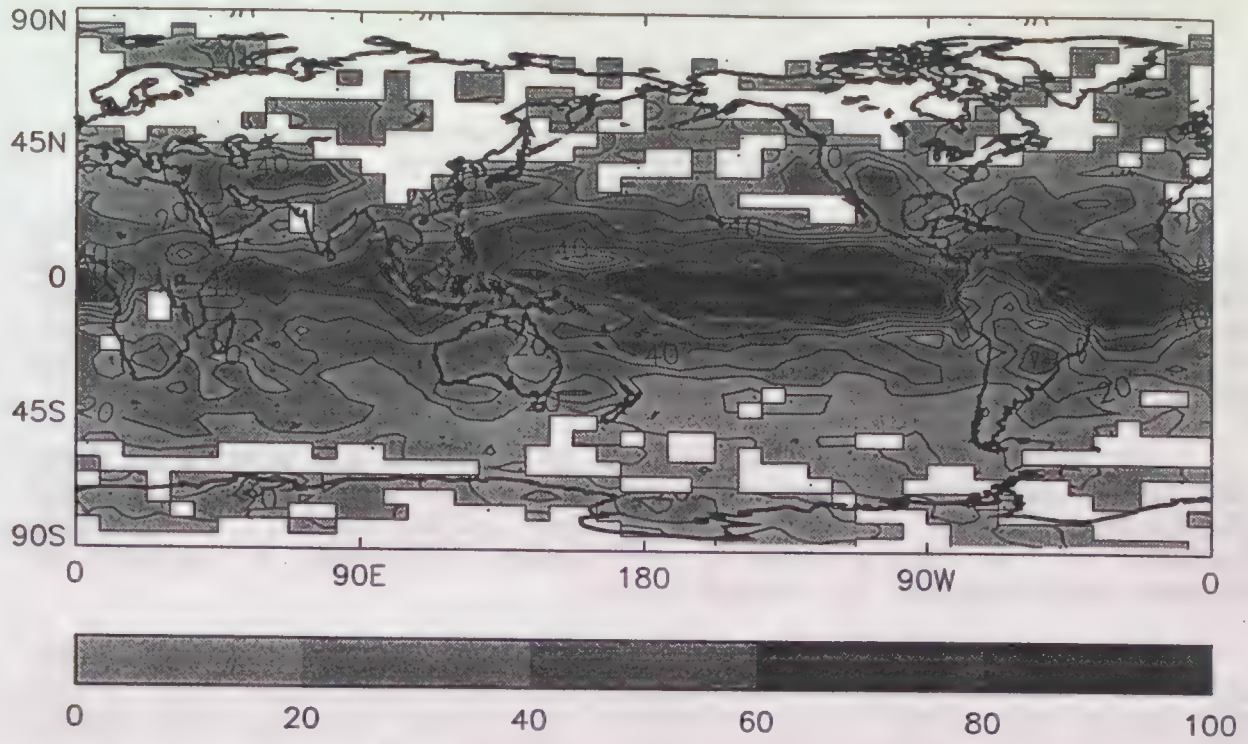

Fig.1 Percentage variance of seasonal (MAM) precipitation due to oceanic forcing, computed from an ensemble of 6 1949-93 runs. Data was first interpolated onto a 5°x7.5° grid (ie. double that of the basic model grid). Contour interval is 10%. White areas show where ρ does not significantly exceed zero at the 5% level, using an F test.

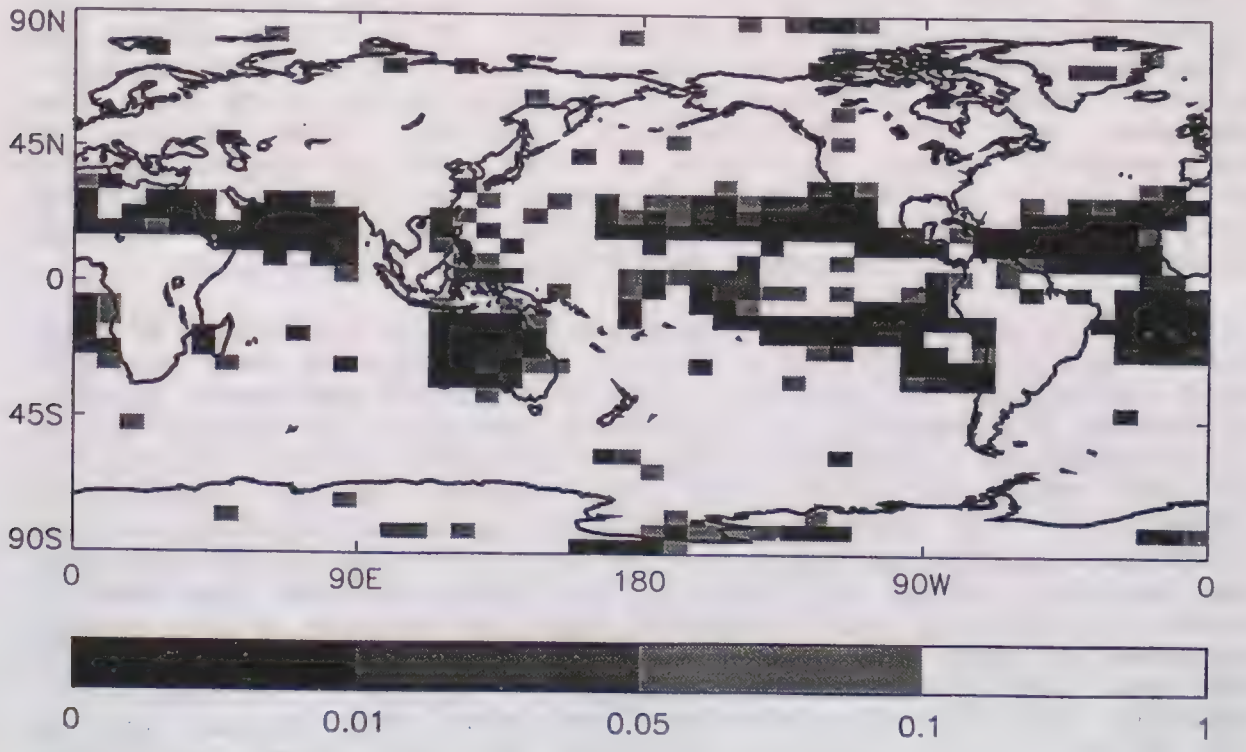

Fig.2 Probability (using a Kolmogorov-Smirnov test) that yearly ensemble spreads of MAM precipitation (on a 5°x7.5° grid) derive from an F distribution. See text for further detail.

Forcing the Hadley Centre model with GISST : Extratropical Response to ENSO.

A.Bevan, D.P.Rowell and C.K.Folland

Hadley Centre for Climate Prediction and Research,
Meteorological office, Bracknell, U.K.

As part of the 'Climate of the 20th century' project, an ensemble of 6 multidecadal integrations has been completed. In these integrations, which cover the period 1948-93, observed SST and sea ice data were used to force the Hadley Centre's AGCM. Further details of the project and integrations are given by Rowell (this volume).

Our ensemble of 6 integrations provides a new source of data for investigating one of the most closely studied of climate phenomena: the EL Nino / Southern Oscillation (ENSO). This study focuses on the extratropical influences of ENSO, a subject of increasing interest in recent years.

Seasonal composites of model anomalies have been created for several variables, in which seasons are selected according to the magnitude and sign of the observed Southern Oscillation Index (SOI). Figure 1 shows winter (DJF) composites of mean sea level pressure (MSLP) for a) high SOI years and b) low SOI years. Each composite is the average of 10 ensemble means, drawn from the years 1949-90. The out of phase relation between the patterns in figures 1a and 1b is striking, even in extratropical regions. Figure 1c shows those areas in which the two composites are significantly different from one another. While these regions are largely concentrated in the tropics, certain extratropical areas are also shown to be strongly affected by the phase of ENSO. The response over the Pacific/North American (PNA) region is particularly strong, and this is also seen in composites for precipitation and surface temperature (not shown). These ENSO related patterns are consistent with those of observational studies, such as Ropelewski and Halpert (1987, MWR 115).

With an ensemble of integrations, the influence of SSTs can be quantified. Figure 2 shows a time series of MSLP averaged over the North East Pacific, showing observed and model values. Following the analysis of variance technique of Rowell et al (1995,QJRMS,in press) it is found that SSTs account for 41.5 % of the model variance. The next stage of our work will investigate how much of the interannual variability of low frequency weather patterns can be accounted for by SST forcing, and how this varies according to the phase of ENSO. The results shown in figures 1 and 2 suggest that the largest extratropical response to ENSO may be found in the PNA region (influencing the PNA and 'Tropical Northern Hemisphere' modes of variability). However, the composites also indicate that other areas, such as the North Atlantic and New Zealand, may also have significant ENSO related signals.

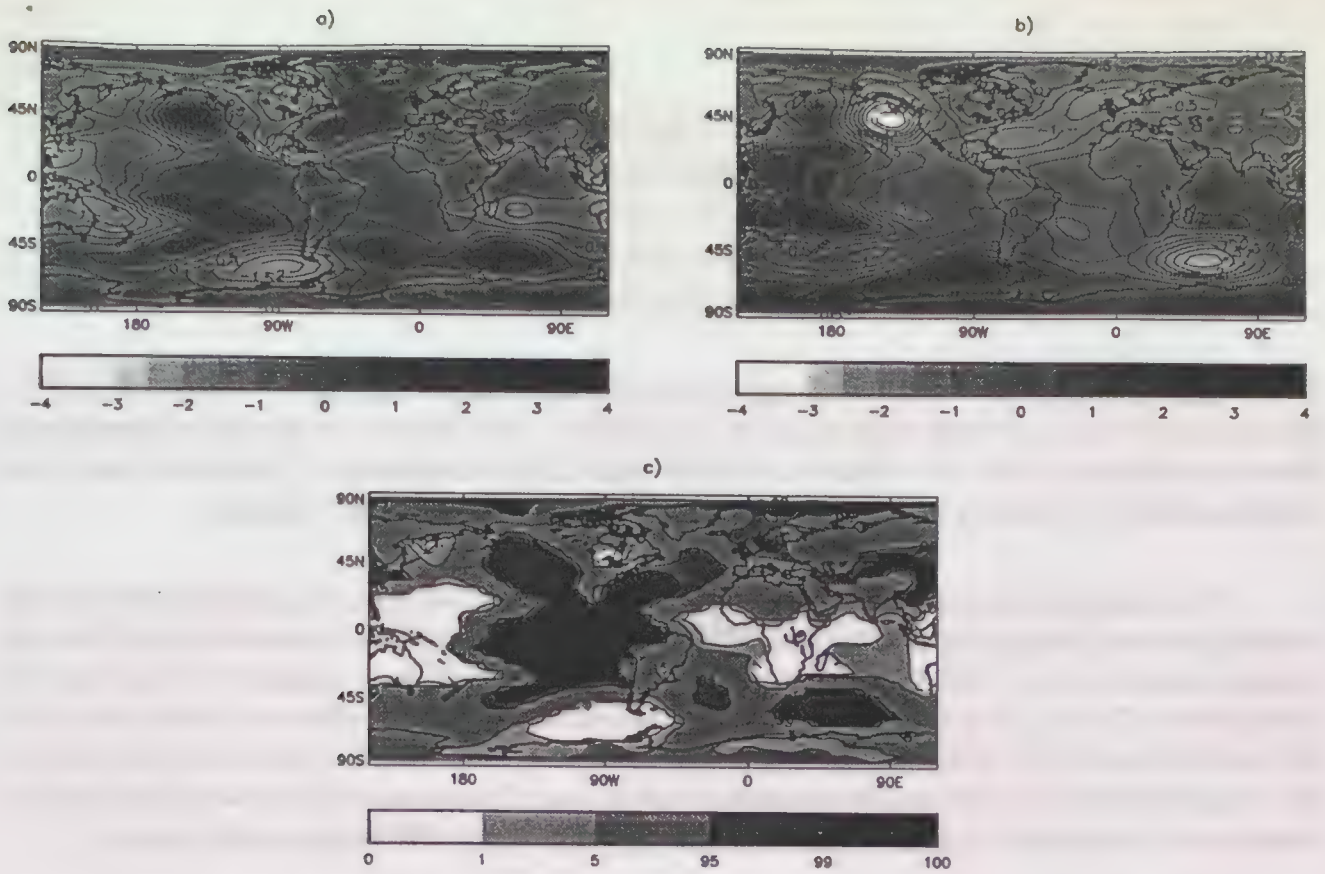

Figure 1: Composite winter (DJF) anomalies of model MSLP, each composite is the average of ensemble means for 10 selected seasons (6 integrations in ensemble). a) composite for high SOI years b) composite for low SOI years. c) areas in which a) and b) are significantly different from each other, calculated using a t-test at each model grid point.

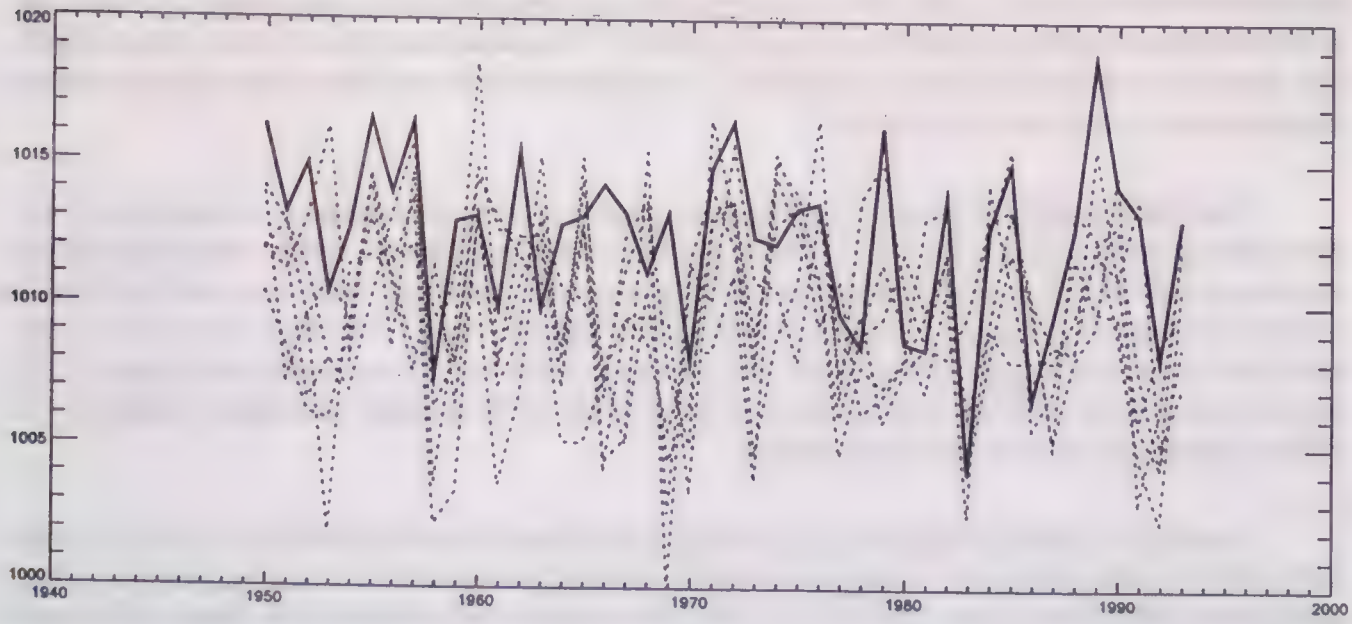

Figure 2. DJF MSLP averaged over the North East Pacific (125-165W, 27.5-62.5N). Heavy line is observed, dotted lines model values. The SSTs account for 41.5% of the variance.

Forcing the Hadley Centre Model with GISST European Variability

J.R. Davies, D.P. Rowell, C.K. Folland
Hadley Centre for Climate Prediction and Research,
Meteorological Office, Bracknell, Berks RG12 2SY

This investigation uses the results of an ensemble of 6 runs of the Hadley Centre 2.5x3.75° 19 level model for the years 1948-1993 forced by the GISST 1.1 SST and sea-ice data set as described by Parker and Jackson (1994, this volume) and with fixed CO_2 concentrations. The runs are part of the Climate of the 20th Century project; for more information see Rowell (this volume).

The seasonal climatologies for the ensemble of 6 runs have been compared to observed climatologies over Europe covering the area 30W to 50E and 30N to 70N. Basnett-Parker (1994, this volume) data has been used for mean sea level pressure (MSLP) and Legates-Willmott used for precipitation. The spatial correlations of the observed versus modelled patterns for MSLP vary from 0.74 in MAM to 0.97 in JJA and SON. For precipitation, they vary from 0.54 in MAM to 0.69 in JJA. The main deficiencies in the model climatology are a lack of penetration of the westerlies into N.E. Europe and Scandinavia in all seasons and a lack of precipitation in W.Europe in all seasons.

The variability of the model and observations has been studied by calculating unrotated covariance EOFs of area weighted monthly anomalies for the region 30W to 30E and 30N to 70N. Figures 1 and 2 show the first EOFs for the observed and modelled MSLP data sets in DJF. Both represent the North Atlantic Oscillation, and explain 34% and 27% of the total variance respectively. The spatial correlation between them is 0.97. The second observed and modelled EOFs explaining 21% and 13% of the variance respectively are shown in figures 3 and 4. The spatial correlation between these is 0.68. The third observed EOF and fourth modelled EOF (explaining 13% and 10% of the variance and not shown) have a spatial correlation of 0.64.

The predictability of the model has been investigated using the technique of analysis of variance (Rowell et al., 1995, QJRMS, in press). Applied to the ensemble of 6 runs, this estimates the fraction of total variance caused by external forcing, ρ ($= \sigma^2_{SST} / \sigma^2_{TOT}$), while the remainder of the variance is assumed to be caused by chaotic internal variability. Figure 5 shows ρ for modelled DJF MSLP in the European region. Calculated values are mostly low over Europe and a peak value of 19% is seen over the SW tip of the British Isles in DJF. A value of 7% or above indicates a probability of 95% or greater that external forcing is present.

Finally, the modelled and observed anomalies have been correlated year by year for the period 1950-1993. Figure 6 shows the correlation of the the ensemble mean MSLP with observations at each grid point in DJF over the area 30W to 30E, 30N to 70N. High values indicate skill. Some skill is seen in the British Isles and western Europe, where the analysis of variance also showed higher values. This indicates that for this period and over this region, not only is the model responding consistently to SST/sea-ice forcing, but it seems to be reproducing the correct teleconnection patterns and so showing useful skill. In MAM and SON, the analysis of variance (not shown) has values of ρ up to 20% for south eastern Europe. However, no significant skill is seen in the correlation with observations for these seasons, suggesting that incorrect teleconnections are present for these seasons.

Figure 1: Model EOF1 (MSLP). 6 runs DJF 1950 to 1993 (normalised).

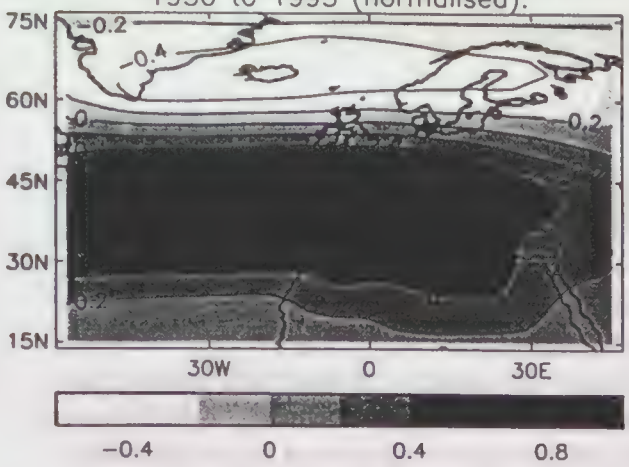

Figure 2: Observed EOF1 (MSLP). DJF 1950 to 1993 (normalised).

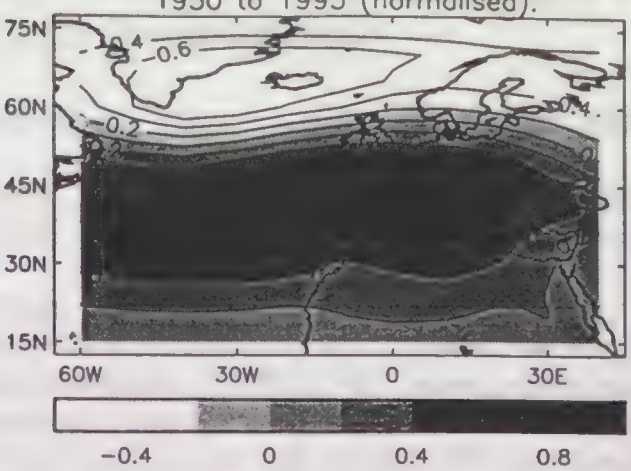

Figure 3:Model EOF2 (MSLP). 6 runs DJF 1950 to 1993 (normalised).

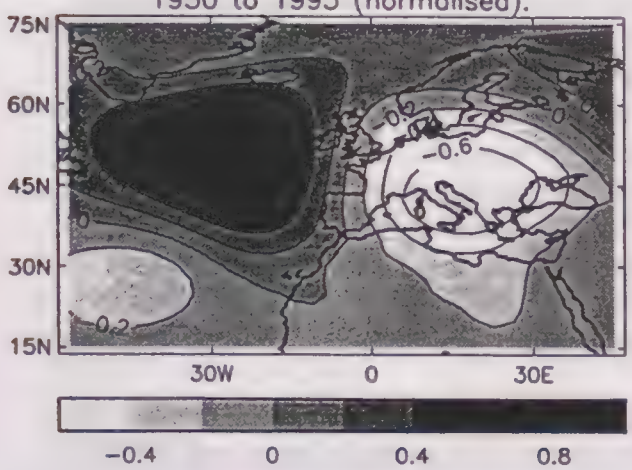

Figure 4: Observed EOF2 (MSLP). DJF 1950 to 1993 (normalised).

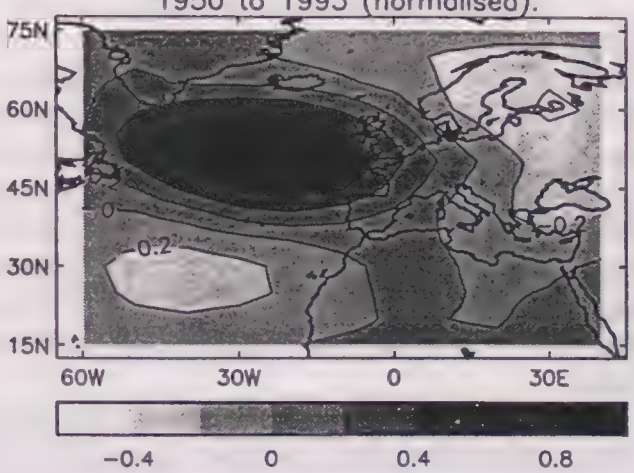

Figure 5: Percentage of total variance explaine by external SST/sea ice forcing. DJF 1950 to 1993

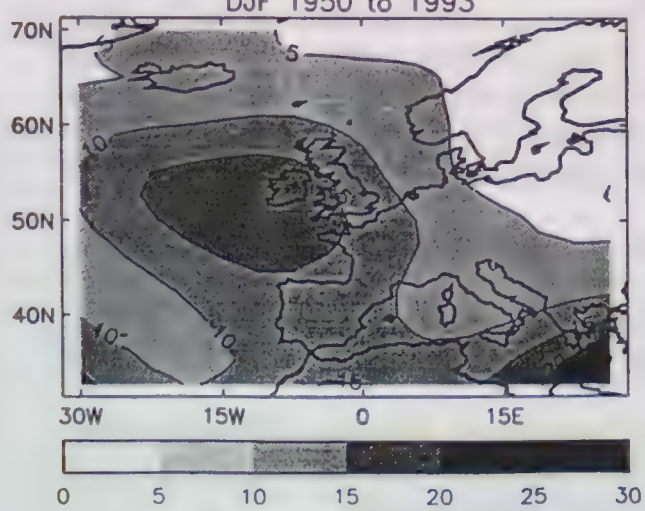

Figure 6: Correlation between ensemble mean of 6runs and observations DJF 1950 to 1993'

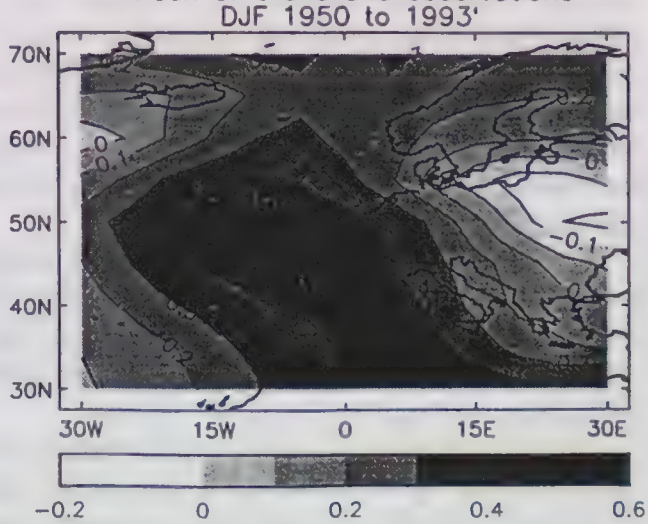

Forcing the Hadley Centre Model with GISST: Interannual Variability of African Wave Activity

C.D. Thorncroft and D.P. Rowell

Department of Meteorology
University of Reading, Reading, U.K.

Hadley Centre for Climate Prediction and Research
Meteorological Office, Bracknell, U.K.

Tropical convection is an extremely important part of the general circulation of the atmosphere and therefore clearly needs to be well represented in climate models. Observations indicate that tropical convection is often organised on synoptic scales and smaller, for example on the synoptic scale, easterly waves are present at various locations in the tropics including Africa (e.g. Reed et al 1977, MWR), the Caribbean and the Pacific. Since there is known to be considerable interannual variability associated with the tropical West African rainfall and since much of this rainfall in the Hadley Centre's 'Climate of the Twentieth Century' GCM integration (see Rowell, this volume) is associated with African easterly waves, the aim of this study is to examine the nature of the waves and their interannual variability.

Figure 1 is a summary of the interannual variability of the easterly wave activity (as determined by the variance of 850mb meridional wind), easterly wave rainfall and the seasonal rainfall between 1949 and 1990 from one of the Hadley Centre integrations (with horizontal resolution 2.5 x 3.75 degrees) and for two different geographical regions. For the Guinea Coast it can clearly be seen that the waves and their associated rainfall are well correlated with the seasonal rainfall anomaly. The correlation between the seasonal wave activity, as measured by the variance of the 850mb wind, and the seasonal rainfall anomaly is in fact 0.94. The same cannot be said for the Sahelian region where the correlation coefficient is close to zero. It is clear from this figure that there exists considerable interannual variability in the wave activity and that the rainfall associated with them is important for determining the seasonal rainfall over the Guinea coast but not the Sahel.

Six years from this GCM integration have been chosen for closer study. The years 1961, 1963, 1972, 1974, 1977 and 1980 have been chosen as they exhibit different wave and seasonal rainfall characteristics. The contrasting nature of two of these years is indicated in Fig. 2 which show time series at (15N,0W) for July to September 1961 and 1980, of 850mb meridional wind and daily convective precipitation. The wave signature in the meridional wind for 1961 is striking with waves in August reaching amplitudes of up to 10m/s and convective rainfall of 10mm/day or more. The daily convective precipitation can clearly be seen to vary at the wave timescale. Interestingly, at this latitude, the convective precipitation is often associated with northerlies, which may indicate that ascent ahead of the trough is crucial to the triggering of convection despite advection of drier air. In 1981 the wave signature can be seen to be much weaker with maximum meridional winds of only 5m/s, and in this particular year, only one wave event has significant convective rainfall.

Longitudinal variations associated with the waves are indicated in Fig. 3 which show Hovmoller plots of the southerly wind at 850mb and 10N. There are marked differences between 1961 and 1980. The waves in 1961 not only have a larger amplitude, but can also be seen to have longer tracks with better organised waves over the Atlantic. This has important consequences for the interannual variability of tropical cyclones.

Further detailed analysis of the waves in individual years is necessary. This will include examining the waves in a limited area model run at 50km horizontal resolution. An examination of observed interannual variability of easterly wave activity is also planned.

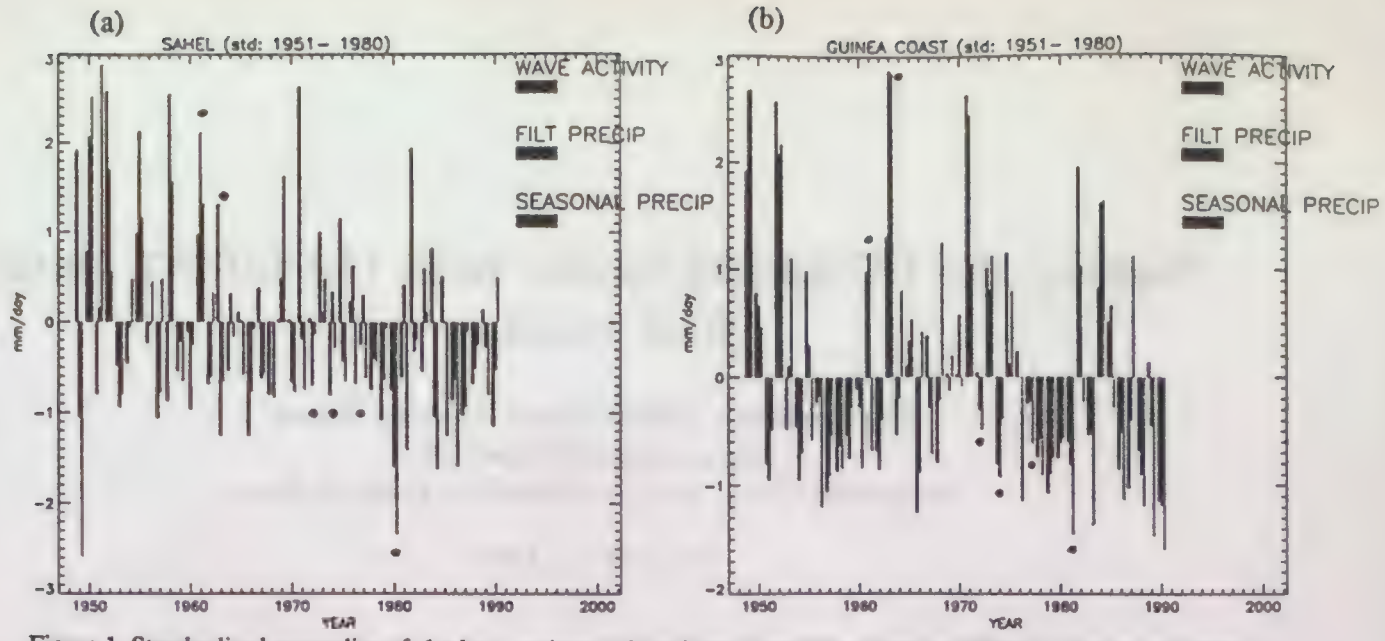

Figure 1. Standardised anomalies of: 1st bar - variance of the filtered meridional wind at 850mb on the west African coast, 2nd bar - variance of filtered precipitation for (a) the Sahel and (b) the Guinea coast and 3rd bar - seasonal precipiation anomaly for (a) the Sahel and (b) the Guinea coast. A 2.5-5 day filter was used to isolate the waves. Dots indicate the years chosen for closer examination.

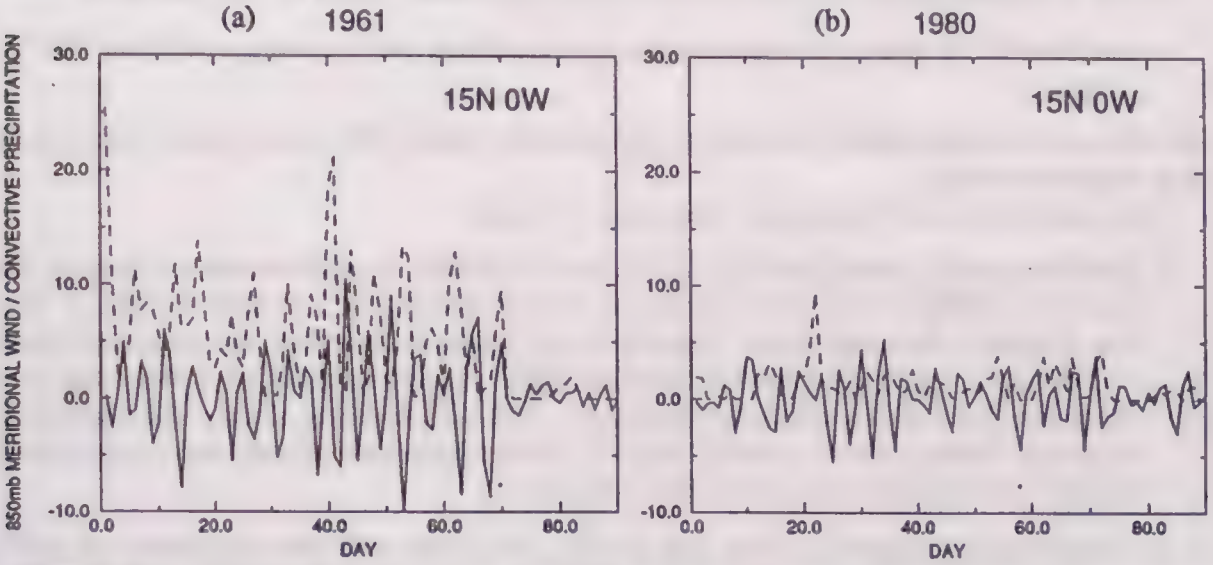

Figure 2. Time-series of unfiltered meridional wind (m/s) and convective precipitation rate (mm/day) at a gridpoint for 1961 and 1980. The solid and dashed lines are the meridional wind and convective precipitation respectively.

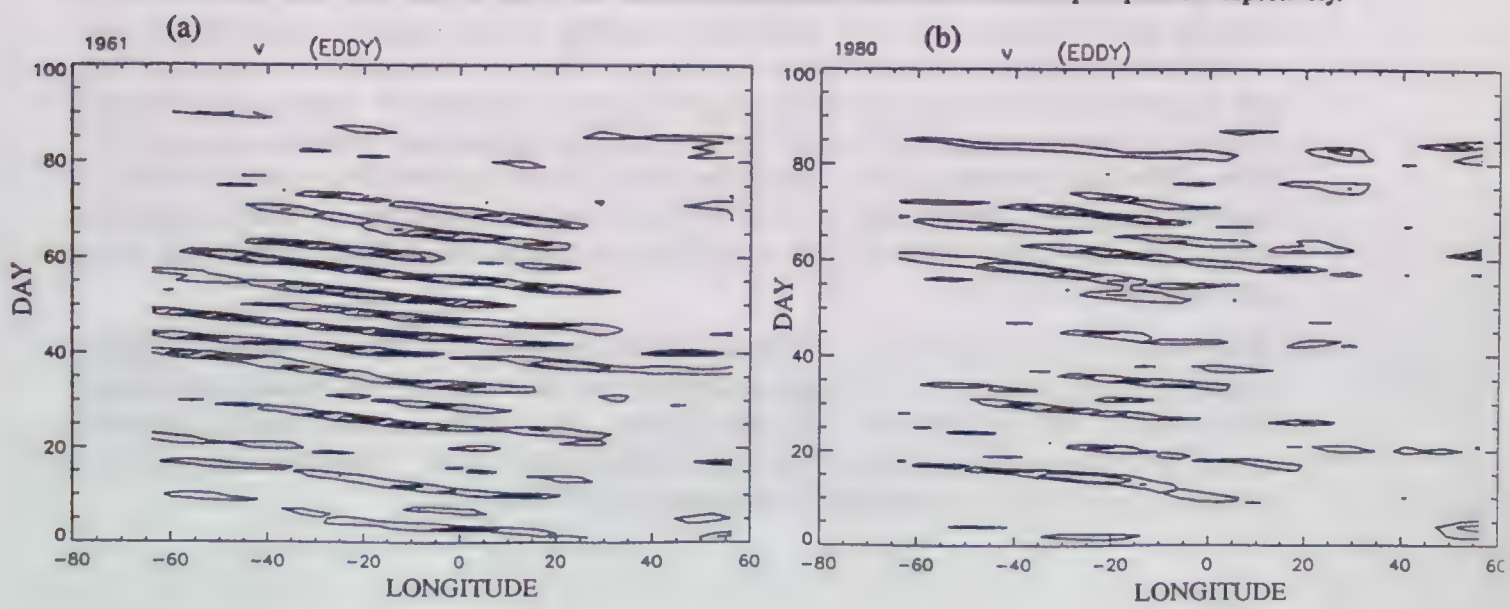

Figure 3. Hovmoller plots of 850mb eddy southerlies (seasonal cycle subtracted) at 10N (unfiltered) for July to September and for 1961 and 1980. Contours are 2, 4, 6, 8 and 10m/s. For clarity northerlies are not included.

Forcing the ECHAM3 model with the GISST data: first results

Andreas Hense, Ulrich Römer, Thomas Heinze
Meteorologisches Institut
Universität Bonn, Auf dem Hügel 20, D-53121 Bonn

October 21, 1994

It is intented to report on the first results of two (possibly three) runs simulating atmospheric variability during the period 1950 - 1989 using

- the ECHAM3 general circulation model (Roeckner et al. 1992) in T21 resolution
- and the GISST data set for the same period providing the boundary conditions SST and ice coverage.

All other external atmospheric forcings (solar radiation input, CO_2 concentration etc.) are kept at their standard values.

The presentation will highlighten three major points.

1. The intercomparison diagnostics: These are at first the ensemble means of pressure in mean sea level (PMSL) and rainfall including a discussion of the systematic error of PMSL in the Atlantic - European area. Secondly we will present the externally generated variability in PMSL as diagnosted from the multiple (two or three) runs. Time series analysis of the Southern Oscillation Index from simulations and observation as well as the analysis of precipitation times series in several tropical / subtropical areas (Sahel, India, Queenland, NE Brazil) will conclude this part of the presentation.

2. Variability of synoptiv activity: The second part of the talk will concentrate on special aspects of decadal variability of intramonthly transients. Variability of synoptic activity in the Atlantic - European sector is measured by an index series of extreme low pressure events over the North Atlantic. No SST generated variability can be found as the correlation between the runs and the observations is close to zero. On the other hand the level of activity, the amplitude of interannual variability and the spatial structure of occurrence of extreme pressure events is comparable between observations and simulations. The interaction of transient eddies and time mean flow in the extratropical Northern hemisphere (north of 20°N) is analysed using the Lorenz energy cycle in quasigeostrophic approximation. Observations and simulation agree quite well except for a trend in the observed data (1967-1989) which is not present in the simulations.

3. The last point to be presented is a comparison of the simulated and satellite observed (ERBE) global radiation balance at top of the atmosphere and the vertically averaged energy fluxes, which can be deduced from the radiation balance. The results indicate modeled poleward energy fluxes being $\simeq$ 15% larger than the satellite data suggest. There are also some discrepencies with respect to the zonal asymmetries of the fluxes.

Forcing the ECHAM3 model with the GISST data: Variability of Storm Tracks

Michael Christoph, Erich Roeckner
Max-Planck-Institut für Meteorologie
Bundesstr. 55
D-20146 Hamburg

A single run of the ECHAM3.2 general circulation model in high resolution (T42) is performed with the GISST data set (period 1949 - 1990) providing the lower boundary conditions.

The activity of storm tracks (as defined by regions of maximum high-frequency variance of geopotential height in 500 hPa) is investigated over large areas of the Atlantic and the Pacific on two different time scales:

- Interannual variability of winter-storm tracks (November - March)
- Seasonal cycle

The results are compared with those obtained from observational data (NMC-analyses, period 1946 - 1989) and from the ECHAM3.2 model forced with climatological SST data (AMIP, mean of 1979 - 1988).

It is found that the interannual variability of winter-storm tracks (as measured by the standard deviation from the long term mean activity) increases significantly using variable SST data compared to using climatological data (fig. 1). Deviations from observations are small (< 15%) and no longer significant. However, a strong non-linear trend in the observed activity with periods of approximately 22 - 24 years is not reproduced by either model version.

The main features of the seasonal cycle of storm track activity are a single maximum over the Atlantic in January and two maxima over the Pacific in the late fall and early spring (no figure). In both model versions the Atlantic maximum is simulated one month later than in the real atmosphere. The representation of the characteristic suppression of baroclinic wave activity in the Pacific area has improved in the model run with variable SST but the amplitude of the cycle is still too weak and the occurence of extremes not at the right time compared to the observations.

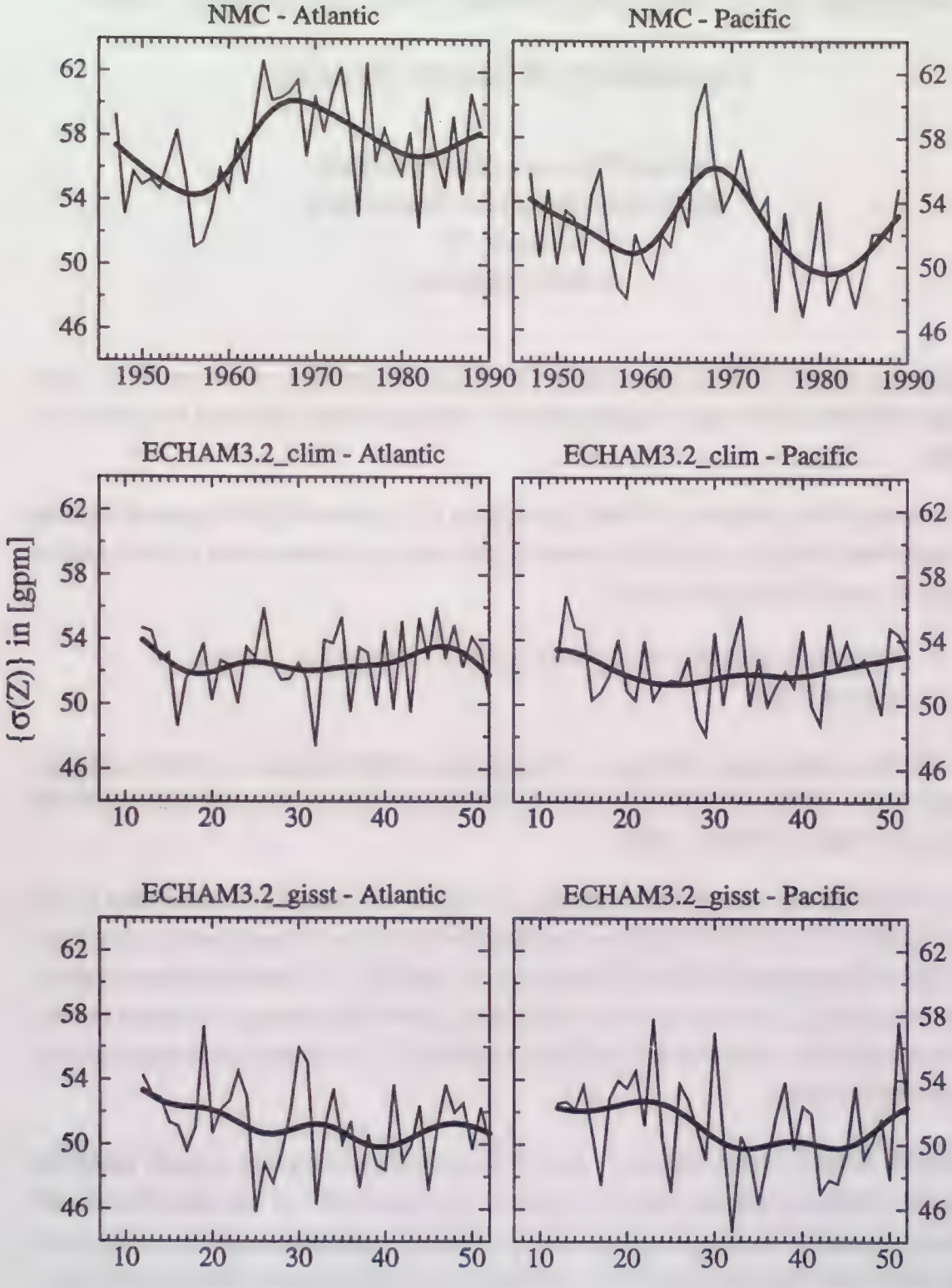

Fig. 1: Interannual variability of 500 hPa winter-storm track activity {σ(Z)} in [gpm].

Forcing the GFDL model with GISST

by W.F. Stern, K. Miyakoda, and J. Anderson
GFDL/ NOAA Princeton University

A 40 year simulation has been completed as a preliminary test. The model used for this test is the same as the one employed in the previous AMIP study, *i.e.*, GFDL/DERF (Stern and Miyakoda 1991; 1994) except for the resolution and the orography. The resolution in the present study has been reduced to T30L18. A "2-dimensional isotropic filter " has been applied to the orogrphy to reduce Gibbs Oscillations (Navarra et al. 1994), as opposed to the unfiltered mountains used in AMIP. The isotropic filtering may appreciably affect the precipitation distribution over India. In this regard, some results for this 40 year run will be presented.

Additionally, a new model is also being applied to GISST. This atmospheric model is used not only for the boundary forced run with GISST or AMIP but also for coupled model forecasts. The main focus of the coupled predictions is an accurate simulation of ENSO and the Asian monsoon. In this regard, some sacrifices have been made in the simulation of other elements of the circulation in order to produce improved simulations of El Niño and the monsoon.

This model differs from the earlier model in the following physical parameterizations: cumulus convection, shallow convection, cloudiness, roughness length over ocean, roughness length over land, surface hydrology, and surface albedo. The new model with the Arakawa-Schubert scheme has run with GISST from 1949 to about 1960 at present. Another version of this model with Moist Convective Adjustment will also run with GISST.

Eventually these simulations will be repeated nine times to study "reproducibility" similar to Stern and Miyakoda (1994) and also employ a statistical test suggested by Anderson (unpublished). One of the major objectives is to investigate the feasibility of predicting droughts over the U.S.

Forcing the BMRC Model with GISST

C.S. Frederiksen, P. Indusekeran, R.C. Balgovind and N. Nicholls.
Bureau of Meteorology Research Centre, Melbourne, Australia.

An ensemble of 5 multidecadal (1950-1991) simulations of the Bureau of Meteorology Research Centre (BMRC) Climate Model (BMRC v2.1) have been conducted. Each simulation has been initialised with different initial atmospheric conditions and forced by observed sea surface temperatures (SSTs) from the Global Ice and Sea Surface Temperature (GISST) dataset. The model is shown to have a reasonable climatology, with global precipitation and circulation features qualitatively similar to the observed in each of the four seasons. Correlations between modelled and observed SOI over this period are consistently greater than 0.8 for all 5 simulations.

In this paper, we concentrate on the Australian region and discuss the extent to which the BMRC model, forced by observed SSTs, is able to reproduce the observed interannual variability in Australian rainfall and its relationship with global SSTs and ENSO. While the model captures the mean annual cycle of Australian rainfall, it generally shows a dry bias. Time series (5 month moving average) plots of modelled and observed rainfall, averaged over the northeast (NE), southeast (SE), northwest (NW) and southwest (SW) quarters of the continent, are presented together with times series of modelled and observed SOI. For example, Figs.1(a) and (b) show the time series of NE rainfall (line) and SOI (shaded) from observations and the 5 run ensemble average. Both plots show a high correlation between rainfall and SOI (0.6 for the observed, and 0.57 for ensemble average). However, the correlation between observed and modelled rainfall is considerably lower at 0.38. For the SE, NW and SW regions the correlations between rainfall and SOI (observed, modelled) are (0.59, 0.52), (0.47, 0.5) and (0.26, 0.31), respectively, while correlations between observed and modelled rainfall are 0.26, 0.16 and 0.14, respectively.

We also present results from an EOF analysis of observed and modelled Australian rainfall for each of the four seasons. A comparison of the observed and modelled results show many qualitative similarities in both the structure of the EOFs and their corresponding time series. In each season, and for both the observed and modelled cases, the first 2 EOFs account for about 40%, or more, of the total variance in rainfall. Varimax rotation of the first 2 EOFs reveals 2 large-scale patterns of variation, with one centred over eastern Australia and the other a broad NW-SE band, centred over southern Australia. Figures 1(c) and (e) show, for example, the second rotated EOF for the observed and modelled cases, respectively, for JJA. Their close association with ENSO can be seen clearly when their time series are correlated with the observed SST time series (Figures 1(d) and 1(f), respectively). These figures show the typical Pacific Ocean structure of the SST anomaly pattern associated with ENSO. The other mode of variation is highly correlated with SSTs to the North/Northwest of Australia, in both cases, and with Indian Ocean SSTs in the observed case. Similar analyses of 6 multidecadal (1948-1993) simulations of the Hadley Centre Unified Model are also discussed and compared.

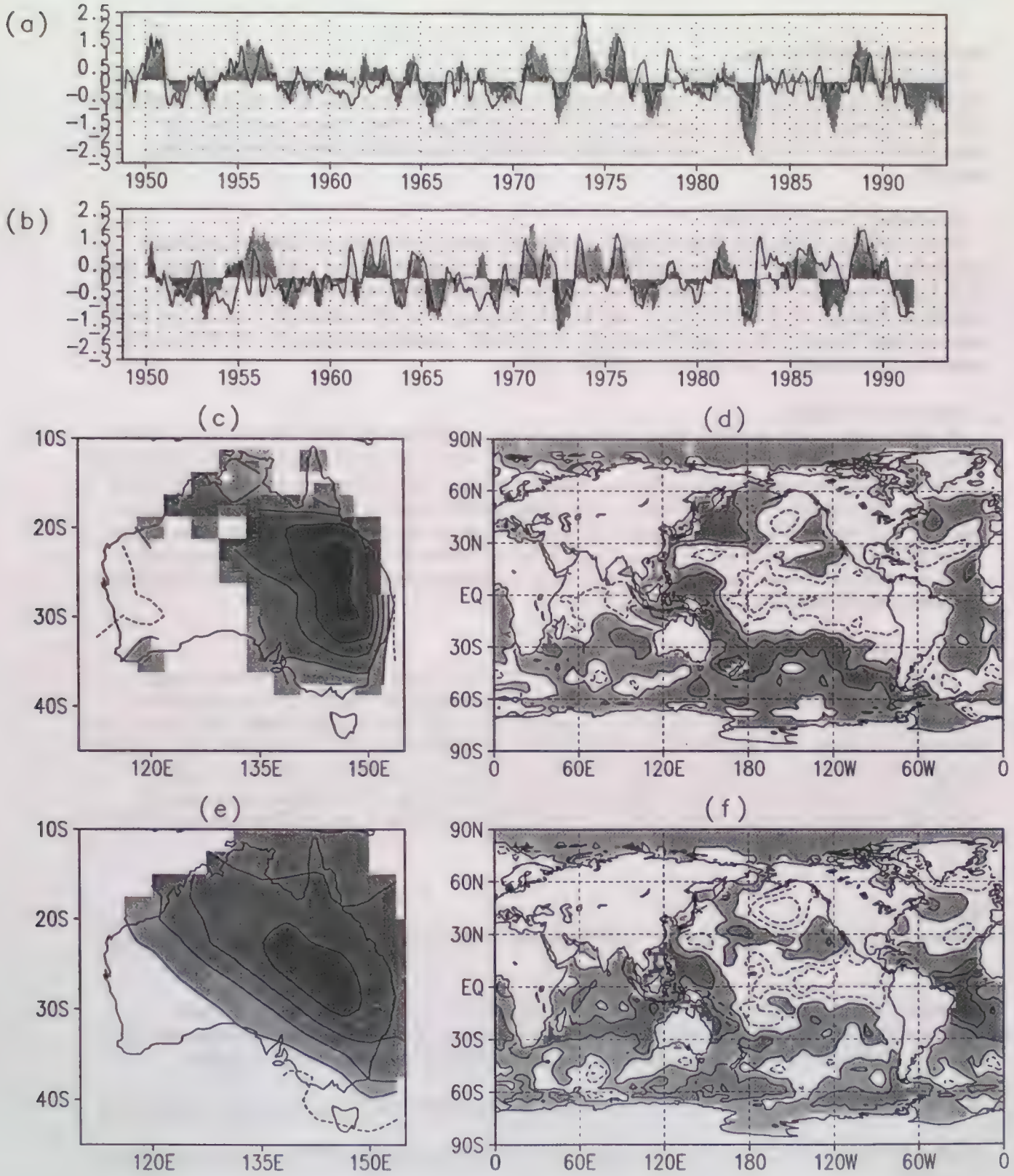

Figure 1: (a) Observed and (b) ensemble average NE Australian rainfall (solid line) against SOI (shaded); (c) second rotated EOF of Australian rainfall (JJA) and its correlation with observed SSTs (1950–1991); (e) and (f), as in (c) and (d) but for ensemble average of modelled rainfall.

Forcing the CSIRO model with GISST and MOHSST

I.N. Smith, B.G. Hunt and R.J. Allan
CSIRO Division of Atmospheric Research

Results using MOHSST data.

Multiple long term climate simulations have previously been performed using CSIRO4 (R21) and MOHSST data for the period 1950-1988. The results from these simulations have been analysed in terms of inter-decadal trends (Smith 1994a) and interannual variability (Smith 1994b). These studies form the background to a current long term simulation using CSIRO9(T63) and GISST data for the period 1871 onwards.

- Inter-decadal trends 1950-1988.

Major results from this study included the simulation of: cooling (warming) over northern (southern) hemisphere land masses; significant rainfall reductions over the Sahel region and evidence of increases over East Africa; a stronger Walker circulation; and inter-hemispheric trends similar to a boreal-winter type circulation. Features not simulated in this study include: the magnitude of the observed warming over land masses; abrupt changes in the circulation over the North Pacific as observed during the mid-1970s; and a trend towards anticyclonic conditions in the North Atlantic.

- Interannual variability

Ensemble mean (N=3) results for selected seasonal fields were subjected to EOF analysis and revealed dominant modes closely associated with ENSO. Comparisons with observations, where possible, reveal many similarities in structure and temporal behaviour providing evidence that a substantial amount of variance at the interannual time scale can be captured by atmospheric models forced by SSTs. Fig.1 shows the mslp mode - a close representation of the Southern Oscillation. However, the signals are strongest in the vicinity of the SST forcing and are relatively weak in remote locations where ENSO effects are important. This raises questions such as how much improvement can be achieved by improved models and how model-based seasonal climate predictions should be formulated.

GISST project

Australian rainfall is affected by, and can even be regarded as in index of ENSO. Late last century, severe drought episodes occurred in 1888 and 1896 while a prolonged La Nina episode spanned 1878 to 1880. Fig.2 shows evidence of the last two events in terms of the SOI and a Pacific Ocean index (Allan and D'Arrigo, submitted) while Fig.3 shows the SST anomaly pattern for SON 1888. A relatively high resolution model is being used (on an 8-processor machine, Rotstayn, in press) to generate results for the earliest available reconstructed SSTs (1871 on) with the aim of simulating some of these large scale events and, eventually, attempting a better understanding of inter-decadal fluctuations in the ENSO phenomenon. Some of the earliest results will be presented.

References

Allan, R.J. and R.D. D'Arrigo 'Persistent' ENSO sequences: How unusual was the recent El Nino. Submitted to Holcene.

Rotstayn, L.D. (in press) Modelling climate with a spectral GCM on a Silicon Graphics Symmetric Multiprocessor. In: Coming of Age- The use of parallel processors in meteorology. Proceedings of the Sixth ECMWF Workshop on the use of parallel processors in meteorology. World Scientific, Singapore.

Smith, I.N. (1994a) A GCM simulation of global climate trends 1950-1988. Journal of Climate,7(5),732-744.

Smith, I.N. (1994b) A GCM simulation of global climate interannual variability 1950-88. Journal of Climate (accepted).

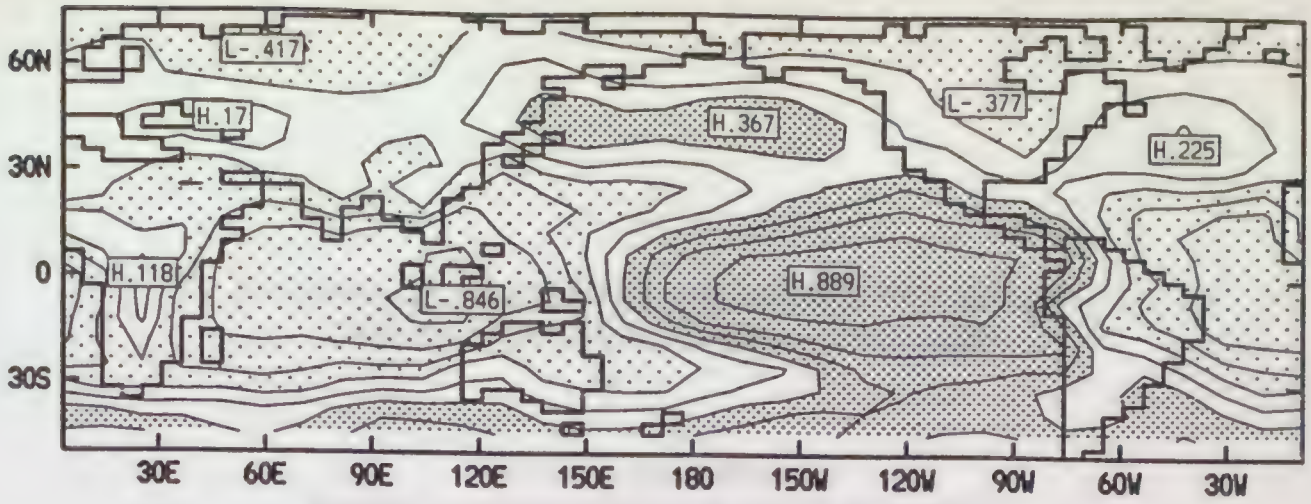

Figure 1. The leading EOF for mean sea level pressure based on the ensemble mean result from three climate simulations (1950-88). Contours represent correlations between the data and the associated time series. Heavy/light stippling indicates values greater/less than +.20/-.20. Contour interval is .20.

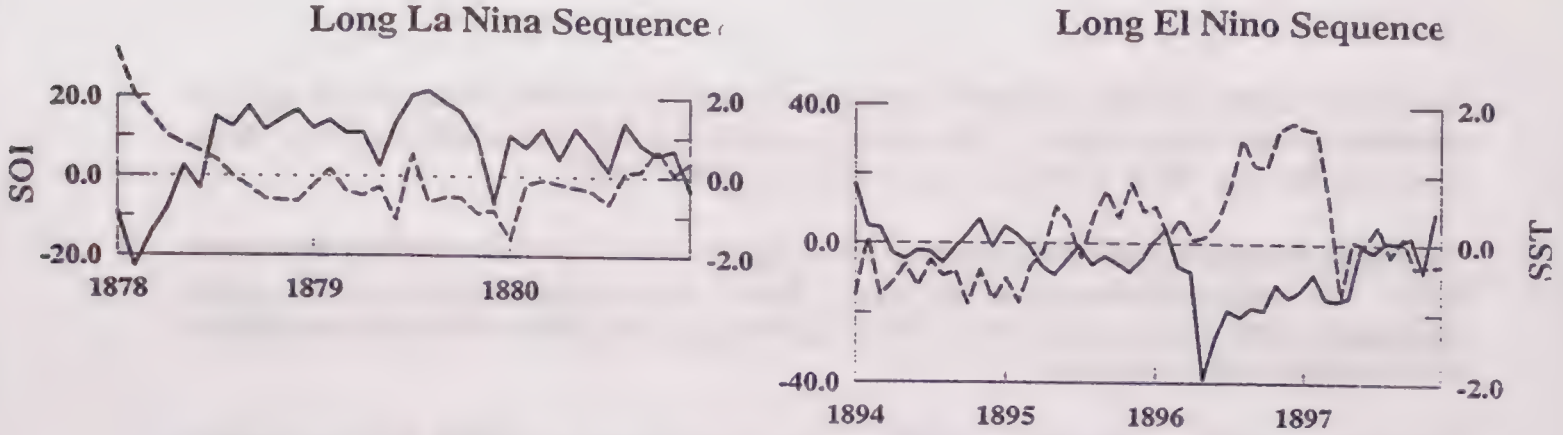

Figure 2. Southern Oscillation Index (SOI) (solid line) and a Pacific Ocean SST index (NINO3+4) (dashed line) for a protracted La Nina event and El nino event.

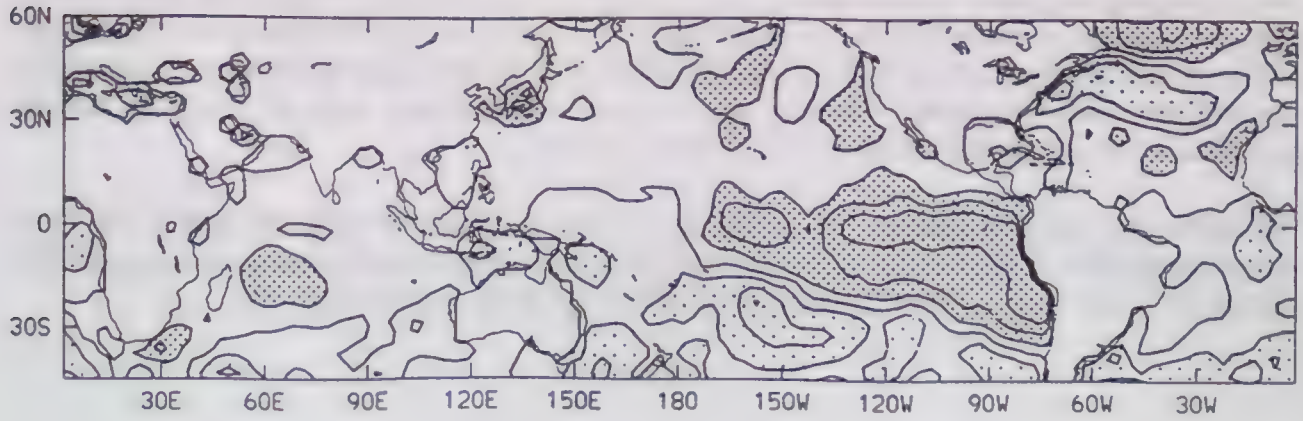

Figure 3. SST anomalies for September-November 1888. Anomalies computed with respect to the full (120+) year GISST data set. Heavy/light stippling indicates values greater/less than +.50/-.50 degC. Contour interval is .50 degC.

Simulation of atmospheric circulation with observed global SST and sea ice during 1949-1992.

J. Shukla and L. Marx
Center for Ocean-Land-Atmosphere Studies
4041 Powder Mill Road, Suite 302
Calverton, MD 20705-3106
U.S.A.

The COLA model has been integrated for 44 years using the monthly mean GISST data set provided by the Hadley Centre. The model resolution is T30 (18 levels), and the initial conditions are taken from a previous long integration of the model.

The model produces realistic simulations of the mean atmospheric climate including the annual cycle. The major deficiencies of the model include the incorrect location of the upper tropospheric ridge over the west coast of North America and insufficient interannual variability of the monthly mean circulation.

The magnitude of the interannual variability of the tropical monsoon rainfall, the Sahel rainfall and the northeast Brazil rainfall is the same as observed. However, the year-to-year changes in the Indian monsoon rainfall are not simulated correctly. The patterns of the extratropical response to warm and cold events in the equatorial Pacific are also comparable to the observations. However, the magnitudes of the simulated 200 mb height anomalies are only about half of the observed. The interannual variability of the Southern Oscillation (SO) and the global-mean surface air temperature over land is simulated extremely well compared to the corresponding 44 years of observations (Fig 1). Such a high degree of similarity between the observed and the modeled surface air temperature anomalies over land suggests that predictions of the global warming of land surface temperatures due to an increase in greenhouse gases, using the coupled ocean-atmosphere models, can be considered reliable only if it can be further established that the predicted SST anomalies are accurate.

We have also made another 10 year integration of the same model using the global SST data produced by CAC (OISST) (Fig. 2b). It is found that the tropical rainfall anomalies using OISST are closer to the observed MSU rainfall anomalies than those using GISST (Fig. 2a).

(Fig. 1.)

Annual Mean
Global Land Surface Temperature Anomalies

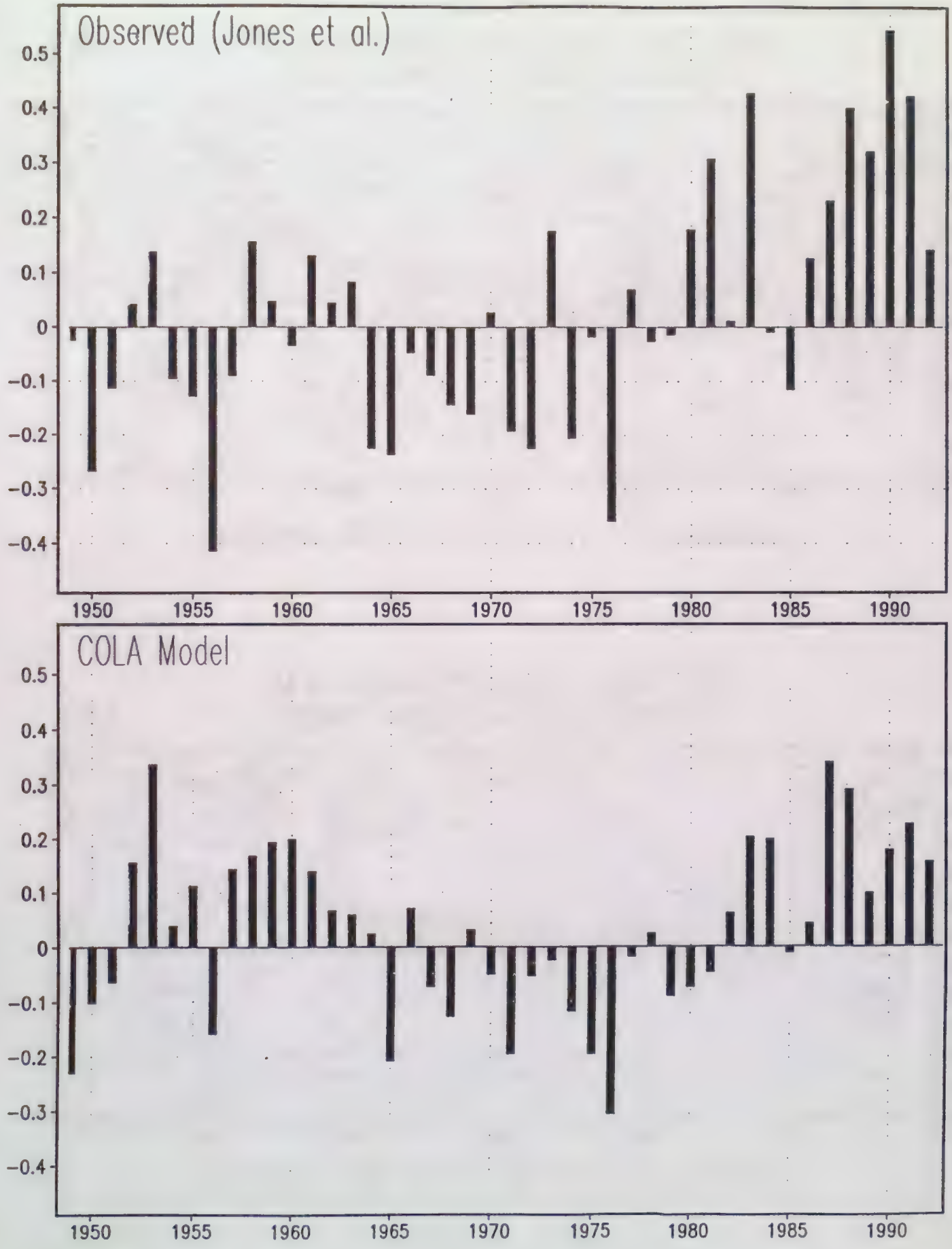

GrADS: COLA/IGES

Fig. 2

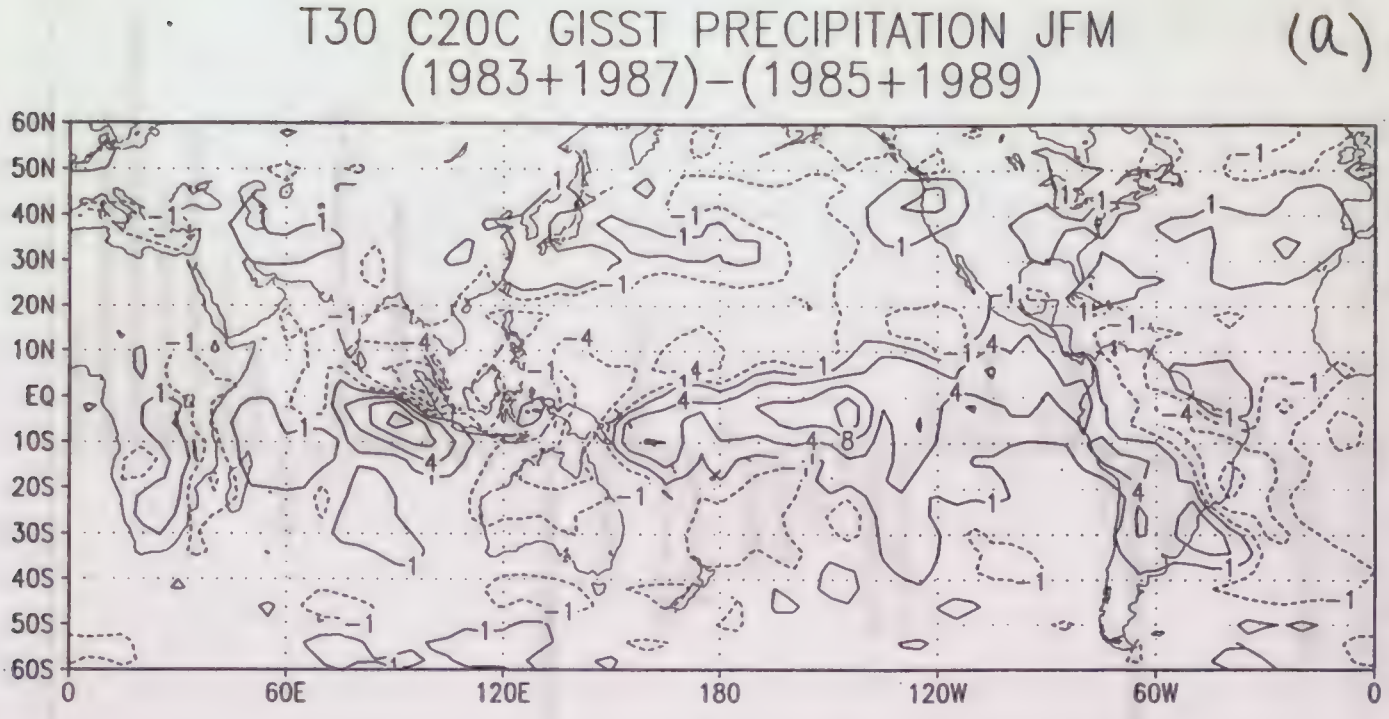
T30 C20C GISST PRECIPITATION JFM
(1983+1987)-(1985+1989)
(a)
60N
50N
40N
30N
20N
10N
EQ
10S
20S
30S
40S
50S
60S
0
60E
120E
180
120W
60W
0
contour +/- 1 4 8 12 16 20 mm/day

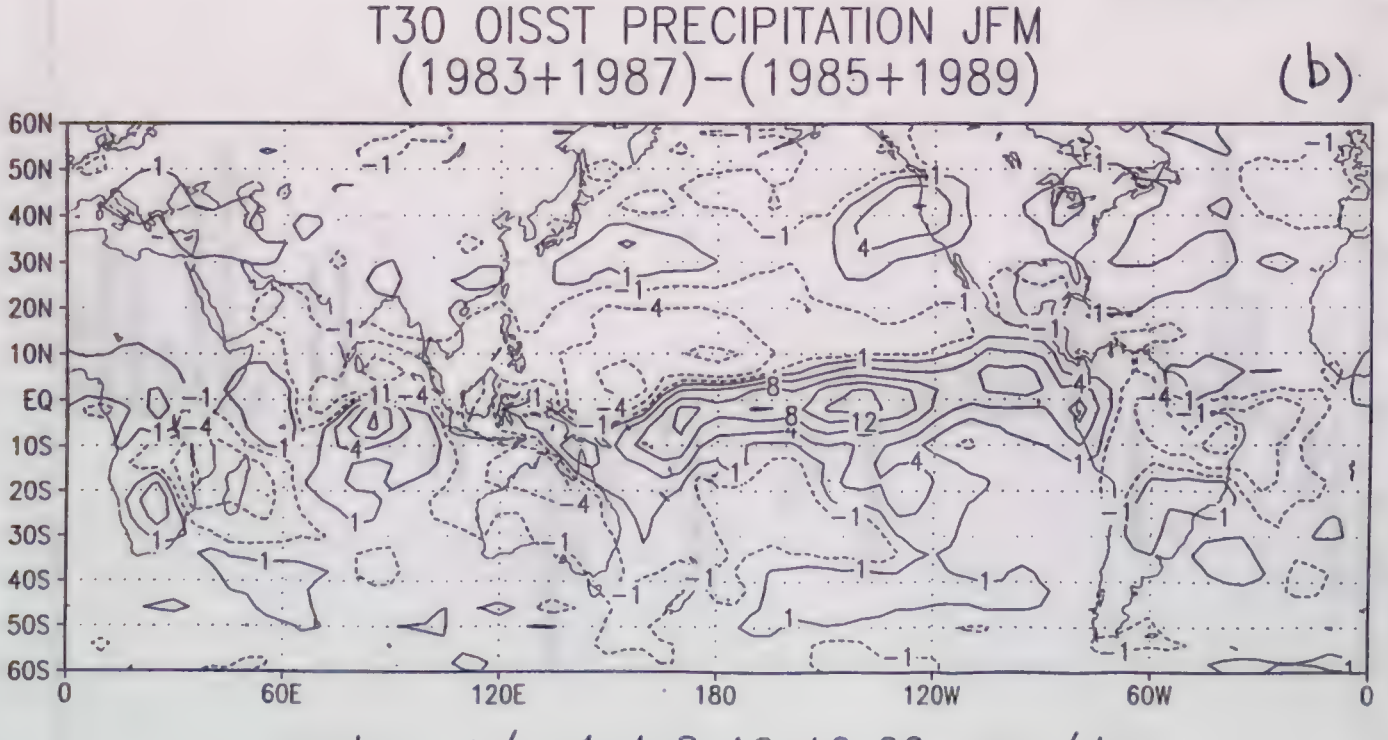
T30 OISST PRECIPITATION JFM
(1983+1987)-(1985+1989)
(b)
60N
50N
40N
30N
20N
10N
EQ
10S
20S
30S
40S
50S
60S
0
60E
120E
180
120W
60W
0
contour +/- 1 4 8 12 16 20 mm/day

Forcing The JMA Global Model with MOHSST

M. Sugi, R. Kawamura (NIED, Tsukuba) and N. Sato (JMA, Tokyo)

Six 34-year integrations of the T42/L21 GCM version of the JMA global model (JMA, 1992) have been performed. Three of them are forced with monthly MOHSST for the 34-year period from January 1955 to December 1988. The other three integrations used climatological SST. In all six integrations, climatological sea ice distribution is used. As in the operational JMA model, Kuo scheme for cumulus parameterization and mean orography are used.

The mean model climate is generally as good as other GCMs (Sugi et al., 1994b,c). Cool bias and zonalization, which are common in many GCMs, are also found in the JMA model. One of the deficiency of the model may be the weak convective activity in the western Pacific around Philippines in Northern Hemisphere summer. This seems to have large influence over the Asian monsoon and the summertime climate over Asia and Pacific.

In spite of these deficiencies, the response of the tropical atmosphere to tropical SST forcing is simulated very well by the model (Fig. 1). In contrast, the interannual variations in extratropics and Asian summer monsoon region are less successfully simulated by the model (Kawamura et al., 1994, Sugi et al., 1994a). This indicates that the internal variability is large in these regions.

The model tropical atmosphere generally shows little internal variability. For example, the interannual variations of the 200 hPa height field over the eastern equatorial Pacific are almost identical among the three real SST integrations. On the other hand, the internal variability is large in the extratropics. Fig. 2 shows the interannual variation of the wintertime 500 hPa height field over the North Pacific region for the three real SST runs. Fairly large difference is found among the three runs. However, if we take the ensemble average of the three real SST runs, the interannual variation of 500 hPa height field over the North Pacific has very good correlation (0.81) with that of 200 hPa height field in the tropics (Fig. 3). This shows clear evidence of the influence of tropical SST forcing on the extratropical interannual variation.

Another interesting interannual variation is that of the Asian summer monsoon. The observed interannual variation of monsoon rainfall is not well simulated by the model. This suggests that the monsoon rainfall is strongly affected by the internal variability and is not dominated by the SST forcing. We can see, however, the evidence of the influence of the SST forcing on the monsoon rainfall in the model. The ensemble mean of the monsoon rainfall of the three real SST runs has significant correlation (0.59) with the eastern equatorial Pacific SST.

References

JMA, 1993: Outline of operational numerical prediction at Japan Meteorological Agency. NPD/JMA, 128pp.

Kawamura, R., M. Sugi and N. Sato, 1994: Interdecadal and interannual variability in the northern extratropical circulation simulated with the JMA global model. (submitted to J. of Climate)

Sugi, M., R. Kawamura and N. Sato, 1994a: Interannual variation of the Asian summer monsoon simulated with the JMA global model. Extended Abstracts of the International Conference on Monsoon Variability and Prediction. Trieste, Italy, 9-13 May 1994, WMO.

_____, _____ and _____, 1994b: The climate simulated by the JMA global model. Part 1: Global feature. Report of NIED. No. 54

_____, R. D. Nair and N. Sato, 1994c: The climate simulated by the JMA global model. Part 2: Tropical precipitation. Report of NIED, No.54.

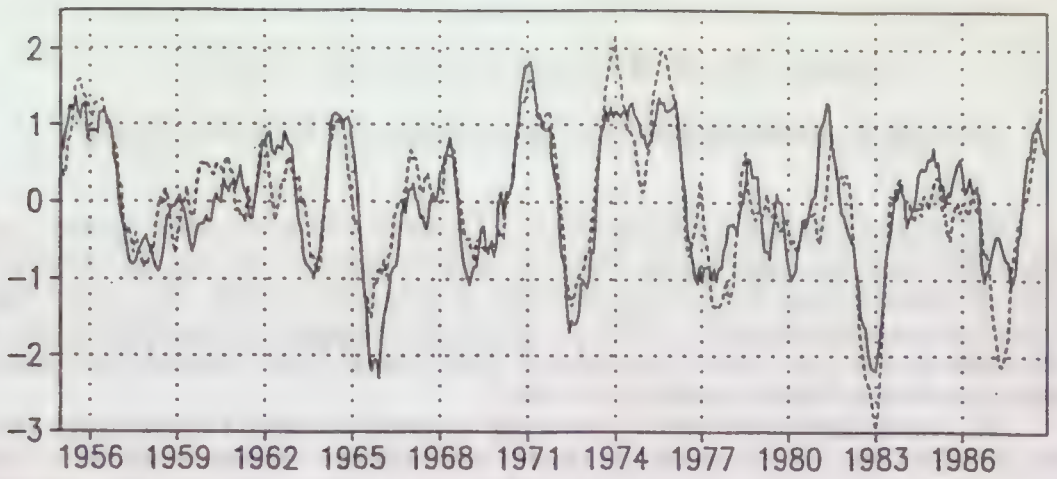

Fig. 1 Observed (dashed line) and simulated (solid line) SOI.

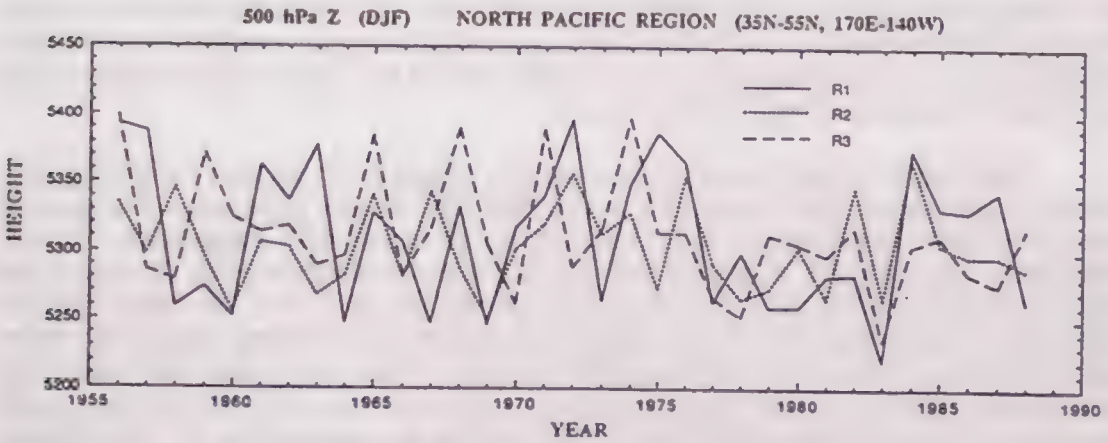

Fig. 2 Interannual variation of the wintertime 500 hPa height field over the North Pacific (35N-55N, 170E-140W) in each real SST run.

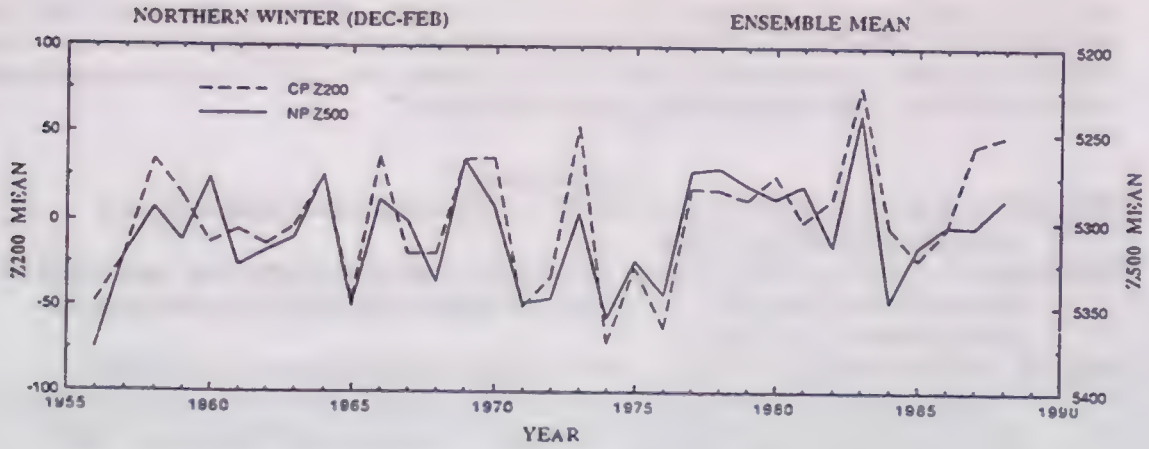

Fig. 3 Interannual variations of the wintertime 500 hPa height field over the North Pacific (35N-55N, 170E-140W) and 200 hPa height filed over the eastern tropical Pacific (10N-10S, 170W-140W) in the ensemble mean of the three real SST runs.

Modelling and Observational studies of a tropic-wide oscillation of boreal summer rainfall

M N Ward, K Maskell, C K Folland, D P Rowell and R Washington

Hadley Centre for Climate Prediction and Research,
Meteorological Office, Bracknell, UK.

Many GCM simulations using observed SST are now being compared with observed atmospheric variability. For a skilful simulation, a model needs to (i) respond correctly to local SST forcing and (ii) generate realistic large-scale teleconnections in the atmosphere. A fundamental stage in GCM verification is to assess the realism of its teleconnections. This note verifies the boreal summer tropical teleconnections of an early version of the UK Met Office model (model details in Rowell et al., 1995 QJRMS in press, and references therein). (More details of the work in this note are in Ward, 1994, Phd thesis and Ward et al., 1994, Hadley Centre CRTN48.)

GCM data: The GCM was forced with global sea-surface temperatures (SSTs) from April to October taken from the UK Met. Office Historical SST dataset for each of the years 1949, 50, 58, 76, 83, 84, 87, 88, 89, 90. Two GCM experiments were run for each year from different initial atmospheric conditions. The model is very skilful at simulating observed West African rainfall variability (Rowell et al, 1995, QJRMS, in press), but here we are concerned with its tropic-wide teleconnections.

Observed data: Observed monthly land station rainfall data were interpolated to grid-boxes by Hulme (in Global Precip. and Clim. Change, in press). The dataset commences in 1900, but here we analysed just the period 1949-90.

GCM and Observed EOF1: The observed and GCM data were placed on a 5°lat x 15°long grid. To identify the principal tropical teleconnection pattern in each dataset, we calculated the first correlation EOF over the domain 20°S to 40°N. The GCM and observed EOF1 patterns (Fig. 1), while differing in details of precise location, show marked broad-scale similarity by linking rainfall anomalies in the monsoon regions of Central America, North Africa and India. The monsoon variations are accompanied by a north-south dipole of rainfall anomaly in the western Pacific. The dipole is weaker in the observed EOF, but the data coverage is sparse in this region. The broad-scale tropic-wide agreement between the GCM and observed EOF1 leads us to argue that the GCM and observed EOFs are describing the same large-scale teleconnection. For brevity, we subsequently refer to this phenomenon as the tropic-wide oscillation (TO). In support of our result, the first EOF of global station precipitation data for June to August 1901-80 found by Lau and Sheu (1991, in Telecon. Linking Worldwide Clim. Anom., Eds Glantz, M H, et al.) is similar in pattern to the EOFs in Fig. 1. However, their EOF was more concentrated in the tropical Pacific, and their interpretation was solely in terms of warm events/cold events in the tropical Pacific. Here, we offer a different interpretation, suggesting that the TO is a natural recurring pattern of atmospheric variability, which certain types of Pacific warm events and cold events can trigger, but which also has variability on longer timescales which during this century has been associated with North-South interhemispheric variations in SST.

Relationship to ENSO: We suggest that the ability of an atmospheric GCM to simulate the TO is an important determinant of its utility for climate studies in boreal summer. Concentration solely on the Tahiti MINUS Darwin Southern Oscillation Index (SOI) may be limited to mainly indicating the ability of the model to respond to local SST. The original SOI of Walker and Bliss (1932, Mem. Roy. Met. Soc.) also included climate variations over India and Africa. Had they sought the SST patterns associated with their index, they would probably have identified what we term type I ENSOs, which involve a strong contrast in SST anomalies from the eastern Pacific to the western Pacific, associated with the strongest zonal migrations of SST maxima in the western Pacific at 5°S. Figure 2 shows the correlation between an index of ENSO and grid-box rainfall in the 17 years that show strongest migration of the SST maximum in the western Pacific 1950-90. Some 26% of boxes are significant at the 5% level, compared to just 6% when the other years are used for the correlation. This suggest that global teleconnections with ENSO become much weaker if ENSO fails to involve strong variations in the western Pacific. This may have tended to occur during the period 1920-50.

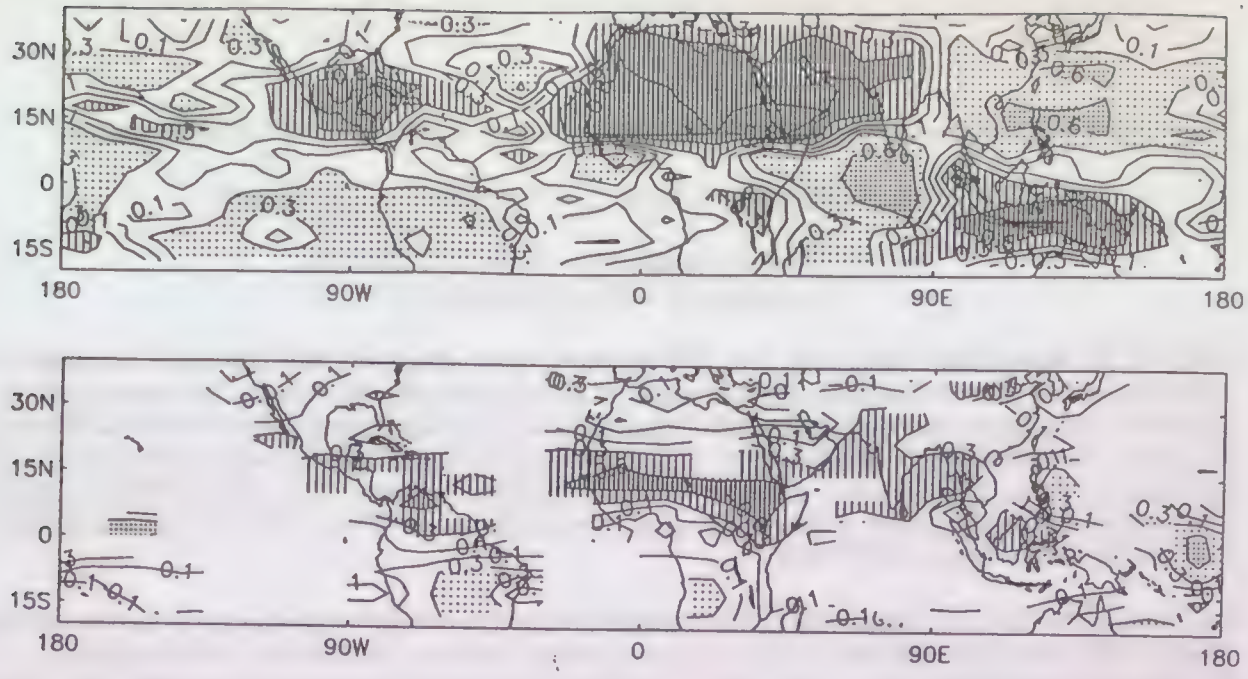

FIG. 1 JAS correlation EOF1 (40°N to 20°S) in (a) GCM simulations and (b) observed data. (a) EOF1 pattern (explaining 25% of the total variance in the dataset) for GCM simulated rainfall from 20 experiments. (b) EOF1 pattern for observed rainfall, 1949-90 (explaining 10% of total variance). Contours for both patterns at +/-.1,.3,.6,.8, shaded above .30, hatched below -.30. In (b), regions with insufficient data for analysis are not contoured.

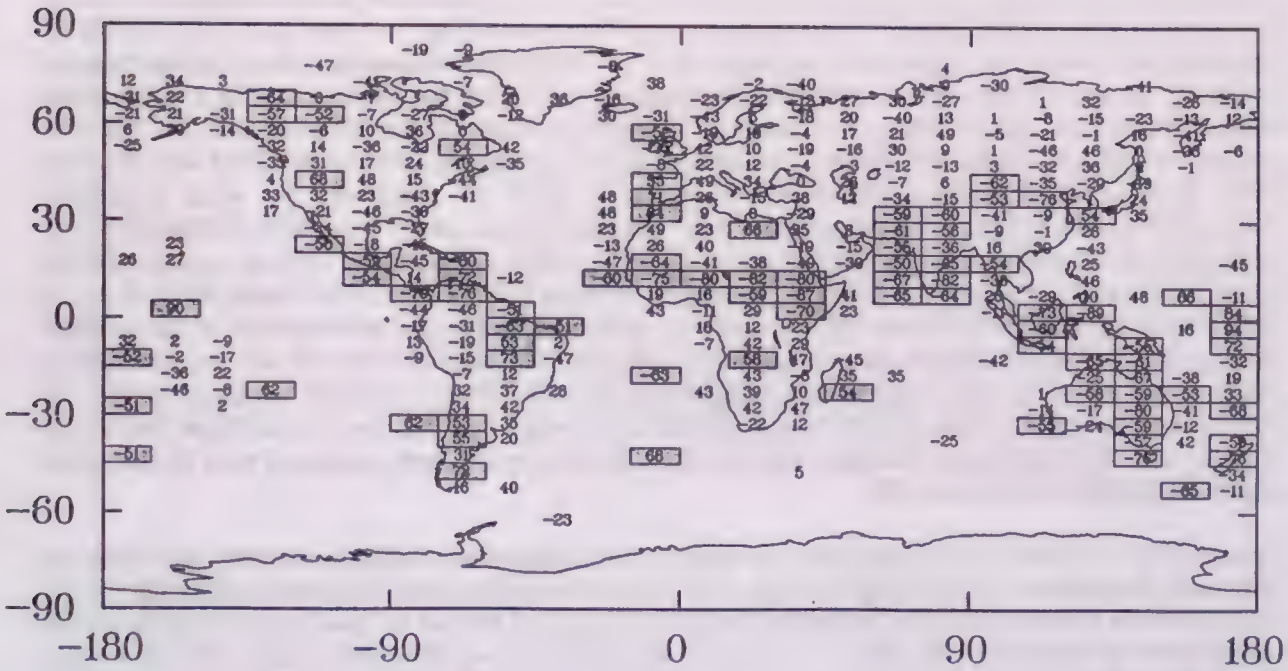

FIG. 2 Correlation of global sea-surface temperature EOF2 time coefficients in JAS (measuring the strength of ENSO) and JAS 5°lat x 15°long rainfall. Included in the correlation are just the 17 years (out of 1950-90) when the SST maximum at 5°S is shifted west of 160°E (50,54,62,64,75,78,81,88) or east of the dateline (51,57,60,65,72,76,77,82,87). Correlations locally significant at the 5% level (26% in total) are boxed. The map of correlations for other years in the period 1950-90 (not shown) has just 6% of all boxes significant at the 5% level. All series were high-pass filtered prior to analysis (passing timescales <11.25 years).

The Atmospheric Model Intercomparison Project (AMIP)

W.L.Gates, P.J.Gleckler, B.D.Santer and K.R.Sperber
Program for Climate Model Diagnosis and Intercomparison
Lawrence Livermore National Laboratory
Livermore, California USA

ABSTRACT

The international Atmospheric Model Intercomparison Project (AMIP) is being carried out by the Program for Climate Model Diagnosis and Intercomparison (PCMDI) with support from the U.S. Department of Energy on behalf of the Working Group on Numerical Experimentation of the World Climate Research Programme. This project calls for the simulation of the decade 1979-1988 by all atmospheric GCMs using the observed monthly-averaged distributions of sea-surface temperature and sea ice, and standardized values of the solar constant and atmospheric CO_2 concentration.

Preliminary analysis of the monthly-mean output from the 30 atmospheric GCMs participating in AMIP shows that they generally simulate the observed large-scale seasonal mean climate reasonably well, although there is a notable spread among the models' results, especially in the case of high-latitude sea-level pressure, tropical precipitation, and cloudiness. In comparison with the ERBE observations, there is evidence for a systematic model underestimate of the net cloud-radiative forcing in lower latitudes, which is believed to be related to deficiencies in the models' parameterizations of clouds, radiation and the boundary layer. More detailed analysis of the AMIP results, including use of the models' simulation history, is being conducted by a series of 26 diagnostic subprojects that are focussed on specific aspects of the models' variability and their simulation of selected phenomena.

Planning is underway for an international AMIP Scientific Conference in May 1995, at which detailed reviews of the AMIP simulations and their diagnosis will be presented, along with descriptions of related model analyses and intercomparisons. It is also proposed to discuss plans for the future of AMIP in the context of a broadened model intercomparison effort.

Intercomparison of Observed and Simulated Potential Predictability

Francis W. Zwiers
Canadian Centre for Climate Modelling and Analysis
Victoria, Canada

1 Introduction

A *potential predictability* calculation is a one-way time-domain analysis of variance (ANOVA) (see, for example, Madden, 1976 or Zwiers, 1987) in which the inter-annual variability of a seasonal or monthly mean is compared to the variation in this mean which is induced by daily weather noise. The inter-annual variance is thought to contain contributions from both external and internal sources which are potentially predictable. On the other hand, the component of inter-annual variance which is weather noise induced in not felt to be predictable on seasonal or longer time scales.

The data used in a potential predictability calculation are typically adjusted prior to analysis by subtracting an estimate of the annual cycle. This step is required to insure that daily variations within seasons are roughly stationary (in the statistical sense).

The inter-annual variance is estimated from the adjusted data in the usual way.

An independent estimate of the contribution to this variance which comes from weather noise is computed by assuming (i) that within season variations behave as white noise at low frequencies; and (ii) that the stochastic character of the weather noise is independent of the seasonal mean state. With these assumptions and the further assumption that between season variations are independent of each other, it can be demonstrated that the inter-annual variance of the seasonal mean contains contributions from external boundary forcing, internal sources of low frequency variation, and weather-noise. Thus F-ratios comparing the inter-annual variance with the induced weather noise variance are computed to ascertain whether the contributions from external and internal sources are significant. F-ratios significantly greater than one imply the presence of long time scale variations in the climate system which are potentially predictable.

Figure 1: *Zonally averaged inter-annual variance of DJF mean 500 mb geopotential computed from 1979-88 NMC analyses.*

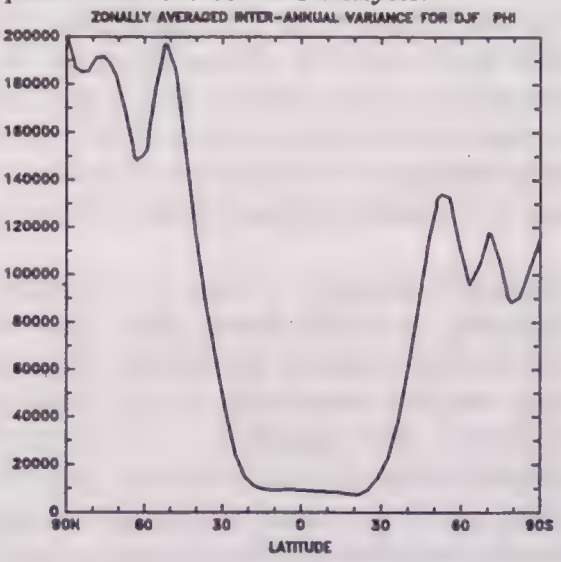

In most cases only a single realization of an observed or simulated climate is available with the consequence that the potentially predictable contributions from external and internal sources are confounded. When multiple runs of the same model are available it is possible to further partition variability according to source.

The CCC GCMII (McFarlane, et al., 1992; Boer, et al., 1992) has been used to generate 6 AMIP simulations (see Gates, 1992, for a description of the AMIP project) from 6 different sets of initial conditions. Each integration experienced the same observed evolution of sea surface temperatures and sea ice boundaries. These 6 integrations can be viewed as 6 independent realizations of the same simulated climate. Under these circumstances one can conduct a 2-way time-domain ANOVA and obtain estimates of the contribution to total inter-annual variance which arises from the initial conditions, the external boundary

Figure 2: *The natural logarithm of the ratio of the inter-annual variance of DJF mean 500 mb geopotential to the weather-noise induced variance of DJF mean 500 mb geopotential (see Zwiers, 1987 for details). The light, medium and dark shading indicate F-ratios which are significantly greater than one at the 10%. 5% and 1.25% significance levels respectively. The contour interval is $ln(2)$.*

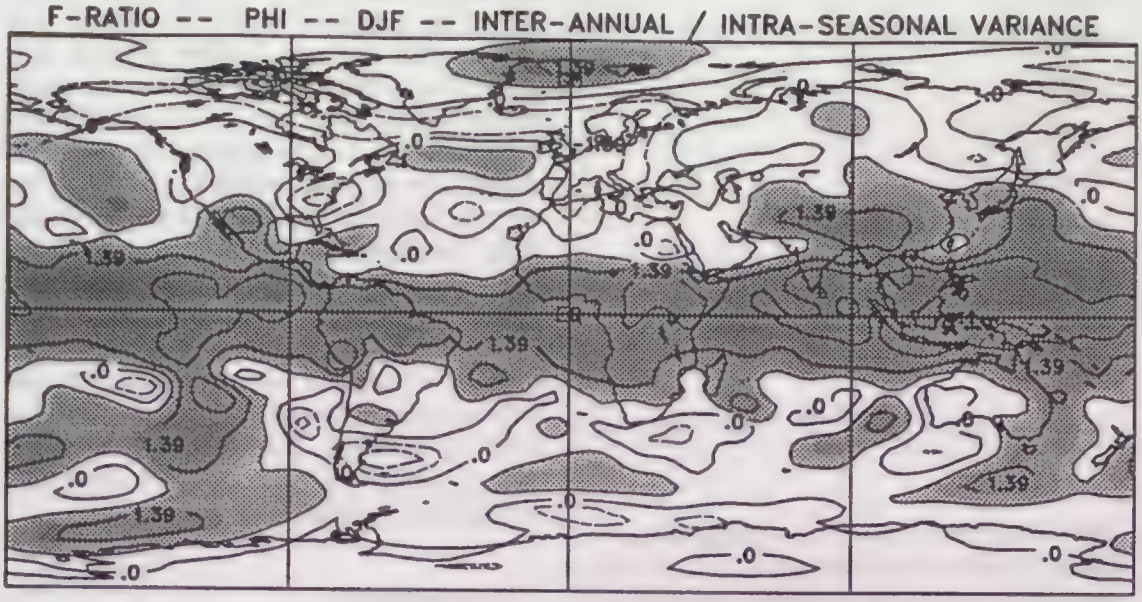

forcing, internal low-frequency sources, and weather noise. It is possible to test null hypotheses that (i) variation induced by varying initial conditions amongst the 6 runs is not potentially predictable; (ii) variation induced by the varying boundary conditions is not potentially predictable; and (iii) that there is no potentially predictable contribution to the inter-annual variance of seasonal means which arises from slowly varying internal sources (such as the atmosphere's internal dynamics and the land surface processes).

The remainder of this short note discusses such potential predictability calculations made with (i) "observations" (1979-1988 NMC analyses of 500 mb geopotential); and (ii) the CCC GCMII ensemble of AMIP simulations (forced with observed 1979-88 SSTs and sea-ice extent).

2 Observations

Figure 1 displays the zonally averaged inter-annual variance of DJF mean 500 mb geopotential as computed from 1979-88 NMC analyses. Note the peak at the north pole (which may be due to sampling variability), a peak at about 75° N which is due to variation over Greenland, and a third peak at about 42° N which reflects the mid-latitude NH storm tracks. Note also the broad tropical trough with variances less than $10^4 g^2 m^2$. The latter represents primarily low-frequency variations in the temperature of the troposphere.

Figure 2 displays locations at which the inter-annual variance of 500 mb geopotential is significantly greater than the variance induced by weather noise alone. Large, significant F-ratios can be seen in a broad tropical band which presumably reflects slow variations in SST in the tropics. Also, note the significant F-ratios in the north-east Pacific, over the southwestern US and Mexico, over China, and a suggestion that variations in the SPCZ are potentially predictable. These findings are in general agreement with those of Madden (1976) who used 1899-1972 NH MSLP station data, but are somewhat at odds with those of Trenberth (1985) who used 1972-80 ECMWF analyses and found significantly large F ratios over Antarctica as well as in the tropics.

3 CCC GCMII AMIP Simulations

Figure 3 displays the zonally averaged inter-annual variance of DJF mean 500 mb geopotential aggregated across the 6 AMIP simulations. Note that the simulated variance is only about 50% of that which is observed. This discrepancy would seem to be much larger

Figure 3: *As Fig. 1, except for DJF mean 500 mb geopotential simulated in the ensemble of 6 CCC GCMII AMIP runs.*

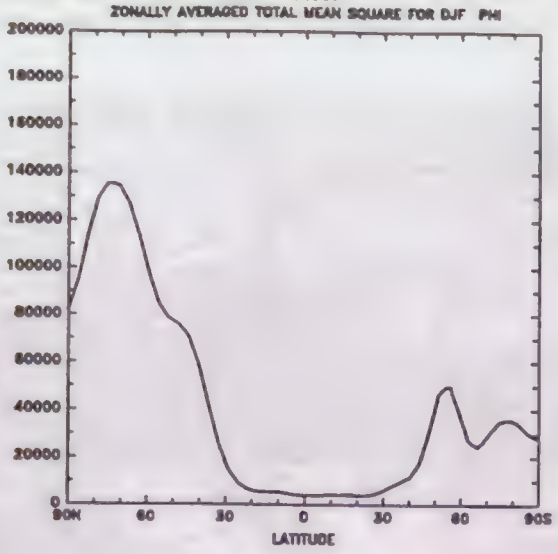

than that which could be attributed to sampling variation (in the observations), observational error, analysis error and the effects of network and analysis system changes during the 10-year AMIP period. The peak at the North Pole is not present in the simulations, the peak at 75° N which is associated with variation over Greenland is present (but not large enough), while the peak associated with northern mid latitude storm tracks is entirely absent. Centers of variation which are associate with these storm tracks are present in the simulated climate but are much weaker than observed. Variation in the tropics is also only about 50% of that which is observed despite the imposition of the observed SSTs at the lower boundary.

Application of the 2-way time-domain ANOVA reveals that there are no significant contributions to the total simulated interannual variability of 500 mb height from either the initial conditions or from sources internal to the model. However there are significant contributions from boundary forcing. This contrasts strongly with Zwiers (1987) who found potential predictability in a 20-year simulation with CCC GCMI (Boer, et al., 1984) from sources apparently internal to that model (SST and sea-ice was prescribed to follow a fixed annual cycle). When the 2-way ANOVA computation is repeated with 850 mb temperature we find strong contributions from boundary forcing and weak evidence that slow land surface variations (which are internal to the model) have a local potentially predictable effect over tropical land masses.

Figure 4 displays the result of the test for potential predictability from external and internal sources for 500 mb geopotential. The general structure of field of test statistics and the magnitude of the statistics is quite similar to that computed from observations. The tropical band of large F-ratios is wider than in the observations, partly because the larger volume of data has increased the sensitivity of the F-test and partly because the simulated climate contains less weather noise than the observed climate. There is a center of activity in the north-eastern Pacific as in the observations as well as large regions of significant F-ratios in the southern Pacific and Atlantic Oceans which roughly correspond to observations. The center of action over the Tibetan Plateau in the observations seems to be absent in the simulations. Consistent with observations, variations at high southern latitudes are not potentially predictable.

References

[1] G.J. Boer, N.A. McFarlane, and M. La zãre. Greenhouse Gas-induced Climate Change Simulated with the CCC Second-Generation General Circulation Model. *J. Climate*, 5:1045–1077, 1992.

[2] G.J. Boer, N.A. McFarlane, R. Laprise, and J.D. Henderson. The Canadian Climate Centre Spectral Atmospheric General Circulation Model. *Atmosphere-Ocean*, 22:397–429, 1984.

[3] W.L. Gates. AMIP: The Atmospheric Model Intercomparison Project, 1992. PCMDI Report No. 7.

[4] R. A. Madden. Estimates of the natural variability of time averaged sea level pressure. *Mon. Wea. Rev.*, 104:942–952, 1976.

[5] N.A. McFarlane, G.J. Boer, J.-P. Blanchet, and M. Lazare. The Canadian Climate Centre Second Generation General Circulation Model and its Equilibrium Climate. *J. Climate*, 5:1013–1044, 1992.

[6] K. E. Trenberth. Potential predictability of geopotential heights over the southern hemisphere. *Mon. Wea. Rev.*, 113:54–64, 1985.

[7] F. W. Zwiers. A potential predictability study conducted with an atmospheric general circulation model. *Mon. Wea. Rev.*, 115:2957–2974, 1987.

X

Figure 4: *As Fig. 2, except the F-ratio is computed as the ratio of the inter-annual variance of the simulated DJF 500 mb geopotential averaged across the 6 run ensemble to the mean weather noise induced variance in the 6 runs. This F-ratio tests the null hypothesis that potential predictability does not arise from either external (boundary) forcing or internal sources. It is also possible to test, separately, the null hypotheses that potential predictability does not arise from external sources, internal sources, or initial conditions.*

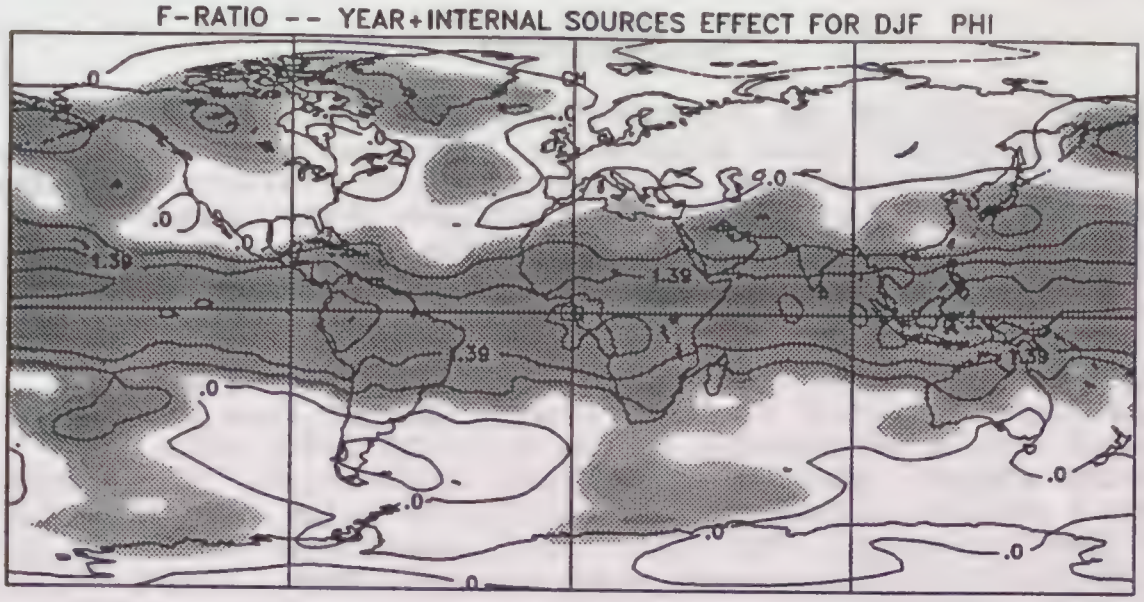

[8] F. W. Zwiers. Aspects of the statistical analysis of climate experiments with mutiple integrations. *MPI Report*, 18:1,33, 1988.

Abstract

SST-Forced Simulation Skill for Versions of the NCEP/MRF Model

Robert E. Livezey, Michiko Masutani, Ming Ji, Hualan Rui, Arun Kumar, and Ants Leetmaa

NCEP/NWS/NOAA

A major objective of the Climate Prediction Center is the exploitation of GCM-based methods for long-lead seasonal prediction. In particular, the capability to evaluate the impact of ENSO-related SST anomalies in situations where linear statistical methods are inadequate -- like those in which non-linearities are important, that are unprecedented, or where temporal resolution is crucial -- is highly desirable.

To begin assessment of the feasibility of the use of GCMs for forecasting a series of ensemble prescribed-SST runs have been conducted with a T40 version of the NCEP/MRF model with more realistic tropics than its operational counterpart. These runs include a series of preliminary simulations using SSTs from the early 1980s to early 1990s and a final ensemble of nine runs for the same period with a common model and different initial conditions. Additionally, a 20-year run with a fixed tropical Pacific SST-anomaly field equal to the standardized anomaly for January, 1992 -- the height of a strong warm episode -- was completed. Simulation accuracy and skill of upper-air fields were examined through a variety of measures by time of year, sector, zone, and time average.

For the nine-member 1980s-90s ensemble much of our *a priori* expectation was met: Convincing simulation skill was found in the northern extratropics for only the cold part of the year over the Pacific/North America sector during major ENSO episodes. This simulation skill was usefully high only for the filtered signal from the ensemble mean. The high-level subtropical flow was also extremely well simulated during the major warm and cold episodes from early winter through early summer.

In the case of the "perpetual" strong warm episode experiment monthly-mean composites were compared month by month to observation-based composites that were thoroughly tested for statistical significance. These two map sequences mutually support each other's suggestion that an ENSO-related signal can be present over North America for much of the year outside of the core of winter. This result had not been previously well-established observationally because of the tendency to composite on the basis of ENSO years rather than month-by-month on the basis of observed SST criteria. Additionally, much of the year the signal represents a considerably smaller percent of the total variance than it does in the winter. Regardless, this and the previously described prescribed SST experiments validate the model as a potentially useful part of a prediction system.

Response of the Asian Summer Monsoon to ENSO

Julia Slingo

Centre for Global Atmospheric Modelling, Department of Meteorology,University of Reading

Simulation of the evolution of the Asian Summer Monsoon has been studied using results from an integration of the U.K. Universities' Global Atmospheric Modelling Programme (UGAMP) General Circulation Model (UGCM). The integration was performed for the Atmospheric Model Intercomparison Project (AMIP) and thus used the observed SSTs for the decade January 1979 to December 1988. A full description of the results is given in Ju and Slingo (1994).

Considerable interannual variability is simulated both in the strength of the monsoon and in its date of onset. By comparing the model results for the dynamical onset of the monsoon with the equatorial SST anomalies, there is a suggestion that years with a delayed onset and weaker monsoon circulation tend to have warm SST anomalies in the central and east Pacific during the northern spring and summer (i.e. 1982, 83 and 87). Those years with an earlier onset and a stronger monsoon circulation tend to have cold SST anomalies (i.e. 1984, 85 and 86). The evolution of the monthly mean 200 and 850 hPa zonal winds over South East Asia (5^0N-20^0N, 40^0E-120^0E) is shown in Figure 1 for the weak and strong monsoon composites. Also shown in Figure 1 are the equivalent results from the ECMWF analyses. If the strength of the monsoon is defined in terms of the anomalous vertical shear of the zonal wind (i.e.$u'_{850} - u'_{200}$) then Figure 2 shows that, even on a year to year basis, the dynamical strength of the large scale monsoon is predictable. This suggests that the boundary forcing associated with the SST anomalies is most likely to be responsible.

The early development of the Somali jet and the low level westerly flow over the Indian Ocean in La Nina years may be related to local heating anomalies over the Indian Ocean and South East Asia. Both satellite data and the model results imply a latitudinal shift of the ITCZ over the Indian Ocean and West Pacific during the preceding spring, in association with the phases of El Nino. During ENSO, SST anomalies prevail in the subtropics, which are of the opposite sign to those in the equatorial central and east Pacific. The patterns of the response by the convection, implied by the OLR anomalies, suggest that these remote SST anomalies may be instrumental in determining the latitudinal position of the ITCZ. This is the basic hypothesis reached from the results of this study, that the influence of El Nino on the large scale monsoon may be through the modulation of the latitudinal position of the ITCZ over Indonesia in the preceding spring. This modulation of the ITCZ appears to be directly related to the SST anomalies prevailing in the subtropical north west Pacific which are themselves part of the global pattern associated with El Nino. SST anomaly experiments to test this hypothesis are currently in progress.

REFERENCES

Ju, J. and J. M. Slingo, 1994 : The Asian Summer Monsoon and ENSO. Quart. J. Roy. Meteorol. Soc. (to appear)

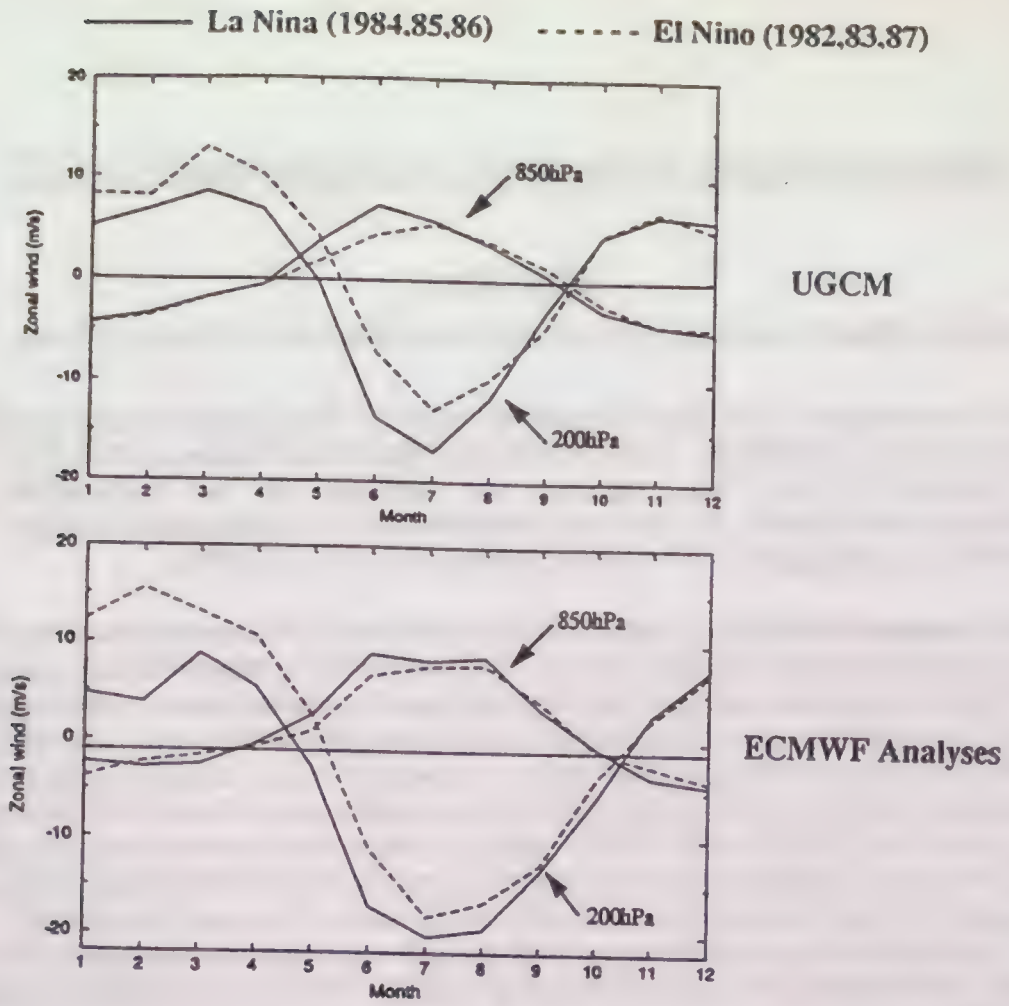

Figure 1 : Composite evolution of monthly mean zonal winds over SE Asia, 5N-20N, 40E-120E

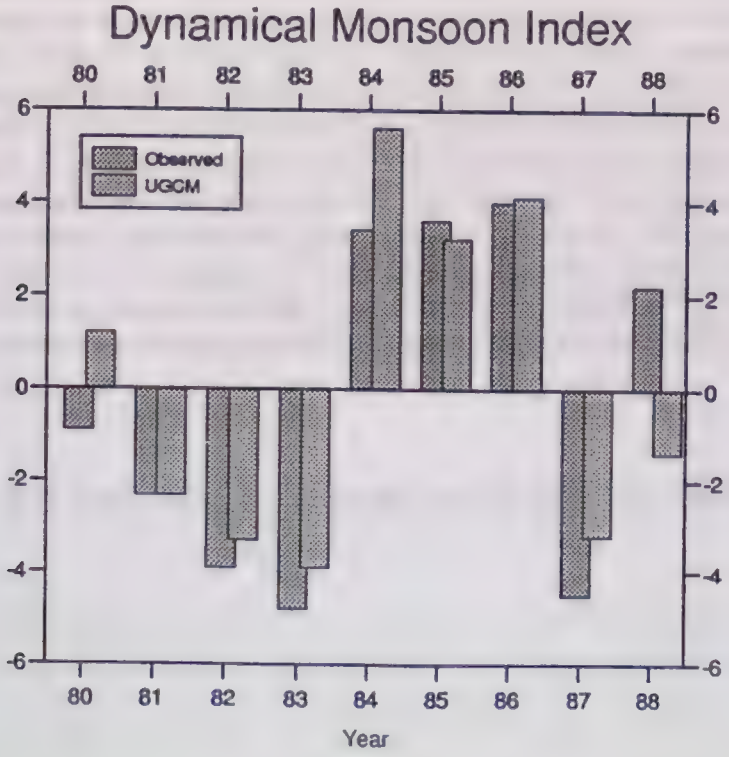

Figure 2 : Dynamical Monsoon Index (u_{850}-u_{200} anomaly) for May and June over SE Asia.

Predictability of Monsoons in ECMWF Seasonal Integrations

Č.Branković and T.N.Palmer

ECMWF, Shinfield Park, Reading, RG2 9AX, England

1. Introduction

The chaotic climate of the atmosphere can be described by a probability distribution function (pdf) over all atmospheric states, and can be estimated from ensemble integrations of an atmospheric model. This pdf is influenced by the atmosphere's lower boundary conditions, in particular, sea surface temperature (SST). Seasonal predictability is, in part, based on the notion that interannual fluctuations in SST can have a notable impact on the atmospheric pdf. In this paper, we study interannual variations in the pdf of the northern hemisphere monsoons through ensembles of seasonal integrations with prescribed SSTs.

A series of 9-member ensembles of seasonal integrations with specified observed SSTs was made with the ECMWF T63L19 model. They were carried out over the 5 summer (JJA) seasons, from 1986 to 1990, with an earlier version of the model, the so-called cycle 36. During this period the equatorial Pacific SSTs evolved between various phases of the El Niño-Southern Oscillation (ENSO). Accordingly, an index linked to the SST anomaly was defined. We focus on the impact of the change in ENSO from the strong warm phase in JJA 1987 (El Niño) to the strong cold phase in JJA 1988 (La Niña). For these summers, ensembles with a more recent model version, cycle 12r1, were also made. For each ensemble, individual members were initiated from consecutive 12Z operational analyses about a month before the calendar summer season. Seasonal averages were computed from the last three months of each individual integration. This work is an extension of Branković *et al.* (1994) who studied seasonal predictability from 3-member time-lagged ensembles.

2. Skill of the model and intra-ensemble variability

Distributions of the skill scores and ensemble consistency have been estimated for 200 mb zonal wind over the tropical region that covers the northern Indian Ocean basin and surroundings, from 22°N to 22°S and from 30°E to 150°E. For the skill scores, we first calculate all possible differences (seasonally and area-averaged) between ensembles from the two years, e_i^{87}-e_j^{88}, where e_i^{87} (e_j^{88}) is a member of the ensemble made with the summer 1987 (1988) SSTs, and both subscripts i and j run from 1 to 9. There are 81 such differences for 9-member ensembles. Then, we correlate each of these differences with the observed difference, o^{87}-o^{88} between the two years. The 81 correlation coefficients obtained in such a way are then categorised into equal bins of 0.2.

We also calculate the internal consistency of the ensemble estimate of interannual difference. For one 'fixed' difference field, e_i^{87}-e_j^{88} (one element from the first ensemble and one element from the second), we calculate correlation coefficients with all possible 81 difference fields from two ensembles, e_k^{87}-e_l^{88}. This is repeated 81 one times (for all different 'fixed' differences), thus obtaining 81x81 correlation coefficients. As for the skill, correlation coefficients measuring consistency have been distributed into equal categories of 0.2.

Fig.1 a,b shows frequency distributions of skill and consistency for cycle 36 (solid bars) and Fig.1 c,d for cycle 12r1 (hatched bars), for the summers of 1987 and 1988. The simulation of the upper atmospheric wind field difference over the northern Indian Ocean basin seems to be quite skilful in both models. The highest skill, with the correlation coefficients between 0.8 and 1.0, takes about 75% of all cases, and the rest of 25% falls into the second highest (0.6 to 0.8) category. There is almost no difference in skill scores between the two versions of the model. Interestingly, the skill for the same field over the adjacent tropical Pacific region is not as high as over the Indian Ocean (not shown).

The ensemble consistency is also high, over 90% in the highest category, indicating little variation between different model realizations and high predictability for this variable. For comparison, the

corresponding cycle 36 distributions for the weak ENSO-index summers (1990 and 1989) is shown in Fig.1 e,f. Clearly, the skill of the model is much reduced and the internal consistency decreased for the case with weak lower boundary forcing. Also, for comparison, in Fig.1 g,h skill and consistency distributions are shown for the Atlantic/European region (86°N to 22°N and 90°W to 30°E), a more ostensibly chaotic part of the atmosphere.

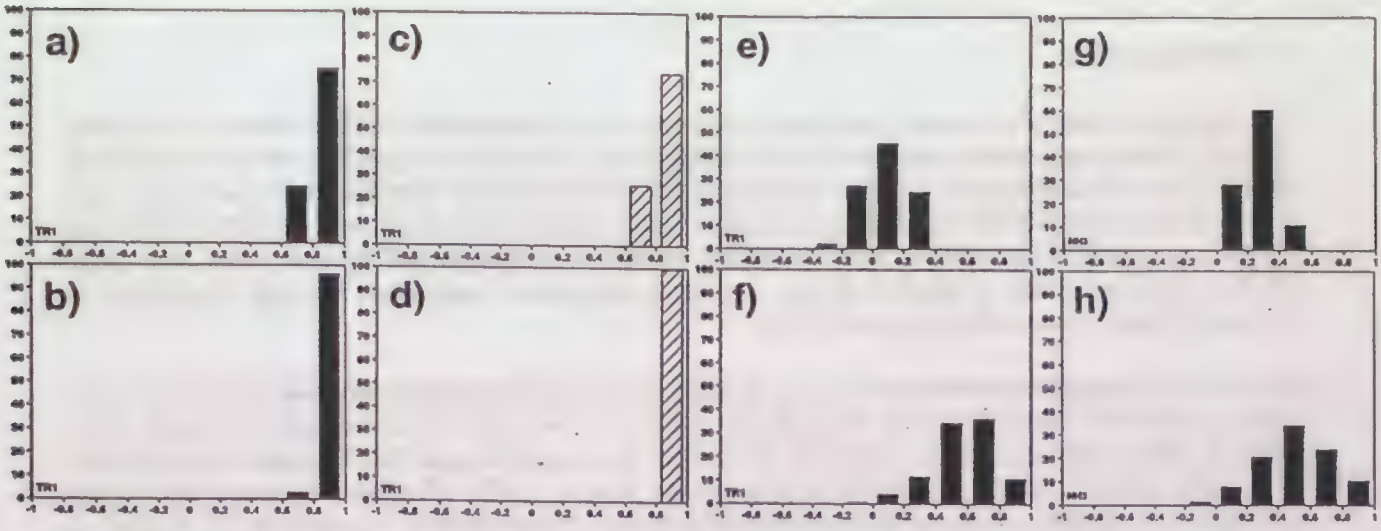

Fig.1 Distributions of JJA 200 mb zonal wind skill scores (top panels) and ensemble consistency (bottom panels) for: a) and b) cycle 36 strong ENSO; c) and d) cycle 12r1 strong ENSO, e) and f) cycle 36 weak ENSO, g) and h) cycle 36 strong ENSO for Atlantic/European region.

3. Relationship between potential predictability and ensemble size

The dependence of potential predictability on ensemble size is assessed for predefined land-regions within the influence of monsoon activity. For a given meteorological variable (rainfall, for example), a t-statistic was derived for ensemble differences from the opposite ENSO-index years. The magnitude of the t-value gives a statistical significance to the simulated ensemble interannual variations. This is first done using all 9 members. The calculation is then repeated for all sub-ensembles that are contained within the 9-member ensemble, i.e. for 8-, 7-, 6-, 5-, 4- and 3-member sub-ensembles. For an n-member sub-ensemble (n<9), the mean t-value averaged over all possible n-member choices within the 9-member ensemble were calculated. For rainfall, the t-statistic is shown in Fig.2 for various chosen regions.

For the Sahel rainfall, the t-variable for the difference between strong ENSO-index summers (JJA 1987 minus JJA 1988) reaches very high values (99% confidence level) even with 3-member ensembles. This suggests that the impact of ENSO on Sahel rainfall is very predictable. This is true for both cycle 36 and a newer cycle 12r1, though somewhat lower values for 12r1 indicate larger intra-ensemble variability with this model cycle. For the weak ENSO-index summers, JJA 1989 and JJA 1990 (open circles in Fig.2), extrapolated t-values indicate that 15- or 16-member ensembles would be required to reach the 99% confidence level.

For India, the predictability of interannual variations of rainfall is not as high as for the Sahel (compare the y-axis values). Though the 90% confidence level with cycle 36 is reached already for 4-member ensembles, a 10-member ensemble would be required to achieve 99% confidence level. Cycle 12r1 has a slightly larger predictability estimates over India, though is broadly comparable with cycle 36 estimates. For the weak ENSO-index years, results suggest that very large ensembles might be needed. For comparison, the results for European region are also shown. In the strong ENSO-index years the significant level of predictability is reached with 5 or 6-member ensembles, though for the weak ENSO-index years, there is little evidence of predictability.

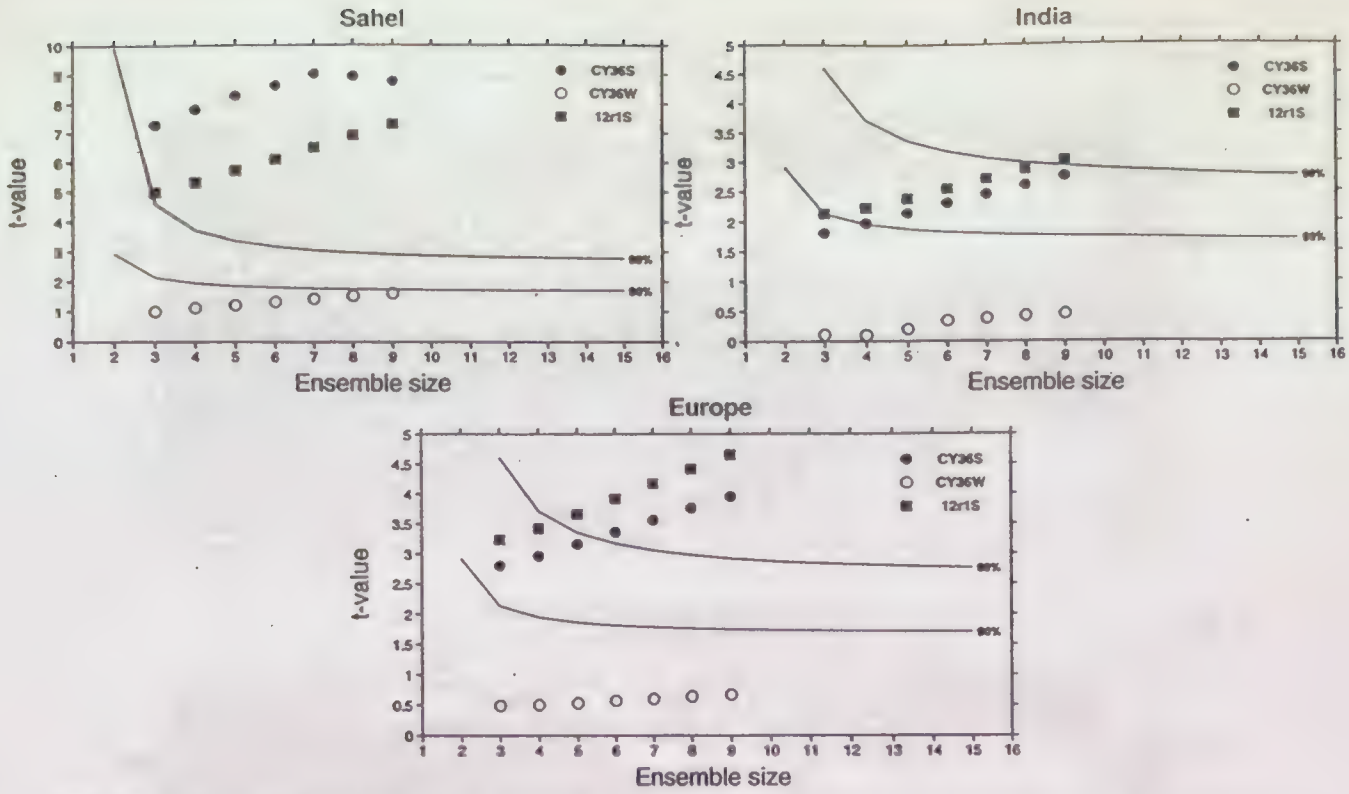

Fig.2 The JJA rainfall t-variable values. Solid circles cycle 36 strong ENSO, open circles cycle 36 weak ENSO, squares cycle 12r1 strong ENSO.

4. Probabilistic representation of ensemble integrations

As discussed in the introduction, ensemble integrations can be used to estimate changes to the atmospheric pdf. Here we show estimates of probability of changes in rainfall. For the 9-member ensembles, all 81 differences between JJA 1987 and JJA 1988 were calculated. From the incidence of both positive and negative rainfall differences, a grid-point probability (or proportion of differences out of total 81) was assigned, indicating whether the El Niño year was wetter (drier) than the La Niña year. Probabilities for both positive and negative differences are then combined into one map with a 60% discriminating contour (Fig.3a).

Over the Sahel, the probability of negative rainfall differences (light stipple) is high, exceeding 90% over much of the region. This result implies that for most of the 81 differences JJA 1987 was drier than JJA 1988. This is in a good agreement with verification differences for the two summers (Fig.3b) obtained from the Global Precipitation Climate Centre (GPCC), Germany (Rudolf 1993).

Over much of India, the probability of negative differences is in excess of 60%, and more than 90% in the north and in the south. Generally smaller probability estimates over India imply lower predictability for that region than for the Sahel. This is associated with a relatively large internal ensemble variability over the Indian subcontinent and is consistent with estimates of the t-variable shown in Fig.2. In cycle 12r1, the internal spread is somewhat larger than in cycle 36 and high probabilities (90 or more%) of negative differences are found only over northern India (not shown).

5. Conclusions

It was demonstrated that the ECMWF model is able to represent satisfactorily interannual variation of summer monsoons. The difference in predictability estimates for the two model cycles indicates that more reliable results may be obtained by combining integrations from various model versions (and using the same initial conditions). We plan to analyse joint ensembles from cycles 36 and 12r1 in future studies.

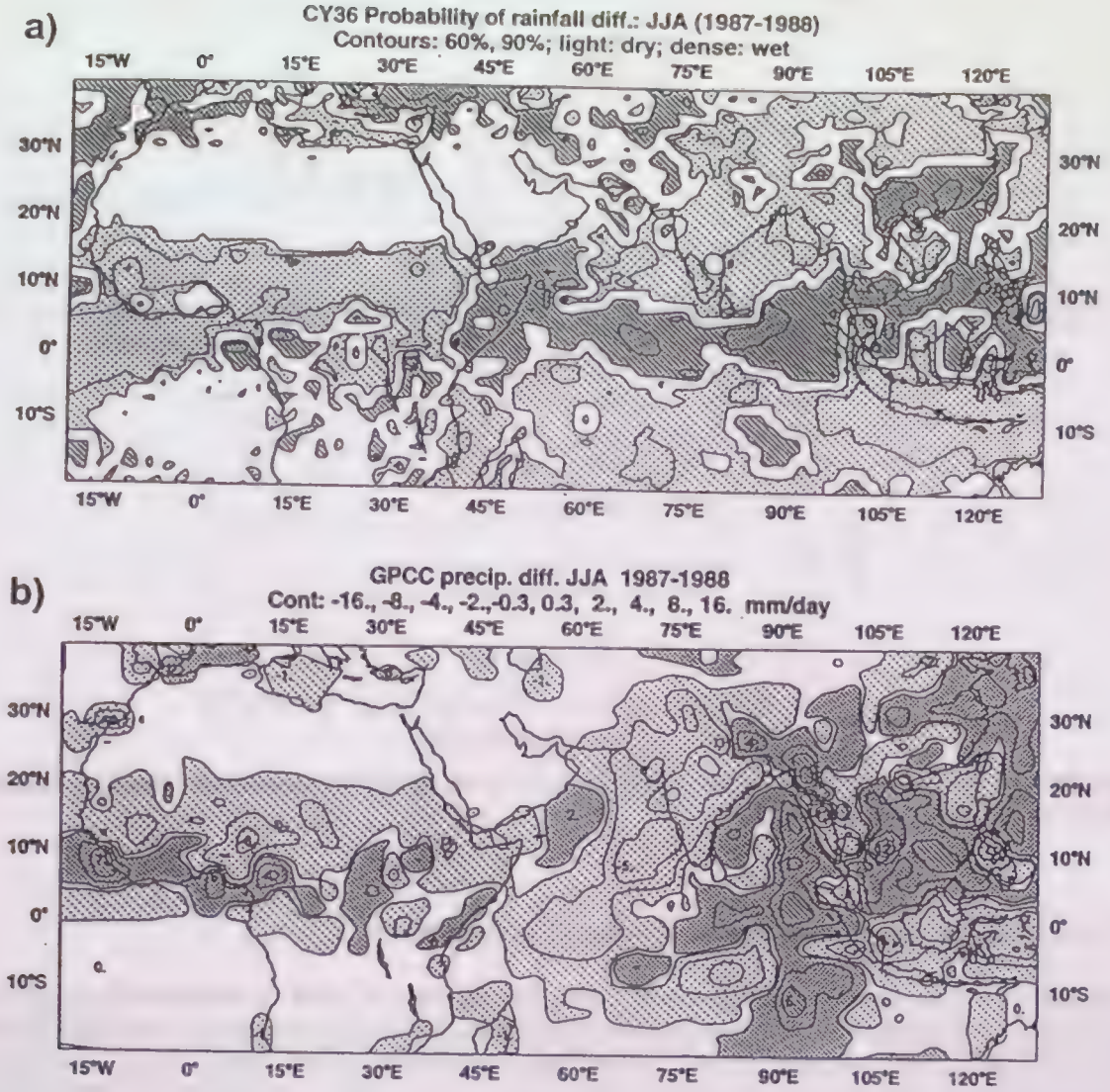

Fig.3 a) Cycle 36 probability of rainfall differences (JJA 1987 minus JJA 1988). Probability of negative differences light shading, positive dense; contours 60% and 90%. b) GPCC rainfall differences.

References:

Branković, Č., T.N.Palmer and L.Ferranti, 1944: Predictability of seasonal atmospheric variations. *J.Climate*, 7, 217-237.

Rudolf, B., 1993: Management and analysis of precipitation data on a routine basis. Proceedings of the Symposium on Precipitation end Evaporation, 20-24 September 1993, Bratislava, Slovak Rep.

Climate Predictability Within Two Nearly Identical Atmospheric GCMs

M. Hoerling[1], A. Kumar[2], M. Ji[2], A. Leetmaa[2], P. Sardeshmukh[1]

[1] *Cooperative Institute for Research in the Environmental Sciences, Boulder, CO*
[2] *National Meteorological Center/Climate Dynamics Group, Washington, D.C.*

1. Background

Predictability of time-averaged atmospheric states arises largely from the "signal" generated by slowly evolving boundary forcings. Of importance is this signal's strength relative to the unpredictable climate "noise" due to natually occurring atmospheric variability. The ratio of signal-to-noise defines the potential for predictability, and that ratio will depend on atmospheric variable, location, and time-averaging interval.

Nature imposes upper limits on climate predictability, and it remains to be seen if these bounds are reachable within state-of-the-art general circulation models (GCMs). The predictable atmospheric component which does exist can be lost due to errors in forecasting the boundary conditions, and due to biases in the atmospheric GCM.

The subject of this paper is the climate predictability within two nearly identical AGCMs forced with the same observed global sea surface temperatures (SSTs). These experiments explore the boundary forced predictability given "perfect SST forecasts". We examine the predictability over the Pacific and North American sectors where a large effect of SST forcing on atmospheric states has been found. A detailed description of the perfomance of these two AGCMs, and a general treatment of assessing a GCM's suitability for making climate predictions appears in Kumar et al. (1994).

2. Experimental Design

GCM simulations of the atmospheric response to observed monthly mean SSTs from February 1982-November 1993 have been conducted. An ensemble of nine parallel integrations have been performed, each starting from different model atmospheric initial conditions on 1 February 1982 but subjected to identically evolving SST forcing.

Two AGCMs, referred to as MRF8 and MRF9, have been used for this purpose. These climate versions originate from NMC's global short range forecast model (Kanamitsu et al. 1991), and our experiments are run at a reduced T40 spectral resolution with 18 sigma levels. The two models differ in their parameterization of convective clouds. In MRF8, convective clouds are divided into discrete low, middle, and high layers for radiation purposes. In contrast, only high clouds are associated with convection in MRF9 (see Kumar et al. 1994).

3. Tropical Boundary Forced Predictability

Five El Niño/Southern Oscillation (ENSO) events occurred during the recent decade, with anomalous tropical Pacific warming during 1982/83, 1986/87 and 1991/92, and anomalous cooling during 1984/85 and 1988/89. Figures 1a and 1b show the MRF8 and MRF9 warm event composite rainfall and 200 mb vector wind anomalies during winter, respectively. This model analysis is of the nine member ensemble mean response for each of the three warm events. The observed composite for the same three cases is shown in Fig. 1c.

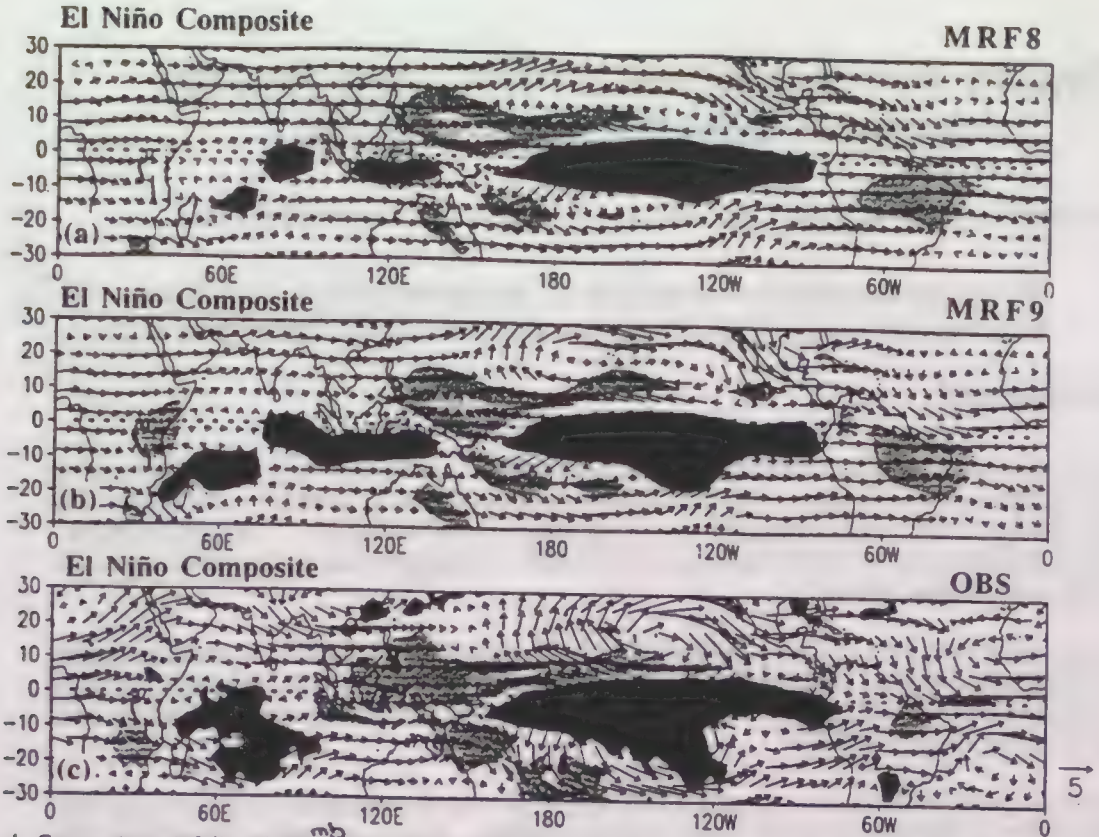

Fig. 1. Composite rainfall and 200 mb vector wind anomalies during the mature phase of El Niño for December-April for (a) MRF8, (b) MRF9, and (c) observations. The model composites are based on the ensemble average of nine atmospheric GCM simulations using global SST anomalies for 1982/83, 1986/87, and 1991/92. The observed composite is the 3-case average of these same events. Observed rainfall anomalies derived from MSU radiances over oceans, and rain guage measurements over land. Dark shading shows positive rainfall anomalies, and maximum values are 7 mm/day just east of the equatorial dateline on all three panels. Light shading highlights negative rainfall anomalies, and the maximum values are -5 mm/day northeast of New Guinea on all three panels.

Both MRF versions exhibit similar tropical responses during El Niño. A narrow band of enhanced rainfall extends from 160°E to the South American coast, and is flanked by off-equatorial suppressed rainfall especially over the western Pacific Ocean. This result agrees closely with the observed composite rainfall anomaly as estimated from the Microwave Sounding Unit (MSU) over oceans and in situ measurements over land (Fig. 1c). Over the tropical land masses, both models simulate suppressed rainfall, although more extensive than that observed, whereas only MRF9 simulates significant rainfall anomalies over Africa. These features are readily reproduced in the AGCMs using only a single realization (equivalent to the single observed time-series) consistent with the fact that the ENSO-related tropical rainfall signal greatly exceeds the inherently unpredictable natural variability.

At upper levels, equatorial westerly anomalies extend from South America to Africa in both model and observations, and these are regions of generally reduced rainfall during the recent El Niño winters. Twin anticyclones straddle the equatorial central Pacific in all three composites. Note that the associated equatorial easterly anomalies span the region of enhanced rainfall in both model and observations, a behavior quite different from a linear Gill-type solution to a steady heat source. It is also worth noting that the ensemble mean MRF composite circulation anomalies are considerably weaker than the observed 3-case mean. Within the framework of a perfect AGCM, this result would indicate that a non-trivial component of even the tropical circulation response to El Niño is not a deterministic outcome of SST forcing. Thus, a weaker model response could arise simply through ensemble averaging which reduces the climate noise yet retains the SST signal. Of course, both GCMs have biases and these may detract from the realism of the responses.

Figure 2 illustrates the MRFs' hindcast skill for 5-month running mean tropical rainfall anomalies during 1982-1993. Model rainfall anomalies are derived from the nine-member ensemble average, and the locations correspond to regions of appreciable interannual rainfall variability in the tropical Pacific. Both MRF8 (dashed line) and MRF9 (light solid line) show nearly the same interannual variability, and this is consistent with the similarity in composite rainfall responses. It is evident, however, that the agreement with observations (dark solid line) is greatest over the central Pacific (Fig. 2a). This result is encouraging since an important dynamical forcing of the global teleconnections during ENSO is believed to originate from such equatorial central Pacific rainfall anomalies. There is also evidence of a significant atmospheric sensitivity to diabatic forcing from the tropical west Pacific (e.g., Simmons et al. 1983), and the predictive skill of both MRF versions in this region is smaller (Fig. 2b).

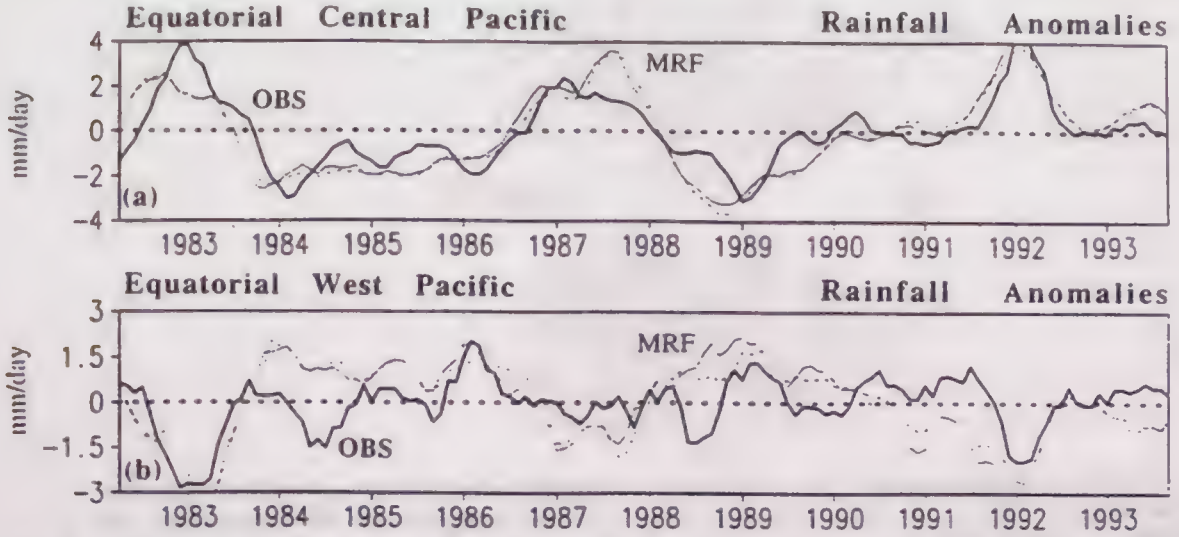

Fig. 2. Time-series of observed and MRF simulated rainfall anomalies for spatial averages centered on the (a) equatorial central Pacific, and (b) equatorial west Pacific. Panel (a) is for the area 10°S-10°N and 180°-140°W. Panel (b) is for the area Equator-15°N, and 120°E-160°E. MRF8 (MRF9) shown in light dashed (solid) line, and the MSU estimated rainfall anomalies are shown in dark, solid line. All anomalies computed relative to either the GCM or observed 1982-1993 base climatology.

4. Extratropical Boundary Forced Predictability

Suffice it to say that there is little evidence for a different tropical sensitivity to anomalous SST forcing among the two MRF versions. This does not preclude the possibility that the two models may exhibit different sensitivity in the extratropics. Indeed, there is evidence that the extratropical response to tropical forcing can be quite sensitive to the background climatological flow, and Kumar et al. (1994) find several important distinctions between such mean flows in MRF8 and MRF9.

An additional issue in the extratropics is the identification of the boundary forced signal itself. Contrary to the tropics, the large climate noise in extratropics can easily mask the boundary forced signal, and reliable detection of that signal in AGCMs requires Monte Carlo methods. Observations on an individual case basis will always be a blend of a predictable climate signal and the background noise, and the verification of AGCM ensemble predictions for individual events is problematic (Kumar and Hoerling 1994).

Thus, it is reasonable to argue that assessments of extratropical climate predictability based on the skill averaged over many cases of significant boundary forcing will be most meaningful. One such evaluation is shown in Fig. 3. The MRF 500 mb height composites (Figs. 3a and b) are for the nine-case ensemble average for each of the 3 El Niño winters in the 1982-1993 period listed in section 3. The observed 500 mb height composite (Fig. 3c) is for 9 El Niño winters since 1950, and is an estimate of the average atmospheric response during El Niño.

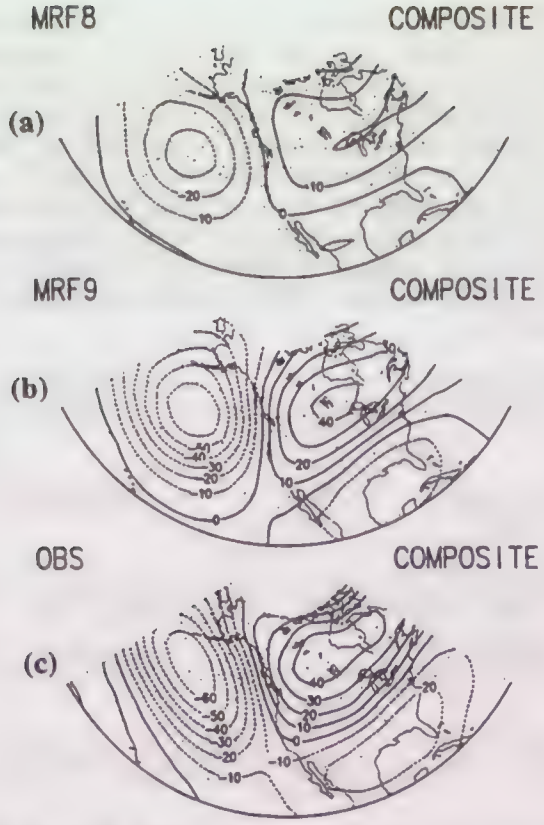

Fig. 3. Departure from zonal symmetry of the composite 500 mb height anomalies for winter (December thru April) during mature El Niño events. Composites are based on (a) MRF8 simulations, (b) MRF9 simulations, and (c) observations. Contour interval is 5 m, and negative contours are dashed. The polar stereographic projection shows the region bounded by 20°-70°N and 180°-60°W. The observations composite the nine warm events (1957-58, 66, 70, 73, 77, 78, 83, 87, 92) The GCM composites consist of 27 El Niño winters derived from the nine-case ensemble for each of 1982-83, 87, 92.

It is evident that the two models possess greatly different extratropical sensitivities to El Niño-related SST forcing. The amplitude of the 200 mb stationary wave anomalies in MRF9 (Fig. 3b) is nearly double that simulated in MRF8. Importantly, the MRF9 response agrees more closely with that observed on average (Fig. 3c). Furthermore, we have verified that both models have similar internal variability of seasonal mean 200 mb heights, and thus the stronger SST-forced signal in MRF9 is also indicative of a larger signal-to-noise ratio. It is thus reasonable to argue that MRF9 is a better suited model for extratropical seasonal predictions, and indeed Kumar et al. (1994) show that MRF9 on average generates more skillful seasonal mean hindcasts over the PNA-region during 1982-1993. While a better GCM for this purpose was not constructed by design, the results highlight the importance of continued model development. Even a subtle change in an otherwise state-of-the-art GCM can significantly impact that model's sensitivity to SST forcing, and its climate predictability.

5. References

Kanamitsu, M., J. C. Alpert, K. A. Campana, E. M. Caplan, D. G. Deaven, M. Iredell, B. Katz, H. L. Pan, J. Sela and G. H. White, 1991: Description of NMC global data assimilation and forecast system. *Wea. Forecasting*, **6**, 425-435.

Kumar, A., M. P. Hoerling, M. Ji, A. Leetmaa and P. D. Sardeshmukh, 1994: Assessing a GCM's suitability for making seasonal predictions. *J. Climate*, submitted.

Kumar, A., and M. P. Hoerling, 1994: Prospects and limitations of atmospheric GCM climate predictions. *Bull. Amer. Meteor. Soc.*, **76**, in press.

Simmons, A. J., J. M. Wallace, and G. W. Branstator, 1983: Barotropic wave propagation and instability, and atmospheric teleconnection patterns. *J. Atmos. Sci.*, **40**, 1613-1630.

Appendix 1: Program of Workshop

28 Nov 1994

0840 Minibus departs Royal Foresters Hotel

0915 Welcome: **D.J.Carson**, Director of the Hadley Centre.

0930 Introduction: **C.K.Folland**

Session 1: Key Climate Data Sets

Chairperson: Larry Gates

0945 **D.E.Parker** and M.Jackson (Hadley Centre): The standard GISST data sets: Versions 1 and 2

1020 **N.Rayner**, M.N.Ward, D.E.Parker and C.K.Folland (Hadley Centre): Using EOF analysis to create a new GISST data set for forcing GCMs

1055 Coffee

1115 **J.Walsh** (Univ. of Illinois): A sea ice database

1150 **M.Hulme** and P.D.Jones (CRU): Global precipitation and surface temperature data sets

1230 Lunch

1340 **T.Basnett** and D.E.Parker (Hadley Centre): A provisional new global mean sea level pressure data set

1410 **D.E.Parker** and D.P.Cullum (Hadley Centre): A provisional new radiosonde temperature data set

1450 **R.E.Livezey** (CAC): NCEP/NCAR 40-year reanalysis, and reconstruction of pre-1980 SST fields

1530 Coffee

Session 2: Simulations using SST

Chairperson: Jagadish Shukla

1550 **D.P.Rowell** (Hadley Centre): Forcing the Hadley Centre model with GISST: Introduction and assessment of seasonal predictability

1605 **A.Bevan**, C.K.Folland and D.P.Rowell (Hadley Centre): Forcing the Hadley Centre model with GISST: Extratropical response to ENSO

1620 **J.R.Davies**, D.P.Rowell and C.K.Folland (Hadley Centre): Forcing the Hadley Centre model with GISST: European variability

1635 **C.D.Thorncroft** (Univ. of Reading) and D.P.Rowell (Hadley Centre): Forcing the Hadley Centre model with GISST: Interannual variability of African wave activity

1650 **A.Hense** (Univ. of Bonn): Forcing the ECHAM3 model with the GISST data: First results

1725 **M.Christoph** (MPI): Forcing the ECHAM3 model with the GISST data: Variability of storm tracks

1740 Close

1800 Minibus returns to Royal Foresters Hotel

1945 Workshop Dinner, Little White Hart Hotel, Henley (coach departs Royal Foresters Hotel at 1905)

29 Nov 1994

0840 Minibus departs Royal Foresters Hotel

Chairperson: Tim Palmer

0900 W.F.Stern, **K.Miyakoda** and J.Anderson (GFDL): Forcing the GFDL model with GISST

0935 **C.S.Fredericksen**, P.Indusekeran, R.Balgovind and N.Nicholls (BMRC): Forcing the BMRC model with GISST

1010 **I.N.Smith**, B.G.Hunt and R.J.Allan (CSIRO): Forcing the CSIRO model with GISST and MOHSST

1045 Coffee

1105 **J.Shukla** and L.Marx (COLA): Simulation of atmospheric circulation with observed global SST and sea ice during 1949-1992

1140 **M.Sugi**, R.Kawamura (National Research Institute for Earth Science and Disaster Prevention, Tsukuba) and N.Sato (JMA): Forcing the JMA global model with MOHSST

1215 **M.N.Ward**, K.Maskell, C.K.Folland, D.P.Rowell and R.Washington (Hadley Centre): Modelling and observational studies of a tropic-wide oscillation of boreal summer rainfall

1235 Lunch

Chairperson: Andreas Hense

1335 **W.L.Gates** (AMIP): The AMIP project

1410 **A.Navarra** (DICE): The DICE project

1430 **F.Zwiers** (CCC): Intercomparison of observed and simulated potential predictability

1450 **R.E.Livezey** (CAC): SST-forced simulation skill for versions of the NCEP/MRF model

1510 Coffee

1530 **J.M.Slingo** (Univ. of Reading): Response of the Asian summer monsoon to ENSO

1550 **T.N.Palmer** (ECMWF): Seasonal predictability experiments at ECMWF

1610 **M.Hoerling** (CIRES): Climate predictability within two nearly identical atmospheric GCMs

Session 3: Discussion, Intercomparison and Recommendations

Chairperson: Chris Folland

1630 General discussion

1700 Commence intercomparison of key diagnostics previously requested; split into 3 groups:
a.Climatologies and ENSO teleconnections (leader: **K.Miyakoda**)
b.SST-forced variability versus internal variability (leader: **F.Zwiers**)
c.Time-series (leader: **R.E.Livezey**)

1745 Close

1800 Minibus returns to Royal Foresters Hotel

30 Nov 1994

0840 Minibus departs Royal Foresters Hotel

0900 Intercomparison of key diagnostics (continued)

1040 Coffee

1100 Intercomparison of key diagnostics (continued)

1200 Summary presentations by leaders, and discussion of intercomparisons.
Plan the final reports.

1300 Lunch

Session 4: Updated input to IPCC 1995 Scientific Assessment Chapter "Climate Models-Validation", mainly on AGCM variability and trends.

Chairperson and lead speaker: Chris Folland

1400 IPCC Session - for those contributing, or intending to contribute, to Chapter 5 "Climate Models-validation" the results of long integrations forced with observed SST, and others interested in the discussion.

1510 Coffee

1530 Continue

1645 (approx) Close

1715 Minibus returns to Royal Foresters Hotel

Appendix 2: Participants

Miss T Basnett
Hadley Centre
Meteorological Office
London Road
BRACKNELL
Berkshire RG12 2SY

FAX 1344-854898
Tel 1344-854063
Email tbasnett@meto.govt.uk

Dr H Cattle
Hadley Centre
Meteorological Office
London Road
BRACKNELL
Berkshire RG12 2SY

FAX 1344-854898
Tel 1344-856209
Email hcattle@meto.govt.uk

Dr D A Bennetts
Hadley Centre
Meteorological Office
London Road
BRACKNELL
Berkshire RG12 2SY

FAX 1344-854898
Tel 1344-856653
Email dabennetts@meto.govt.uk

Dr M Christoph
Max-Planck-Inst fur Meteologie
Bundesstrasse 55
D-20146 HAMBURG
GERMANY

FAX 49-40-41173-298
Tel 49-40-41173-373
Email Christoph@dkrz.d400.de

Miss A Bevan
Hadley Centre
Meteorological Office
London Road
BRACKNELL
Berkshire RG12 2SY

FAX 1344-854898
Tel 1344-856904
Email abevan@meto.govt.uk

Mr D P N Cullum
Hadley Centre
Meteorological Office
London Road
BRACKNELL
Berkshire RG12 2SY

FAX 1344-854898
Tel 1344-856079
Email dpncullum@meto.govt.uk

Dr D J Carson
Hadley Centre
Meteorological Office
London Road
BRACKNELL
Berkshire RG12 2SY

FAX 1344-854898
Tel 1344-856611
Email djcarson@meto.govt.uk

Mr J R Davies
Hadley Centre
Meteorological Office
London Road
BRACKNELL
Berkshire RG12 2SY

FAX 1344-854898
Tel 1344-856875
Email jdavies@meto.govt.uk

Dr M Fiorino
PDMDI/LLNL
P O Box 808,L-264
LIVERMORE
California 94550
USA

FAX 510-422-7675
Tel 510-423-8505
Email fiorino@typhoon.llnl.gov

Dr P Gleckler
PDMDI/LLNL
P O Box 808,L-264
LIVERMORE
California 94550
USA

FAX 510-422-7675
Tel 510-422-7631
Email gleckler@airsea.llnl.gov

Mr C K Folland
Hadley Centre
Meteorological Office
London Road
BRACKNELL
Berkshire RG12 2SY

FAX 1344-854898
Tel 1344-856646
Email cr@meto.govt.uk

Dr D Gregory
Hadley Centre
Meteorological Office
London Road
BRACKNELL
Berkshire RG12 2SY

FAX 1344-854898
Tel 1344-856204
Email dgregory@meto.govt.uk

Dr C Frederiksen
BMRC
GPO Box 1289K
MELBOURNE
VIC 300
AUSTRALIA

FAX 61-3-669-4660
Tel 61-3-669-4407
Email csf@bom.gov.au

Mr C D Hall
Hadley Centre
Meteorological Office
London Road
BRACKNELL
Berkshire RG12 2SY

FAX 1344-854898
Tel 1344-854490
Email cdhall@meto.govt.uk

Prof L Gates
PDMDI/LLNL
P O Box 808,L-264
LIVERMORE
California 94550
USA

FAX 510-422-7675
Tel 510-422-7626
Email gates5@llnl.gov

Dr M Harrison
Numerical Modelling Research
Meteorological Office
London Road
BRACKNELL
Berkshire RG12 2SZ

FAX 1344-854026
Tel 1344-856295
Email mharrison@meto.govt.uk

Prof Dr A Hense
Meteorologisches Institut
Universitat Bonn
Auf dem Hugel 20
D-5300 BONN 1
Germany

Fax 49-228-735188
Tel 49-228-735184
Email UNF42D@IBM.rhrz.uni-bonn.de

Prof D Karoly
CRC, Southern Hemisphere Meteo
Monash University
8 Redwood Drive
Notting Hill, VIC 3168
AUSTRALIA

FAX 61-3-550-9181
Tel 61-3-550-9169
Email djk@vortex.shm.monash.edu.au

Dr M Hoerling
Climate Research Division
NOAA/ERL
325 Broadway
BOULDER
Colorado 80303
USA

FAX 303-497-7013
Tel 303-492-1114
Email mph@noaacdc.colorado.edu

Dr R Livezey
Climate Analysis Center
W/NMC51, Room 604
World Weather Building
5200 Auth Road
WASHINGTON DC 20233
USA

FAX 301-763-8395
Tel 301-763-8155
Email N/A

Dr M Hulme
Climatic Research Unit
University of East Anglia
NORWICH
Norfolk NR4 7TJ

FAX 1603-507784
Tel 1603-593162
Email m.hulme@east-anglia.ac.uk

Prof K Miyakoda
GFDL
Princeton University
Forrestal Campus, Route 1
PO Box 308
PRINCETON, NJ 08540
USA

FAX 609-987-5063
Tel 609-452-6545
Email km@gfdl.GOV

Mr M Jackson
Hadley Centre
Meteorological Office
London Road
BRACKNELL
Berkshire RG12 2SY

FAX 1344-854898
Tel 1344-856238
Email mjackson@meto.govt.uk

Dr A Navarra
IMGA - CNR
Via Emilia Est 770
41100 MODENA
ITALY

Fax 39-5937-4506
Tel 39-5936-2388
Email navarra@rigoletto.bo.cnr.it

Ms F Nortley
CGAM, Dept of Meteorology
University of Reading
2 Earley Gate
Whiteknights
READING, RG6 2AU

FAX 1734-318316
Tel 1734-318954
Email Fay@met.reading.ac.uk

Dr D P Rowell
Hadley Centre
Meteorological Office
London Road
BRACKNELL
Berkshire RG12 2SY

FAX 1344-854898
Tel 1344-856077
Email DPRowell@meto.govt.uk

Dr T N Palmer
ECMWF
Shinfield Park
READING
Berkshire RG2 9AX

FAX 1734-869450
Tel 1734-499600
Email N/A

Dr J Shukla
Inst of Global Env & Soc, Inc
COLA
4041 Powder Mill Rd, Suite 302
CALVERTON
MD 20705-3106
USA

FAX 301-595-9793
Tel 301 595-9755
Email N/A

Mr D E Parker
Hadley Centre
Meteorological Office
London Road
BRACKNELL
Berkshire RG12 2SY

FAX 1344-854898
Tel 1344-856649
Email deparker@meto.govt.uk

Dr J Slingo
CGAM, Dept of Meteorology
University of Reading
2 Earley Gate
Whiteknights
READING, RG6 2AU

FAX 1734-318316
Tel 1734-318424
Email swsslingo@met.reading.ac.uk

Miss N Rayner
Hadley Centre
Meteorological Office
London Road
BRACKNELL
Berkshire RG12 2SY

FAX 1344-854898
Tel 1344-854063
Email nrayner@meto.govt.uk

Dr I Smith
CSIRO
Private Bag No 1
MORDIALLOC
Victoria 3195
AUSTRALIA

FAX 61-3-586-7600
Tel 61-3-586-7666
Email ins@dar.csiro.au

Dr K Sperber
PDMDI/LLNL
P O Box 808,L-264
LIVERMORE
California 94550
USA

FAX 510-422-7675
Tel 510-422-7720
Email sperber@space.llnl.gov

Dr J E Walsh
Dept of Atmos Sciences
Univ Illinois, Urbana-Campaign
105 South Gregory Avenue
URBANA
IL 61801, USA

FAX 217-244-4393
Tel 217-333-7521
Email walsh@wx.atmos.uiuc.edu

Dr M Sugi
Atmos & Hydrospheric Sci Div
Nat Res Inst, Earth Science
3-1 Tennodai, Tsukuba
IBARAKI 305
JAPAN

FAX 81-298-51-1622
Tel 81-298-51-1611
Email sugi@ess.bosai.go.jp

Dr M N Ward
Hadley Centre
Meteorological Office
London Road
BRACKNELL
Berkshire RG12 2SY

FAX 1344-854898
Tel 1344-856080
Email mnward@meto.govt.uk

Dr R Sutton
Dept of Atmospheric Physics
Clarendon Laboratory
Parks Road
OXFORD OX1 3PU

FAX 1865-272923
Tel 1865-272085
Email
atmrts@Toga1.atm.ox.ac.uk

Mr R Washington
C/o Hadley Centre
Meteorological Office
London Road
BRACKNELL
Berkshire RG12 2SY

FAX 1344-854898
Tel 1344-854089
Email rwashington@meto.govt.uk

Dr C Thorncroft
Dept of Meteorology
University of Reading
2 Earley Gate
Whiteknights
READING RG6 2AU

FAX 1734-352602
Tel 1734-316688
Email swsthcri@met.reading.ac.
uk

Dr F Zwiers
Climate Modelling & Anal Div
University of Victoria
PO Box 1700 MS 3339
VICTORIA, B.C.
CANADA V8W 2Y2

FAX 604-363-8247
Tel 604-363-8229
Email fzwiers@uvic.bc.doe.ca

CLIMATE RESEARCH TECHNICAL NOTES

CRTN 1	Oct 1990	Estimates of the sensitivity of climate to vegetation changes using the Penman-Monteith equation. P R Rowntree
CRTN 2	Oct 1990	An ocean general circulation model of the Indian Ocean for hindcasting studies. D J Carrington
CRTN 3	Oct 1990	Simulation of the tropical diurnal cycle in a climate model. D P Rowell
CRTN 4	Oct 1990	Low frequency variability of the oceans. C K Folland, A Colman, D E Parker and A Bevan
CRTN 5	Dec 1990	A comparison of 11-level General Circulation Model Simulations with observations in the East Sahel. K Maskell
CRTN 6	Dec 1990	Climate Change Prediction. J F B Mitchell and Qing-cun Zeng
CRTN 7	Jan 1991	Deforestation of Amazonia - modelling the effects of albedo change. M F Mylne and P R Rowntree
CRTN 8	Jan 1991	The role of observations in climate prediction and research. D J Carson
CRTN 9	Mar 1991	The greenhouse effect and its likely consequences for climate change. D J Carson
CRTN 10	Apr 1991	Use of wind stresses from operational N.W.P. models to force an O.G.C.M. of the Indian Ocean. D J Carrington
CRTN 11	Jun 1991	A new daily Central England Temperature series, 1772-1991. D E Parker, T P Legg and C K Folland
CRTN 12	Jul 1991	Causes and predictability of Sahel rainfall variability. D P Rowell, C K Folland, K Maskell, J A Owen, M N Ward

CLIMATE RESEARCH TECHNICAL NOTES

CRTN 13	Jul 1991	Modelling changes in climate due to enhanced CO2, the role of atmospheric dynamics, cloud and moisture. C A Senior, J F B Mitchell, H Le Treut and Z-X Li
CRTN 14	Sep 1991	Sea temperature bucket models used to correct historical SST data in the Meteorological Office. C K Folland
CRTN 15	Aug 1991	Modelling climate change, and some potential effects on agriculture in the U.K. P R Rowntree, B A Callander and J Cochrane
CRTN 16	Aug 1991	The Boreal Forests and Climate G Thomas and P R Rowntree
CRTN 17	Aug 1991	Development of a Stratosphere-Troposphere Data Assimilation System. R Swinbank.
CRTN 18	Sep 1991	A study of asynchronous coupling using a simple climate model. M K Davey.
CRTN 19	Sep 1991	The Oceanic Carbon Cycle. N K Taylor
CRTN 20	Nov 1991	Worldwide ocean-atmosphere surface fields in Sahel wet and dry years using provisionally corrected surface wind data. M N Ward
CRTN 21	Dec 1991	Coupled tropical ocean global atmosphere models at the UKMO. M K Davey, C Gordon, S Ineson and S Lawrence
CRTN 22	Dec 1991	Empirical parameterisation of tropical ocean-atmosphere coupling. M Allen, M K Davey, D L T Anderson and P D Killworth
CRTN 23	Feb 1992	The temporal evolution of Equatorial Currents in the Indian Ocean D L T Anderson, D J Carrington, R A Corry and C Gordon
CRTN 24	Feb 1992	Stratospheric analyses provided by the U.K. Meteorological Office M J Bailey, A O'Neill and V D Pope

CLIMATE RESEARCH TECHNICAL NOTES

CRTN 25	Feb 1992	Modelling interannual variability in the Indian Ocean using momentum fluxes from the UKMO and ECMWF operational weather analyses. D L T Anderson and D J Carrington
CRTN 26	Mar 1992	A GCM simulation of the impact of Amazonian deforestation on climate using an improved canopy representation J Lean and P R Rowntree
CRTN 27	Mar 1992	The parameterization of rainfall interception in GCMs A J Dolman and D Gregory
CRTN 28	Jun 1992	Development of worldwide marine data eigenvectors since 1985 A W Colman
CRTN 29	Jun 1992	A tropical ocean model with reduced physics M K Davey
CRTN 30	Jun 1992	International Temperature Workshop, Boulder, Colorado, USA, 16 January 1992 Edited by D E Parker
CRTN 31	Jul 1992	Simulation of clear-sky outgoing longwave radiation over the oceans using operational analyses A Slingo and M J Webb
CRTN 32	Sep 1992	A prediction of the transient response of climate J M Murphy
CRTN 33	Nov 1992	LEPS scores for assessing climate model simulations and long-range forecasts. C K Folland
CRTN 34	Jan 1993	Stratospheric Data Assimilation System Guide Editer: R Swinbank
CRTN 35	Mar 1993	A Stratosphere-Troposphere Data Assimilation System R Swinbank and A O'Neill
CRTN 36	Mar 1993	Validation of hydrological schemes for climate models against catchment data. P R Rowntree and J Lean

CLIMATE RESEARCH TECHNICAL NOTES

CRTN 37	Apr 1993	Modelling of palaeoclimates: Examples from the recent past J F B Mitchell
CRTN 38	May 1993	A simulation of seasonality in ENSO forecast skill M K Davey, D L T Anderson and S Lawrence
CRTN 39	Jul 1993	ENSO Prediction experiments using a simple ocean-atmosphere model D-H Wu, D L T Anderson and M K Davey
CRTN 40	Sep 1993	Diagnosis of dynamic sea-surface and sea-level changes from the Cox ocean model J M Gregory
CRTN 41	Sep 1993	Seasonal variations of the clear-sky greenhouse effect: the role of changes in atmospheric temperatures and humidities M J Webb, A Slingo and G L Stephens
CRTN 42	Nov 1993	Sea-level changes under increasing atmospheric CO_2 in a transient coupled ocean-atmosphere GCM experiment. J M Gregory
CRTN 43	Dec 1993	Global and regional patterns of climate change: recent predictions for the Arctic P R Rowntree
CRTN 44	Feb 1994	The effect of changing horizontal diffusion in the atmospheric version of the unified climate model C D Hall and R A Stratton
CRTN 45	Mar 1994	Simulation of El-Niño/Southern Oscillation like variability in a global AOGCM and its response to CO_2 increase. S F B Tett
CRTN 46	Apr 1994	Global data required for monitoring climate change. D E Parker and C K Folland
CRTN 47	May 1994	Seasonal uptake of anthropogenic CO_2 in an ocean general circulation model. N K Taylor

CLIMATE RESEARCH TECHNICAL NOTES

CRTN 48	Jun 1994	A tropic-wide oscillation of boreal summer rainfall and patterns of sea-surface temperature. M N Ward, K Maskell, C K Folland, D P Rowell and R Washington
CRTN 49	Jun 1994	Simulation of the tropical Pacific using a simplified ocean model M A Balmaseda, D L T Anderson and M K Davey
CRTN 50	Sep 1994	Simulation of global mean temperature using a box-diffusion climate model P R Rowntree
CRTN 51	Sep 1994	Seasonal dependence of ENSO prediction skill M A Balmaseda, M K Davey and D L T Anderson
CRTN 52	Nov 1994	Simulation of the Indian Monsoon and Tropical Intraseasonal Variability by a General Circulation Model P M Inness and D Gregory
CRTN 53	Mar 1995	A comparison of modelled surface fluxes with climatological estimates. C Gordon and D K Wright
CRTN 54	Mar 1995	The representation of moist convection in atmospheric models. D Gregory
CRTN 55	Mar 1995	A consistent treatment of the evaporation of rain and snow for use in large-scale models D Gregory
CRTN 56	Apr 1995	Workshop on simulations of the Climate of the Twentieth Century using GISST, 28-30 November 1994, Hadley Centre, Bracknell, UK Edited by C K Folland and D P Rowell